In vivo dynamics of DnaA and its regulators

Inauguraldissertation
zur Erlangung der Doktorwürde
der Fakultät für Chemie der Philipps-Universität Marburg

vorgelegt von
Diplombiologin Katrin Schenk
geboren in Freiburg i. Br.

Februar 2015

Vom Fachbereich Chemie der Philipps-Universität Marburg (Hochschulkennziffer 1180) als Dissertation am _____. _____. _____ angenommen.

Erstgutachter:	Prof. Dr. Peter L. Graumann Fachbereich Chemie, Philipps-Universität Marburg
Zweitgutachter:	Prof. Dr. Martin Thanbichler Fachbereich Biologie, Philipps-Universität Marburg
Tag der Disputation:	27.03.2015

Die Untersuchungen zur vorliegenden Dissertation wurden in der Zeit vom April 2011 bis Dezember 2014 unter der Leitung von Herrn Prof. Dr. Peter L. Graumann an der Albert-Ludwigs-Universität Freiburg und der Philipps-Universität Marburg durchgeführt.

EIDESSTATTLICHE ERKLÄRUNG

(gemäß § 10, Abs. 1 der Promotionsordnung der Mathematisch-Naturwissenschaftlichen Fachbereiche und des Medizinischen Fachbereichs für seine mathematisch-naturwissenschaftlichen Fächer der Philipps-Universität Marburg vom 15.07.2009)

1. Ich erkläre hiermit, dass ich die vorliegende Arbeit ohne unzulässige Hilfe Dritter und ohne Benutzung anderer als der angegebenen Hilfsmittel angefertigt habe. Die aus anderen Quellen direkt oder indirekt übernommenen Daten und Konzepte sind unter Angabe der Quellen gekennzeichnet. Insbesondere habe ich hierfür nicht die entgeltliche Hilfe von Vermittlungs- beziehungsweise Beratungsdiensten (Promotionsberater oder anderer Personen) in Anspruch genommen. Niemand hat von mir unmittelbar oder mittelbar geldwerte Leistungen für Arbeiten erhalten, die im Zusammenhang mit dem Inhalt der vorgelegten Dissertation stehen.
2. Die Arbeit wurde bisher weder im In- noch im Ausland in gleicher oder ähnlicher Form einer anderen Prüfungsbehörde vorgelegt.

Ort, Datum	Katrin Schenk

Zusammenfassung

Die Verdopplung des Chromosoms ist ein entscheidender Schritt des bakteriellen Zellzyklus. Um die Anzahl der Chromosomen pro Zelle konstant zu halten, muss dieser Prozess streng reguliert werden. Die Replikation wird am Replikationsursprung durch das hochkonservierte Initiationsprotein DnaA initiiert. Dazu bindet DnaA an spezifische DNA-Sequenzen in der Ursprungsregion und bildet einen helikalen Nukleo-Protein-Komplex, der die lokale Aufwindung des Doppelstrangs herbeiführt. Dies muss kontrolliert geschehen, um eine Initiation zu einem falschen Zeitpunkt zu vermeiden. Für *Bacillus subtilis* sind zwei Regulationsproteine bekannt, YabA und Soj (ParA). YabA erfüllt zwei Funktionen: Zum einen wirkt es als Anti-Kooperativitäts-Faktor für DnaA und zum anderen rekrutiert es, vermittelt duch eine Interaktion mit DnaN, DnaA und die Replikationsmaschinerie. Das Protein Soj hingegen kann ATP-abhängig ein Dimer bilden und als solches fördernd auf die DnaA-Aktivität wirken, während es in seiner ADP-gebundenen Form als Monomer vorliegt und am Ursprung die Ausbildung der rechtsgängigen DnaA-Helix verhindert.

Die vorliegende Arbeit zeigt, dass die Lokalisation von YabA im Bezug auf den Replikationsursprung und die Replikationsmaschinerie einem ähnlichen Muster folgt, wie es für DnaA bekannt ist. Dabei stellt sich heraus, dass YabA hauptsächlich am Replisom, aber auch am Ursprung lokalisieren kann.

Unter Zuhifenahme von FRAP (*fluorescence recovery after photobleaching*) konnte ich *in vivo* zeigen, dass DnaA einen hohen Turnover am Ursprung und an der Replikationsmaschinerie hat, der im Bereich von nur wenigen Sekunden liegt. Des Weiteren verringert eine Deletion von *yabA* und *soj-spo0J* den Turnover von DnaA. YabA hingegen zeigt ein ähnliches Verhalten wie DnaA.

In einem zweiten Ansatz wurde Einzel-Molekül-Mikroskopie an lebenden Zellen durchgeführt. Die Untersuchung von DnaA-Einzelmolekülen bestätigt, dass es sich bei DnaA um ein sehr dynamisches Protein handelt, das für nicht mehr als wenige Millisekunden an seinen Bindestellen verweilt. Da DnaA auch als Transkriptionsfaktor wirkt, beinhalten diese Bindestellen nicht nur den Ursprung und die Replikationsmaschinerie, sondern auch mehrere über das ganze Chromosom verteilte Promotoren. Des Weiteren führt eine Deletion von *soj-spo0J* zu verkürzten Verweildauern, was im Einklang mit den FRAP-Daten steht. Im Gegensatz dazu verweilt eine DnaA-Variante, die eine Aminosäuresubstitution trägt, welche die ATPase-Aktivität und die Initiationsrate beeinträchtigt, deutlich kürzer. Folglich führen selbst geringe Unterschiede in der Verweildauer zu untypischen Initiationsfrequenzen. YabA-Einzelmoleküle hingegen sind statischer, was darauf hindeutet, dass DnaA und YabA nicht gemeinsam, als Komplex, die DNA scannen.

Erstaunlicherweise war für *E. coli*-DnaA eine Oszillation der DnaA-Moleküle zwischen den zwei Zellhälften zu beobachten. Die Diffusionskonstante und die Verweildauer ähnelten denen von *B. subtilis*-DnaA, was eine hohe Dynamik von DnaA Proteinen in zwei Bakterienspezies zeigt.

Die Beobachtung, dass *E. coli*-DnaA oszilliert, lässt weiterhin einen Mechanismus vermuten, bei dem ein regulatorisches Protein DnaA verfolgt und es von seinen Bindestellen löst, was zu dem beobachteten Muster führen könnte. Hohe Änderungsraten können vorteilhaft sein um viele regulatorische Impulse in die Entscheidung über eine Initation zu integrieren. In *B. subtilis* könnten die zwei Regulatoren YabA und Soj teilweise durch eine Stimulation der zeitlichen Änderungsrate von DnaA am Ursprung und an der Replikationsmaschinerie agieren.

Synopsis

An important step during the bacterial cell cycle is the duplication of the chromosome. This key process has to be tightly regulated to ensure that the number of chromosomes per cell remains constant. Chromosomal DNA replication is initiated at the origin of replication by the highly conserved initiator protein DnaA. DnaA binds to specific DNA sequences at the *oriC* region and initiates replication by forming a stable, helical right-handed nucleoprotein complex, which leads to local unwinding of the double-stranded DNA. To prevent untimely and overinitiation the initiation step is highly regulated. In *B. subtilis*, YabA and Soj (ParA) play major roles in regulating the initiation of replication. YabA functions as an anti-cooperativity factor of DnaA and furthermore tethers DnaA to the replication machinery. Soj, on the other hand, was shown to stimulate DNA replication in its dimeric form and to inhibit DnaA helix formation as a monomer.

This study reveals that the localization of YabA with respect to the origin of replication and the replication machinery is similar to the pattern previously observed for DnaA, indicating that YabA can localize at the origin of replication but that it is primarily localized at the replisome.

By using *in vivo* fluorescence microscopy after photobleaching (FRAP), I could show that the exchange rates of DnaA molecules bound to the origin of replication or at the replication machinery are similar and in the lower second range. Furthermore, a deletion of *yabA* or *soj-spo0J* significantly decreased the turnover of DnaA. In addition, YabA was shown to have similar recovery half-times as DnaA.

As a second approach single molecule microscopy in live cells was applied. The study of DnaA at the single molecule level reveals that DnaA is indeed a highly mobile protein and does not rest for more than a few hundred milliseconds at its individual binding sites. Because DnaA also acts as transcription factor at several sites throughout the chromosome, these sites also include several promotor sites, and not only *oriC* or the replication forks. Furthermore, a deletion of *soj-spo0J* increased the residence time of DnaA molecules, which is in accordance with results obtained in FRAP experiments. On the contrary, a DnaA variant carrying a single amino acid substitution, which renders it impaired in ATPase activity and leads to an underinitiation of replication, displays an even shorter residence time than wild type DnaA. Therefore, even mild differences in residence time can lead to aberrant initiation frequencies. YabA molecules, on the other hand, tend to be significantly more static, indicating that DnaA and YabA are not scanning together over the chromosome.

Strikingly, *E. coli* DnaA showed an oscillation of DnaA molecules between the two cell halves and a diffusion constant and residence time similar to *B. subtilis* DnaA, revealing that DnaA is highly dynamic in two different bacterial species. Subsequently, the observation that DnaA in *E. coli* oscillates might support the notion of a mechanism in which DnaA is chased by a slower regulatory protein that upon interaction induces the release of DnaA from its binding

site, thereby inducing the alternating pattern of DnaA. Fast turnover rates may be advantageous to integrate many regulatory inputs into the decision whether to initiate or not. In *B. subtilis* the two regulators YabA and Soj could act in part through a stimulation of DnaA turnover at *oriC* and the replication machinery, thereby regulating the initiation of replication.

Contents

1. Introduction

1.1. The cell cycle of *Bacillus subtilis*

Bacillus subtilis is a Gram-positive, endospore forming rod shaped bacterium. It contains a single circular chromosome with a size of approximately 4.2 Mbp encoding around 4100 genes[1]. Its growth can be divided into an exponential and a stationary phase.
During exponential phase nutrition is avaible and the *B. subtilis* cells proliferate. DNA replication is initiated at a unique site within the chromosome, the origin of replication (figure 1 a). Once initiation has occurred, the DNA replication proceeds in a bidirectional manner (figure 1 b). During ongoing replication the duplicated origin regions are segregated towards the opposite cell poles, while the replisome remains in the cell center (figure 1 c). As soon as the active replication forks reach the terminus region, the replisome disassembles (figure 1 d). Once the division plane is free of DNA, the cell divides by binary fission (figure 1 e).

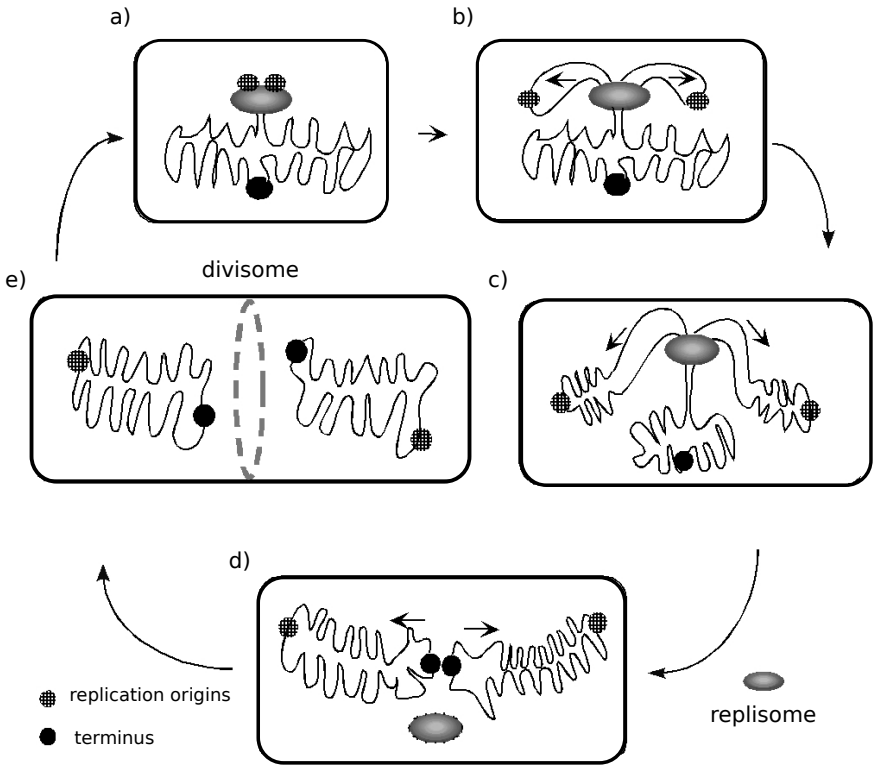

Figure 1: Cell cycle of *B. subtilis*.
Schematic display of the replicative cell cycle of *B. subtilis*. Replication starts at the origin of replication (a) and proceeds in a bidirectional manner (b). During ongoing replication the origin regions are segregated towards opposite cell poles, while the replisome stays in the cell center (c). Once the replication forks reach the terminus region, the replisome disassembles (d) and cell division occurs (e). Figure adapted from Soufo *et al.*[2].

Upon high nutrient availability, *B. subtilis* can, like *E. coli*, grow with overlapping replication cycles. Newly divided cells thus inherit active replication forks on partially duplicated chromosomes. The initiation of replication in these cells occurs at multiple origins simultaneously[3].
The entry into stationary phase is triggered upon nutrient deprivation. Cells stop dividing and alternative genetic programs are pursued.
One of them is the formation of a specialized, metabolically dormant cell, a so-called endospore. This spore is resistant to extreme temperatures, desiccation and radiation. An asymmetric cell division, separating the cell in a smaller and a bigger compartment, termed forespore and mother cell, respectively, mark the physiological entry point into sporulation. The interplay of sequentially activated sigma factors in the two compartments drive the differentiation of the forespore into a spore, which is finally released upon lysis of the mother cell.
Alternatively, upon activation of the transcription factor ComK, *B. subtilus* cells can become naturally competent. In competent cells a complex DNA uptake machinery is assembled at the cell pole. It mediates the uptake of external DNA that can be either integrated into the chromosome via homologous recombination or degraded to serve as nutrient source.

1.2. Initiation of DNA replication

Doubling of the genome is an essential and important event for all cells during their cell-cycle. In all three domains of life the initiation of DNA replication is triggered at specialized genomic regions (origin of replication) through highly conserved initiator proteins. Upon binding of the initiator proteins the double-stranded DNA in the origin region is unwound and a so-called pre-replication complex (pre-RC) is formed. Subsequently the replication machinery is recruited and DNA replication commences. A more detailed account of this process is given in the following sections.

1.2.1. Initiation of DNA replication in *E. coli*

The Gram-negative γ-proteobacterium *Escherichia coli* serves as a model organism for the initiation of DNA replication in bacteria. *E. coli* cells contain a single circular chromosome with an unique origin of replication, *oriC*. The AAA+ (ATPases associated with diverse cellular activities) protein DnaA is the initiator of DNA replication, which is highly conserved in bacteria.
DnaA binds specifically to 9-nucleotide long DNA sequences (5'-TTATNCACA) inside the *oriC* region, the so-called DnaA boxes[4;5]. Three tandem repeats of AT-rich 13-mer sequences and an AT-cluster form the DNA unwinding element (DUE), the site inside the *oriC* region where the double strand opening occurs[6]. The DnaA protein is able to bind to ADP and ATP, but it can only initiate replication in its ATP-bound form[7]. The DnaA protein has different affinities to the DnaA boxes, due to nucleotide mismatches to the consensus sequence, low affinity sites can only be bound by DnaA in its ATP-bound state. Besides DnaA also the integration host

factor (IHF) and the DnaA initiator-associating protein (DiaA) play a crucial role during the initiation of DNA replication[8;9]. With the help of IHF and DiaA, DnaA-ATP can multimerize in a cooperative manner along the DNA thereby forming a right-handed helix[10]. The so formed nucleoprotein complex stimulates double strand opening in the AT-rich sequence, a process called open-complex formation[11].

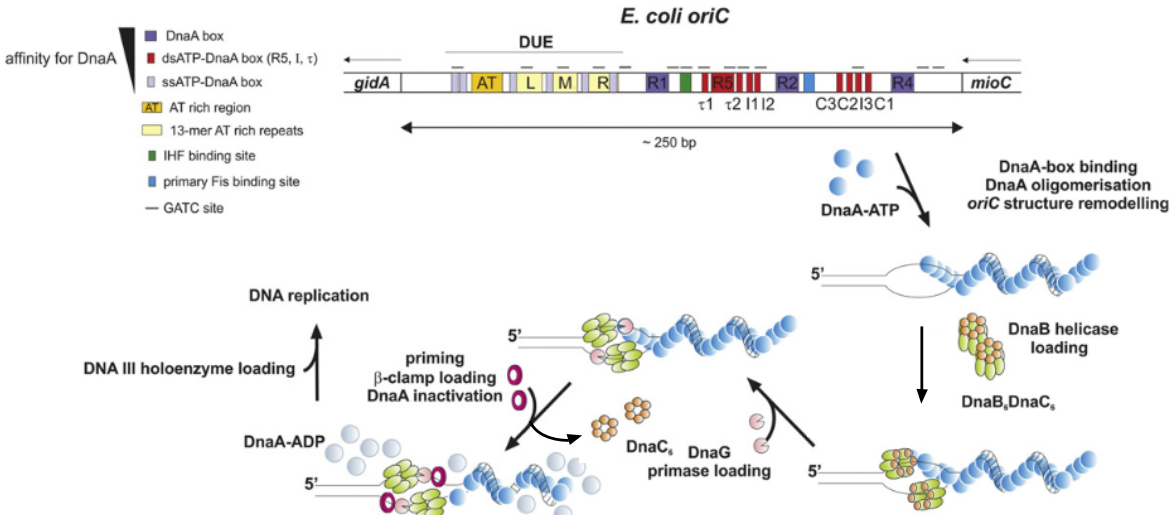

Figure 2: Fundamental steps during the initiation of DNA replication in *E. coli*.
Schematic display of the fundamental steps during initiation of replication in *E. coli*. The initiation process starts by binding of ATP-DnaA to DnaA boxes inside the origin of replication. DnaA multimerizes into a nucleoprotein complex resulting in doublestrand opening at the DNA unwinding element (DUE). The replicative helicase DnaB together with the helicase loader DnaC are loaded on the unwound DNA, forming the pre-priming complex. Then the primase DnaG associates and upon priming DnaC is released and DnaB expands the unwound part of the DNA. In a next step, the β-clamp and subsequently the DNA polymerase III holoenzyme are loaded and DNA replication commences. Figure modified after Donczew *et al.*[12].

The emerging single stranded region is stabilized by DnaA and by the single-stranded DNA-binding protein (SBB)[13]. The replicative helicase DnaB forms a stable complex with the helicase loader DnaC ($DnaB_6$–$DnaC_6$), which inhibits the helicase and ATPase activity of DnaB[14]. Two such complexes, one for each strand, are recruited into the opened double strand via interaction with DnaA, forming the prepriming complex[15;16].

Upon association of the primase DnaG, small RNA primers are synthesized and DnaC and DiaA are released from the *oriC* region[15;17;18]. The helicase DnaB, now free from its inhibitor DnaC, starts unwinding of the double stranded DNA and interacts with a dimer of the DNA polymerase III holoenzyme, which binds to the ends of the previously synthesized primers.

Replication proceeds in a bidirectional manner. At each replication fork leading and lagging strand synthesis occur through an interplay of the helicase DnaB, a dimer of the DNA polymerase III holoenzyme and the primase DnaG, which continuously synthesizes the primers needed for

Okazaki fragment synthesis[19].

1.3. The DnaA protein

DnaA is the conserved initiator of bacterial DNA replication and belongs to the family of AAA+ proteins. It is capable of ATP and ADP binding, but is considered active in its ATP-bound form[7]. It displays an intrinsic ATPase activity. The functional, eukaryotic homolog to DnaA is the origin recognition complex (ORC, consisting of six subunits, Orc1–Orc6).
Based on biochemical studies, *E. coli* DnaA can be divided into four functional domains, responsible for the following functions[20;21]:
Domain I (amino acids 1–90) is responsible for protein-protein interactions[22]. It mediates self-oligomerization of DnaA as well as binding of DnaA to the helicase DnaB and the DnaA-binding protein DiaA[9;16;23].
Domain II (amino acids 91–130) is a non-conserved linker domain separating the interaction domain I and the AAA+ domain III[16;23]. Functional fluorescence sandwich fusions contained the fluorophor inside domain II[24;25].
Domain III (amino acids 131–346) is the highly conserved AAA+ domain. It contains the following motifs: the Walker A/B, the sensor I/II and the box VII motif. ATP binding and hydrolysis as well as DnaA protomer oligomerization are mediated by this domain[10]. Furthermore, a role in single-stranded (ss) DNA binding was reported[26].
Domain IV (amino acids 347–467) contains a helix-turn-helix and a basic loop motif responsible for double-stranded (ds) DNA binding[27]. Furthermore a short amphipathic helix, located between domain III and IV, mediates interaction of DnaA with membrane lipids[28].

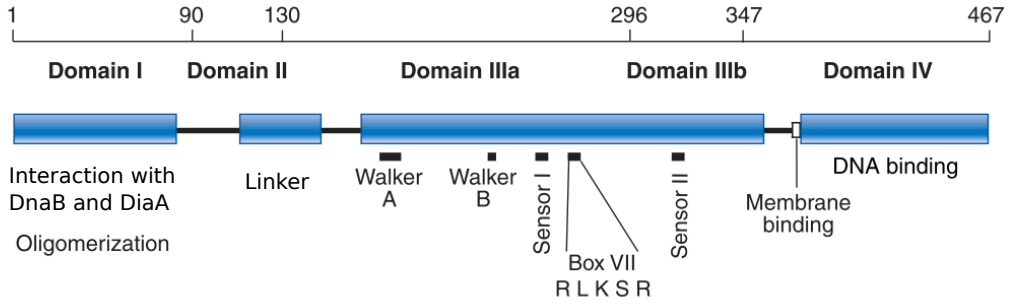

Figure 3: Overview of the functional domains of *E. coli* DnaA.
Scheme displaying the four functional domains of DnaA (blue boxes). Domain I (amino acids (aa) 1–90) interacts with the helicase DnaB and the regulator DiaA and mediates self-oligomerization. Domain II (aa 91–130) is a non-conserved linker domain. ATP binding and hydrolysis is executed through domain III (aa 131–347), which is the highly conserved AAA+ domain, whereas the helix-turn-helix motif in domain IV (aa 348–467) mediates dsDNA binding. Figure modified after Kaguni 2006[29] .

Besides its function as the initiator of DNA replication, the DnaA protein serves as a sequence specific transcription factor[30]. In *B. subtilis* 56 genes in 20 operons are regulated by DnaA[31]. One

example of the genes regulated is *dnaA* itself, which controls its own transcription by a negative feedback loop *dnaA*[32].
M. Eisemann biochemically and physiologically characterized the effect of several single amino acid substitutions, which were introduced into the *B. subtilis* DnaA protein[33].
Analysis of the effect of the amino acid substitution A163V revealed a loss of ATP-binding and ATPase capacity aside from residing as a constitutive multimer. Moreover cells expressing YFP-DnaAA163V overinitiated replication.
Exchanging glutamic acid 183 into glutamine resulted in a 2-fold reduced ATP-binding and 6–7-fold reduced ATPase activity, which yielded a reduced oligomerization capacity of the protein[33]. Furthermore cells expressing YFP-DnaAE183Q in a merodiploid strain displayed highly elongated cells[33].
Substitution of R260A resulted in a 1.5-fold reduced ATP-binding and a 2-fold reduced ATPase activity compared to wild type DnaA. Notably, *B. subtilis* cells expressing YFP-DnaAR260A were significantly shorter than wild type cells[33].
The amino acid substitution R387C renders DnaA DNA binding deficient[33].

1.4. Organization of the origin region

The origin of replication is the starting point of DNA replication. Although the structure of the origin regions may vary between different bacterial species, they all share the same basic features[34]. A cluster of DnaA boxes, an AT-rich region, where the local DNA unwinding occurs and additional DNA sequences, which are recognized by regulatory proteins.
The minimal functional *oriC* region of *E. coli* consist of around 250 bps (figure 4)[35]. It contains five so-called R-boxes, conserved 9-mer DNA sequences (5'-TTATCCACA-3'), of which R1, R2 and R4 display a high affinity for DnaA (figure 4, blue triangles)[36;37]. Further investigations identified six additional 9-mer and two 6-mer sequences, showing a low affinity for DnaA, termed C1-3, I1-3 and τ1, τ2, respectively (figure 4, purple triangles)[23;38]. Hence, AT-rich sequences, the so-called DUE element, are a crucial part of each *oriC* region. It consists of three 13-mer AT-rich repeats (5'-GATCTnTTnTTTT-3')[6;23]. In addition binding sites for regulatory proteins, like Fis and IHF are part of the *E. coli oriC* region[8;39]. GATC sequences, the target site for the DAM methylase and the regulatory protein SeqA, partially overlap with DnaA low affinity sites (figure 4, black squares)[40].
The high affinity sites R1, R2 and R4 are permanently bound by DnaA molecules,[40] and serve as nucleation centers for binding of DnaA to the proximal low affinity sites[41]. At the time of initiation, the transition between origin recognition and the pre-replication complex occurs rapidly, once ATP-DnaA binds to the low affinity sites[40;41]. Two DNA bending proteins modulate the availability of these sites. Fis is associated with the *oriC* region during most of the cell cycle, inhibiting pre-RC assembly, until it is displaced by DnaA prior to initiation[42]. IHF binding as well as DiaA stimulate pre-RC assembly. Directly after initiation of replication the SeqA protein

binds to hemimethylated GATC sites, partially overlapping with low affinity DnaA boxes and thereby inhibits untimely pre-RC assembly[40].

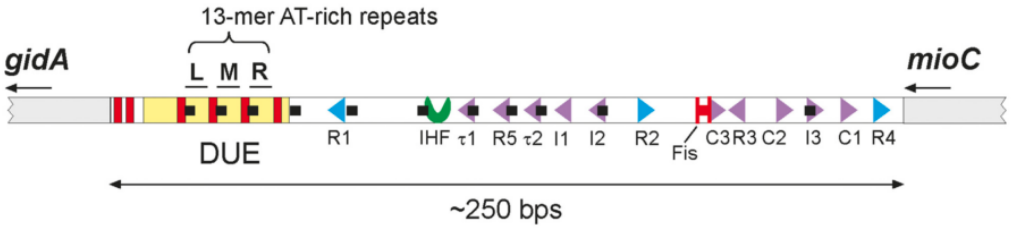

Figure 4: Overview of the organization of the *E. coli* minimal origin region.
Schematic display of the *oriC* region of *E. coli* consisting of high (blue triangles) and low (purple triangles) affinity DnaA binding sites, a DUE element and recognition sequences for regulatory proteins (Fis, red and IHF, green). Figure adapted from Wolański *et al.*[34]

The origin region of the *B. subtilis* chromosome contains two DnaA box regions, a larger one (*oriC1*) upstream of the *dnaA* gene and a smaller one (*oriC2*) downstream (figure 5)[43]. The *oriC1* region, which can be further subdivided into *incA* and *incB*, contains three AT-rich 16-mers (figure 5, gray squares), three DnaA boxes matching the consensus sequence (5′-TTATCCACA-3′, figure 5 black arrows), six boxes with one and five boxes with two mismatches (figure 5 hatched and empty arrows, respectively)[44]. The *oriC2* region, also called *incC*, contains an AT-rich 27-mer, one DnaA box matching perfectly the consensus sequence, two DnaA boxes with one and four with two mismatches and the DUE[44;45].
Both DnaA box regions are required for replication initiation[46].
Regulation of the initiation of replication through Spo0A, the master transcriptional regulator of sporulation, will be discussed in section 1.5.6.

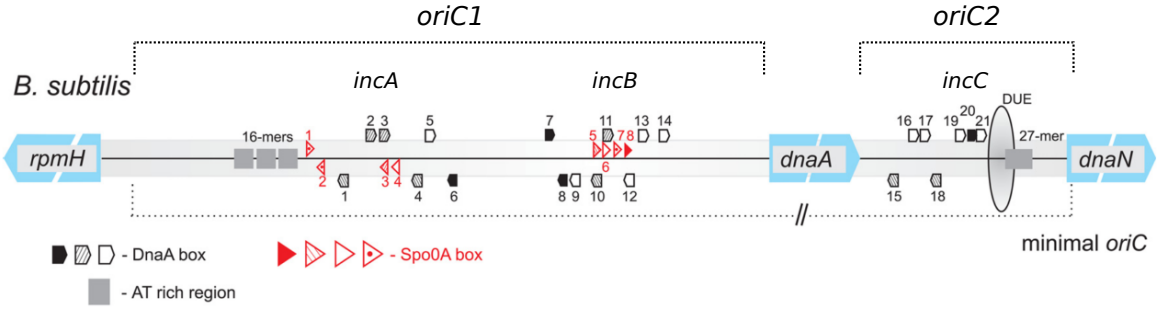

Figure 5: Overview of the organization of the *B. subtilis* origin region.
Schematic display of the biparted *B. subtilis oriC* region. gray squares, AT-rich sequences; black arrows, DnaA boxes perfectly matching the consensus sequence; hatched arrows, DnaA boxes with one mismatch; empty arrow, DnaA boxes with two mismatches. Spo0A binding sites are shown in red. Figure modified after Wolański *et al.*[47]

1.5. Regulation of the initiation of DNA replication

Regulation of DNA replication occurs mainly at the initiation step. The timing of replication initiation during the cell cycle must be precisely coordinated, to avoid untimely- or overinitiation of replication, which would alter the cellular DNA concentration. Regulation of the initiation of DNA replication is best understood in the Gram-negative bacterium *E. coli*. But based on the highly conserved initiator protein DnaA similar regulatory strategies for other bacterial species are likely.

Regulatory mechanisms either directly target the initiator DnaA or block its access to the origin region. This following section gives some examples on known regulatory mechanism in *E. coli* and *B. subtilis*.

1.5.1. SeqA mediated origin sequestration

Inside the *oriC* region of the *E. coli* chromosome the specific DNA sequence GATC is found with high frequency[48;49]. GATC is the recognition site for the DNA adenine methylase (Dam), an enzyme responsible for methylating the adenine nucleotide included in its recognition sequence. As DNA replication proceeds in a semi-conservative manner, hemimethylated GATC sites emerge. These are preferentially bound by a protein named SeqA (sequestration protein)[50]. SeqA binding regions partially overlap with low affinity DnaA boxes, bound SeqA thus prevents ATP-DnaA from binding to these boxes and hence inhibits initiation of DNA replication[50 40 51]. Furthermore a SeqA bound GATC sequence is inaccessible for Dam methylation, resulting in a hemimethylated state of the *oriC* region for around one third of the cell cycle[52;53].

A further GATC site resides within the promotor region of the *dnaA* gene lying downstream of the origin of replication, which bound by SeqA leads to a block of transcription of the initiator of DNA replication[53].

Deletion of *seqA* results initiation asynchrony in the prescence of multiple origins during rapid growth.

1.5.2. Regulatory inactivation of DnaA

Immediately before initiation the cellular ATP-DnaA level increases[54]. To prevent untimely reinitation *E.coli* uses a process called RIDA (regulatory inactivation of DnaA)[55]. The active ADP-Hda protein, which is stably bound to the sliding clamp (DnaN) of the DNA polymerase III holoenzyme, interacts with the AAA+ domain of the DnaA protein and thereby stimulates the ATP-hydrolysis of DnaA[56;57]. As Hda is bound to DnaN, which localizes to the replication machinery, RIDA supposedly targets ATP-DnaA bound to DNA, representing a replication-coupled negative feedback loop[49;58].

1.5.3. Titration of DnaA – the *datA* locus

Around 300 high affinity DnaA boxes are distributed throughout the *E. coli* chromosome a[59]. Five of them are clustered with 25 low affinity boxes to form the *datA* (DnaA titration) site[60;38]. The 1 kb big locus is located 450 kb away from *oriC* and is replicated towards the end of the sequestration period in fast growing cells[61]. This site is capable of binding up to 60 DnaA molecules and probably functions as a sink, titrating DnaA away from *oriC*[61;38]. A deletion of *datA* leads to extra initiations and is especially deleterious during rapid growth[61].
On the *B. subtilis* chromosome six similar DNA sequences, termed DnaA-box cluster (DBC), were detected, which when deleted led to overinitation of replication[62].
In addition an IHF dependent ATP-hydrolysis of ATP-DnaA molecules bound to the *datA* locus was reported (DDAH, *datA*-dependent ATP-DnaA hydrolysis)[63], providing further means of DnaA regulation.

1.5.4. DnaA reactivating sequences

Only ATP-DnaA can initiate DNA replication[7]. The nucleotide exchange from ADP-DnaA to ATP-DnaA is promoted by two DNA sequences positioned half way towards the terminus region on the left and right arm of the chromosome[64]. On this DARS (DnaA reactivating sequence) sequences multiple ADP-DnaA molecules form a complex which facilitates the release of ADP. Apo-DnaA molecules are released from the DARS sequence, probably based on their reduced complex binding capacity. Due to higher cellular ATP than ADP-levels the Apo-DnaA rapidly binds to ATP and can initiate replication[64].
Recently Kasho *et al.* showed that the proteins Fis and IHF are required for DARS2 activation *in vitro*[65]. Furthermore recruitment of Fis and IHF to the DARS2 site occurred in a growth phase and cell-cycle-dependent manner, respectively[65].

Most mechanisms to regulate initiation of replication described so far are limited to *E. coli*. For the Gram-positive bacterium *B. subtilis* no homologues for SeqA or Hda are described. Although the initiator is highly conserved in eubacteria, the means to regulate it are not. The following examples give a brief insight into regulation of initiation in *B. subtilis*.

1.5.5. Autoregulation of *dnaA* transcription

In *B. subtilis* the initiator of DNA replication DnaA is encoded in an operon together with DnaN, the β-clamp of the DNA III polymerase. The promotor region of this operon contains DnaA boxes. For *B. subtilis*, as for *E. coli*, an autoregulation of *dnaA* transcription was shown[32]. Upon overexpression of DnaA a downregulation in the transcription of the *dnaA-dnaN* operon was observed, finally resulting in induction of the SOS response, probably due to low DnaN levels[32].

1.5.6. Binding of Spo0A to *oriC* inhibits initiation of replication

Cells committed to sporulation require exactly two copies of the chromosome, one for the mother cell and one for the forespore, respectively. Spo0A-P is the master transcriptional regulator of sporulation and inhibits initiation of replication by direct binding to Spo0A boxes partially overlapping with DnaA boxes in the *oriC* region (figure 5, red arrows)[66;67]. Furthermore Spo0A controls the transcription of SirA (sporulation inhibitor of replication A), a protein inhibiting the initiation of replication in cells committed to sporulation by direct binding to DnaA domain I[68;69;70].

In vegetative cells the intrinsically unstable protein Sda (suppressor of *dnaA1*) inhibits initiation of sporulation by binding to KinA/B and thereby preventing the phosphorylation of Spo0A[71]. DnaA induces transcription of Sda, which is actively proteolysed, opening a small window of opportunity to commit to sporulation before initiation of replication occurs[72].

1.5.7. YabA inhibits cooperativity at *oriC* and tethers DnaA to the replication machinery

YabA is a small protein capable of binding to the replication initiator DnaA and the sliding clamp of the DNA polymerase DnaN[73]. Deletion of *yabA* results in overinitiation of replication whereas overproduction of YabA inhibits replication initiation, whence YabA is reported to be a negative regulator of replication initiation in *B. subtilis*[74;73].

Based on localization studies a spatially sequestration model was proposed, in which YabA tethers DnaA to the replication machinery and thereby inhibits untimely DnaA binding to the *oriC* region[2].

Overproduction of DnaN, however, resulted in a YabA-dependent overinitiation, indicating an antagonizing effect of DnaN on DnaA inhibition by YabA[74;75]. Furthermore YabA was reported to reduce the ATP-dependent cooperative binding of *oriC* DNA by DnaA and to inhibit DnaA helix formation *in vitro*[75;76].

1.5.8. Regulation of DnaA activity by Soj/Spo0J

Soj and Spo0J are the *B. subtilis* orthologues of ParA and ParB, which are plasmid-partitioning proteins[77]. Soj is an ATPase that dimerizes upon binding to ATP, which renders it capable of unspecific DNA binding[78].

Soj was reported to act as a molecular switch for DnaA activity, because it inhibits DnaA in its ADP or Apo-form while ATP-Soj stimulates DnaA activity upon dimerization[79]. The conversion from the dimeric to the monomeric state is controlled by Spo0J, which stimulates the weak intrinsic ATPase activity of Soj[79]. Recently Scholefield *et al.* identified the underlying mechanism of DnaA inhibition by monomeric Soj. They were able to show a direct interaction of Soj with the AAA+ domain of DnaA, leading to the inhibition of DnaA helix formation[80].

1.6. YFP-DnaA localizes in a cell-cycle-dependent manner

So far localization studies of DnaA have been performed in the Gram-negative bacterium *E.coli*[24;25] and the Gram-positive bacteria *Mycobacterium tuberculosis*[81] and *B. subtilis*[2].
The *E.coli* DnaA sandwich fusions were reported to either localize as discrete foci[24], colocalizing with the *oriC* region or the *datA* locus or in a helical pattern along the long axis of the cell[25].
In *M. tuberculosis* DnaA-GFP localized as foci at midcell or at the cell poles, showing a similar localization pattern to cardiolipin-enriched regions[81].

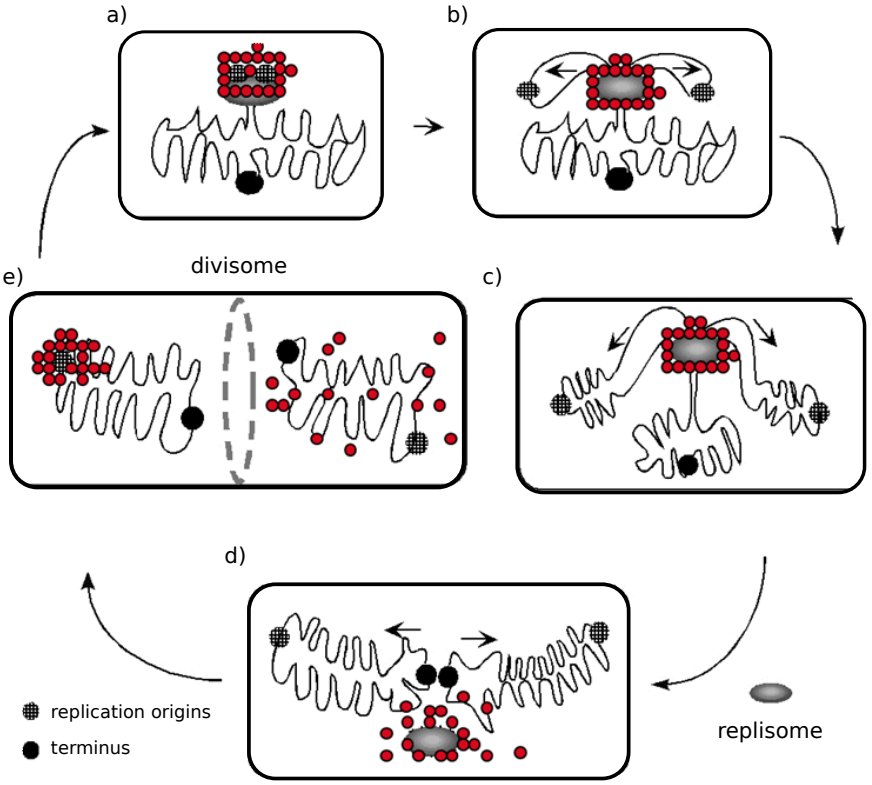

Figure 6: Cell-cycle-dependent localization of *B. subtilis* YFP-DnaA.
Schematic display of the cell-cycle-dependent spatial sequestration of DnaA in *B. subtilis*. Red points represent YFP-DnaA.
During initiation of replication, YFP-DnaA localizes at the origin of replication (a). Replication proceeds in a bidirectional manner. During ongoing replication the origin regions are segregated towards opposite cell poles, while the replisome and YFP-DnaA (through interaction with YabA) remain in the cell center (b, c). Once the replication forks reach the terminus region, the replisome disassembles (d) and YFP-DnaA is free to initiate a new round of DNA replication (e). Figure adapted from Soufo *et al.*[2].

Localization of a functional YFP-DnaA fusion in *B. subtilis* displayed a cell-cycle dependent spatial sequestration of DnaA[2]. During most of the cell cycle a colocalization of DnaA with DnaX, the τ-subunit of the replication machinery, was observed[2]. A colocalization of YFP-DnaA

with the origin, using repressor/operator system to indirectly label the *oriC* region, occurred during early and late stages of the cell-cycle[2].
Deletion of *yabA* was reported to cause overinitiation of replication[82;83]. Localization of YFP-DnaA in a *yabA* deletion strain revealed a change in the YFP-DnaA localization pattern, now YFP-DnaA localizes in multiple foci, which colocalize with the origin in 95% of all cases[2]. Similar results were obtained for YFP-YabA fusions impaired in DnaA or DnaN interaction[2]. The existence of a higher-molecular weight complex consisting of DnaA and YabA was reported[2].
Based on these results a model for the localization of YFP-DnaA was proposed (figure 6). At the beginning of the cell cycle, during initiation of replication, YFP-DnaA colocalizes with the replication origin. Once replication starts and the origin regions are segregated towards opposite cell poles, YFP-DnaA remains at the replication machinery in the cell center, through interaction with YabA. Thereby DnaA is spatially sequestered away from the origin region. Once replication reaches the terminus region and the replisome disassembles, YFP-DnaA is released from the replication machinery and is free to bind to the *oriC* region and initiate another round of DNA replication.

1.7. Aims of research

DNA replication is a central process during the cell cycle of each species. Asynchronous initiation events can lead to severe growth defects or even cell death. Replication is mainly regulated at the initiation step. In different species different regulatory mechanism have evolved to ensure that initiation occurs only once per cell cycle.
For *B. subtilis* YabA, a protein capable of interacting with DnaA and the sliding clamp (DnaN) of the DNA polymerase III holoenzyme, was reported to be a negative regulator . YabA is thought to tether DnaA to the replication machinery directly after initiation, thereby preventing DnaA from reinitiation through spatially sequestering it from the origin region. Recently YabA was shown to inhibit cooperativity of DnaA at *oriC*. Localization studies on YabA revealed a predominant colocalization of YFP-YabA with the replication machinery.
During this work we were interested in localizing YFP-YabA with respect to the origin of replication and the replication machinery and to investigate a possible colocalization with the origin region and its extend.
Deletion of *yabA* or *soj-spo0J* are reported to overinitiate replication to some extent. Although previously reported to be lethal, we aimed at generating a *soj-spo0J yabA* triple deletion and investigating its effect on cell growth, cell length and initiation of replication.
Localization studies on DnaA in *B. subtilis* revealed a cell-cycle-dependent localization of YFP-DnaA. Discrete foci were reported to either colocalize with the origin of replication or the replication machinery.
We were interested in the dynamics underlying this observed localization pattern. Using time lapse microscopy we studied the localization of YFP-DnaA with respect to the origin of replication.
Furthermore we used FRAP (Fluorescence recovery after photobleaching) and single molecule microscopy to investigate the recovery half-time, the diffusion coefficient and the average residence time of YFP-DnaA molecules. Using the same methods we analyzed the behavior of YFP-DnaA upon deletion of *yabA*, *soj-spo0J* and *yabA soj-spo0J* and in strains harboring single amino acid substitutions in the YFP-labeled DnaA protein.
We then extended our research to investigating the dynamics of YFP-YabA, using the same methods.
The DnaA protein is highly conserved among bacterial species. *E. coli* and *B. subtilis* DnaA share a sequence similarity of 63%. Using single molecule microscopy we compared dynamics of YFP-labeled DnaA proteins of *B. subtilis* and *E. coli*.

2. Material and methods

2.1. Material

2.1.1. Chemicals and kits

Chemicals used in this work were ordered from Carl Roth GmbH and Co (Karlsruhe), AppliChem GmbH (Darmstadt) and Sigma-Aldrich Chemie GmbH (München).
Enzymes and DNA ladders were purchased from New England Biolabs GmbH (Frankfurt). Prestained Protein ladder was obtained from Thermo Scientific (Schwerte).
Kits for plasmid extraction were supplied by the following companies: Zymo Research (Freiburg) *ZR Plasmid Miniprep^{TM}-Classic*, PEQ-lab (Erlangen) *peqGOLD Plasmid Miniprep Kit I* and VWR (Darmstadt) Omega *E.Z.N.A ® Plasmid DNA Mini Kit I*.
Kits to purify nucleic acids were purchased from Qiagen. For PCR purification the *QIAquick® PCR Purification Kit* was used and for gel extraction the *QIAquick® Gel Extraction Kit*.

2.1.2. Media and supplements

Table 1: List containing antibiotics and their concentrations used in this work

Antibiotic	Abbreviation	Stock solution	Final concentration
Ampicillin	amp	100 mg/ml in $_{dd}H_2O$	100 µg/ml
Chloramphenicol	cm	50 mg/ml in 50% EtOH (v/v)	5 µg/ml
Spectinomycin	spec	25 mg/ml in 50% EtOH (v/v)	100 µg/ml
Kanamycin	neo	10 mg/ml in $_{dd}H_2O$	10 µg/ml
Tetracyclin	tet	10 mg/ml in 50% EtOH (v/v)	5 µg/ml
Lincomycin	lin	25 mg/ml in 50% EtOH (v/v)	25 µg/ml
Erythromycin	erm	4 mg/ml in 100% EtOH	1 µg/ml
Zeocin		20 mg/ml in $_{dd}H_2O$	20 µg/ml

E. coli and *B. subtilis* strains were cultivated in Luria-Bertani (LB) medium (Carl Roth) and on LB agar (Carl Roth) plates. For sterilization purposes the growth media was autoclaved for 30 min at 121 °C and 2 bar.
Media and agar were supplemented with the appropriate antibiotic (concentrations listed in table 1). To induce expression of genes under the xylose promotor a final concentration of 0.1 or 0.5% xylose (stock: 50% (w/v)) was used. Transcription was inhibited using 200 µg/ml rifampicin.

B. subtilis cells that were subsequently used for fluorescence microscopy were cultured in $S7_{50}$ (table 3) or M9 minimal medium (table 2). Sterilization was accomplished by using sterile filtration (pore size 0.2 µm; filters: Sarstedt, Numbrecht).
Transformation of *B. subtilis* cells with plasmids encoding a spectinomycin resistance was performed on agar plates with difco sporulation media (DSM, refer to table 3). Selection for Zeocin resistance was performed in low salt LB medium (ref. table 3).

Table 2: Media used to culture *B. subtilis* and *E. coli* strains

Media	**Composition**	**Final concentration**
M9 minimal medium	M9 5×stock solution	1×
	100×trace elements	1×
	Glucose	0.15% (w/v)
	$MgSO_4$	1 mM
	$CaCl_2$	100 µM
	$FeCl_3$	50 µM
	K-glutamat	0.1% (w/v)
Adjust pH to 7.0 with HCl		
M9 5×stock solution	Na_2HPO_4	238 mM
	KH_2PO_4	110 mM
	NH_4Cl	93 mM
	NaCl	43 mM
M9 100×trace elements	$MnCl_2$	0.5 mM
	$ZnCl_2$	1.25 mM
	$CuCl_2$	0.25 mM
	$CoCl_2$	0.25 mM
	Na_2MoO_4	0.25 mM

Table 3: Media used to culture *B. subtilis* and *E. coli* strains

Media	Composition	Final concentration
DSM medium	Nutrient broth (Roth)	0.8% (w/v)
	$MgSO_4 \times 7\ H_2O$	0.012% (w/v)
	KCl	0.1% (w/v)
	NaOH	0.5 mM
	Agar (Bacto)	1.5% (w/v)
Add sterile after autoclaving:		
	$Ca(NO_3)_2$	1 mM
	$MnCl_2$	0.01 mM
	$FeSO_4$	1 µM
$S7_{50}$ medium	10× $S7_{50}$ salts	1×
	100×$S7_{50}$ metals	1×
	Glucose	1% (w/v)
	K-glutamat	0.1% (w/v)
	casamino acids	0.004% (w/v)
10×$S7_{50}$ salts	MOPS	0.5 M
	$(NH_4)_2SO_4$	100 mM
	KH_2PO_4	50 mM
	adjust pH to 7.0 using KOH	
100×$S7_{50}$ metals	$MgCl_2$	0.2 M
	$CaCl_2$	70 mM
	$MnCl_2$	5 mM
	$ZnCl_2$	0.1 mM
	Thiamine-HCl	0.01% (w/v)
	HCl	2 mM
	$FeCl_3$	0.5 mM
Low salt LB	Tryptone	1%
	Yeast extract	0.5%
	NaCl	0.5%
Adjust pH to 7.5		

2.1.3. Oligonucleotides

Oligonucleotides were ordered from Sigma-Aldrich Chemie GmbH (Steinheim) or Metabion International AG (Planegg/Martinsried). They were adjusted to a concentration of 100 pmol/µl with $_{dd}H_2O$ and stored at -20 °C.

Table 4: List of oligonucleotides used during this study

Number	Sequence from 5′→3′	Amplicon (vector)
828	gca aaa gaa cag ctt ccg g	test-PCR Δ*yabA*
829	ctt ttt gaa tcg gaa cgt acg	
2582	gtg gga aaa atc ata gca att ac	test-PCR Δ*soj-spo0J*
2583	tga ttc tcg ttc aga caa aag	
1053	ctg **gaa ttc** tga ttc tcg ttc aga caa aag	*spo0J*
2132	atc **ggg ccc** gct tta tta gaa aac ctt cag	(pSG1164*cerulean*)
1036	ctg **gct agc** aga aag gag att cct agg atg	*yfp-yabA* (pDR111)
4737	cat **gca tgc** cta ttt ttt att taa gaa tga cag	
4131	cat **gct agc** gtt agg agg ata aaa atg aaa ttc	*dnaN* (pDP150)
2726	cat **gca tgc** cta ata ggt tct gac agg aag g	
4097	cat ggt aga tca ggt tat ctg atc	test-PCR *thrC* integration
4098	cat ctg aca ttt atg cac agc ag	

The recognition site of the restriction endonuclease is indicated in bold letters.

2.1.4. strains

All strains used during this study are listed in table 5 and table 6. Table 6 contains the strains constructed during this work. As wild type strain the *B. subtilis* PY79 was used[84].
In order to construct KS103, the last 500 base pairs (bp) of the *spo0J* gene were cloned into the pSG1164- *cerulean* (ref. section 2.1.5.1.) plasmid using the *Apa*I and *Eco*RI restriction sites. The fragment was amplified using primer 1053 and 2132. Transforming *B. subtilis* wild type cells with pKS103 resulted in the generation of strain KS124.
To express DnaN from an ectopic locus, the strain KS115 was constructed. Using primer 4131 and 2726 the complete *dnaN* gen including its ribosomal binding site (rbs) was amplified and cloned into pDP150 (ref. section 2.1.5.2.) via the *Sph*I and *Nhe*I restriction site. Transformation of wild type *B. subtilis* cells with the pKS115 resulted in KS19.

KS125 was obtained by transforming KS19 cells with pKS103. In order to make the influence of various DnaN levels on YFP-DnaA localization visible, competent cells of KS125 were transformed with the plasmid *pSG1729-yfp-dnaA* (ME1) resulting in KS21. To generate KS112, competent cells of KS19 were transformed with the plasmid *pSG1729-yfp-dnaA* (ME1). Analogously KS131 was constructed to investigate the effect of DnaN levels on the localization of YFP-YabA. To this end KS19 cells were transformed with chromosomal DNA of JDS190.
In order to study the localization behavior of YFP-YabA with respect to the origin of replication and the replication machinery, a strain with a CFP-tagged origin and an mCherry-tagged replication machinery were generated. To combine the CFP tagged origin with YFP-YabA, competent cells of PG208 were transformed with chromosomal DNA of JDS190, which gave rise to strain KS119. To change the chloramphenicol resistance to tetracylcline resistance, PG1159 was transformed pCm::Tet (ref. section 2.1.5.5.) resulting in strain KS114. In a final step cells of KS119 were transformed with chromosomal DNA of KS114 to obtain KS140.
To study the localization of the GTPase Era, wild type cells were transformed with the plasmid *pSG1164NLMV-era-mvenus* (PG2393) resulting in KS144.
To investigate the localization behavior of YFP-DnaA in different deletion backgrounds, the following strains were constructed. To analyze YFP-DnaA in a Δ*yabA* background, KS171 was generated transforming competent CDS2 cells with chromosomal DNA of KS183. To test for successful *yabA* deletion a test-PCR was performed. To study YFP-DnaA in a Δ*soj-spo0J* background, CDS2 cells were transformed with chromosomal DNA of AG1505, giving rise to KS175. Competent cells of KS171 were transformed with chromosomal DNA of AG1505 resulting in a strain carrying a triple deletion combined with YFP-DnaA (KS180).
For single molecule microscopy a strain with an ectopic copy of *yfp-dnaA* in a Δ*soj-spo0J* background was generated. To this end AHV2 cells were transformed with chromosomal DNA of AG1505 resulting in KS192.
To integrate the *soj-spo0J* deletion in the PY79 background, competent wild type cells were transformed with chromosomal DNA of AG1505 to give rise to KS182. Combining the *soj-spo0J* deletion with a *yabA* deletion resulted in a strain carrying a triple deletion. To generate the triple deletion (KS178), competent KS183 cells were transformed with chromosomal DNA of AG1505. To verify the deletions, test-PCRs were performed.
To construct a strain with YFP-YabA under an IPTG (isopropyl β- D -1-thiogalactopyranoside) inducible promotor, *yfp-yabA* was amplified from chromosomal DNA of JDS190 using primer 1036 and 4737 and cloned into pDR111 via *Nhe*I and *Sph*I restriction sites (KS142). Competent wild type cells were transformed using *pDR111-yfp-yabA* to generate KS149. Competent KS183 cells were transformed with the plasmid pKS142 or chromosomal DNA of JDS190 to give rise to KS173 and KS167, respectively.

Table 5: Strains used during this study

Strain	Genotype (resistance)	Reference
E. coli		
DH5α	F$^-$ *ϕ*80d*lacZ*ΔM15 Δ(*lacZYA-argF*) U169 *recA1 endA1 hsd*R17(rk-, mk+) *phoA supE*44 *λ-thi*-1 *gyrA*96 *relA*1	[85]
MG1655	*dnaA-eyfp*	[24]
PG2393	*pSG1164NLMV-era-mvenus* [pPG2393]	D. Cavalcanti de Lucena
PSL354	*pPSL38-cgeD::P$_{pen}$-tetR-yfp*	[86]
ME1	*pSG1729-yfp-dnaA*	PhD thesis M. Eisemann
B. subtilis		
PY79	*wild type, prototroph*	[84]
PG208	*spo0J(359°)::lacOcassette* (cm^R, 359°) *thrC::lacI-cfp* (mls^R) (*origin-cfp*)	laboratory strain
PG1159	*dnaX-mcherry* (cm^R)	laboratory strain
CDS2	*P$_{xyl}$ yfp-dnaA* (cm^R)	[2]
JDS190	*amyE::P$_{xyl}$yfp-yabA* (spec^R)	Joel Defeu Sofou
AG1505	Δ*soj-spo0J::spec* in wild type JH642	[87]
PSL37	Δ*soj-spo0J::spec yyaC::pDL175 lacOcassette* (cm^R) *thrC::lacI-gfp* (mls^R)	[86]
DCL696	*yyaC (359°)::pDL175 lacO cassette* (cm^R) *thrC::lacI-gfp* (mls^R)	[88]
HM123	*spo0J::tetO array* (kan^R)	H. Murray
ME15	*origin-cfp* (cm^R, mls^R) *amyE::yfp-dnaA* (spec^R)	PhD thesis M. Eisemann
ME16	*origin-cfp* (cm^R, mls^R) *amyE::yfp-dnaAA163V* (spec^R)	PhD thesis M. Eisemann
ME17	*origin-cfp* (cm^R, mls^R) *amyE::yfp-dnaAD214N* (spec^R)	PhD thesis M. Eisemann
ME18	*origin-cfp* (cm^R, mls^R) *amyE::yfp-dnaAR260A* (spec^R)	PhD thesis M. Eisemann
ME19	*origin-cfp* (cm^R, mls^R) *amyE::yfp-dnaAW8A* (spec^R)	PhD thesis M. Eisemann
ME20	*origin-cfp* (cm^R, mls^R) *amyE::yfp-dnaAE183Q* (spec^R)	PhD thesis M. Eisemann
ME21	*origin-cfp* (cm^R, mls^R) *amyE::yfp-dnaAR387C* (spec^R)	PhD thesis M. Eisemann
KS198	Δ*yabA::phleo* in wild type 168	[73]
KS183	Δ*yabA::phleo*	S. Geers
AHV2	*amyE::P$_{xyl}$yfp-dnaA* (kan^R)	Ana Hervas Veguillas

Table 6: *Bacillus subtilis* and *Escherichia coli* strains constructed during this study

Strain	Relevant genotype (resistance, inducer) [plasmid name]
B. subtilis	
KS19	*thrC::dnaN* (mls^R, IPTG)
KS21	*thrC::dnaN* (mls^R, IPTG) *spo0J-cerulean* (cm^R) *amyE::yfp-dnaA* ($spec^R$, xyl)
KS112	*thrC::dnaN* (mls^R, IPTG) *amyE::yfp-dnaA* ($spec^R$, xyl)
KS114	*dnaX-mcherry* (tet^R)
KS119	*origin-cfp* (cm^R, mls^R) *amyE::yfp-yabA* ($spec^R$, xyl)
KS124	*spo0J-cerulean* (cm^R)
KS125	*spo0J-cerulean* (cm^R) *thrC::dnaN* (mls^R, IPTG)
KS131	*thrC::dnaN* (mls^R, IPTG) *amyE::yfp-yabA* ($spec^R$, xyl)
KS140	*origin-cfp* (cm^R, mls^R) *amyE::yfp-yabA* ($spec^R$, xyl) *dnaX-mcherry* (tet^R)
KS144	*era-mvenus* (cm^R, xyl)
KS149	*amyE::yfp-yabA* ($spec^R$, IPTG)
KS167	Δ*yabA::phleo amyE::yfp-yabA* ($spec^R$, xyl)
KS171	Δ*yabA::phleo yfp-dnaA* (cm^R, xyl)
KS173	Δ*yabA::phleo amyE::yfp-yabA* ($spec^R$, IPTG)
KS175	Δ*soj-spo0J::spec yfp-dnaA* (cm^R, xyl)
KS178	Δ*yabA::phleo* Δ*soj-spo0J::spec*
KS180	Δ*soj-spo0J::spec* Δ*yabA::phleo yfp-dnaA* (cm^R, xyl)
KS182	Δ*soj-spo0J::spec*
KS188	*spo0J::tetO array* (kan^R) *cgeD::*P_{pen} *tetR-yfp* (tet^R)
KS192	Δ*soj-spo0J::spec amyE::yfp-dnaA* (kan^R, xyl)
KS193	*thrC::lacI-cfp* (mls^R) *yyac::lacO* (cm^R)
KS194	*thrC::lacI-cfp* (mls^R) *yyac::lacO* (cm^R) Δ*soj-spo0J::spec*
KS196	*thrC::lacI-cfp* (mls^R) *yyac::lacO* (cm^R) Δ*yabA::phleo*
KS197	*thrC::lacI-cfp* (mls^R) *yyac::lacO* (cm^R) Δ*yabA::phleo* Δ*soj-spo0J::spec*
E. coli	
KS103	*pSG1164-spo0J-cerulean* [pKS103]
KS115	*pDP150-dnaN* [pKS115]
KS142	*pDR111-yfp-yabA* [pKS142]

In order to investigate the localization of specific DNA sites the fluorescence repressor operator system can be used. To this end, a repressor (e.g.: LacI) is fused to a fluorescence protein and several copies of the operator sequence (e.g.: 256 copies of *lacO* sequence) are integrated into the chromosome at your site of interest. In order to construct a strain with a CFP-tagged origin with the *lacO* cassette integrated downstream of the *yyaC* gene, competent cells harboring *lacI-cfp* at the *thrC* site were transformed with chromosomal DNA of DCL696, resulting in KS193. To combine the CFP-tagged origin with the *soj-spo0J* deletion, competent *lacI-cfp* cells were transformed with chromosomal DNA of PSL37 resulting in KS194. To analyze the localization behavior of the origin of replication in a *yabA* deletion background, competent KS193 cells were transformed with chromosomal DNA of KS183 resulting in KS196. To combine the triple deletion with the CFP-tagged origin of replication, competent KS194 cells were transformed with chromosomal DNA of KS183 resulting in KS197.
To generate a strain, where the origin of replication is tagged with a YFP, competent cells harboring a *tetO* array inside the *spo0J* gene were transformed with the plasmid *pPSL38-*P_{pen}*tetR-yfp* to give rise to KS188.

2.1.5. Plasmids and vectors

Table 7: Plasmids used in this study

Vectors	Properties	Reference
pSG1164*cerulean*	cm^R, C-terminal mCerulean-fusion, original locus	F. Dempwolff
pSG1164NLMV*	cm^R, C-terminal mVenus-fusion, original locus	D. Cavalcanti de Lucena
pSG1729	$spec^R$, 5'*amyE*, 3'*amyE*, P_{xyl} promoter	[89]
pHJDS	cm^R, N-terminal GFP fusion, original locus, P_{xyl}	[90]
pDP150	ery^R, integrates into the *thrC* site, $P_{hyper-spank}$ promoter	[91]
pDR111	$spec^R$, integrates into the *amyE* site, $P_{hyper-spank}$ promoter	Gift of D. Rudner
pCm::Tet	exchanges cm^R to tet^R	[92]

All plasmids carry an amp^R resistance for selection in *E. coli*. *NLMV: *new linker mvenus*

2.1.5.1. pSG plasmids

The pSG plasmids are used to fuse a protein of interest to a fluorescent protein[89]. After successful transformation of *B. subtilis* cells with the plasmid, the construct will be integrated into the *B. subtilis* chromosome via homologous recombination.

- **pSG1164*cerulean***

  This plasmid is a derivate of the original pSG1164 plasmid[89] that encodes for the fluorescent protein mCerulean. It is used to create a C-terminal fusion that integrates via a single cross over event at the original locus of the target gene. Transcriptional control of downstream genes can be ensured using the encoded xylose promoter (P_{xyl}). For selection purposes in *B. subtilis* a chloramphenicol resistance is provided. A plasmid map is depicted in figure 7.

- **pSG1164NLMV**

  Another derivate of the original pSG1164 plasmid[89] encoding for a monomeric variant of the Venus fluorescent protein (A206K). In this plasmid a new longer linker was inserted which contains mostly uncharged amino acids. This changes the multiple cloning site (mcs) from the original pSG1164 plasmid (mcs_{new}: *Avr*II-start-*Kpn*I-*EcoR*I-*EcoR*V-*Apa*I). It is used to construct C-terminal fusions of a target protein with mVenus. Once integrated into *B. subtilis* the construct will be under the control of the original promoter. This plasmid was constructed by Daniella Cavalcanti de Lucena (Philipps-University Marburg, Germany).

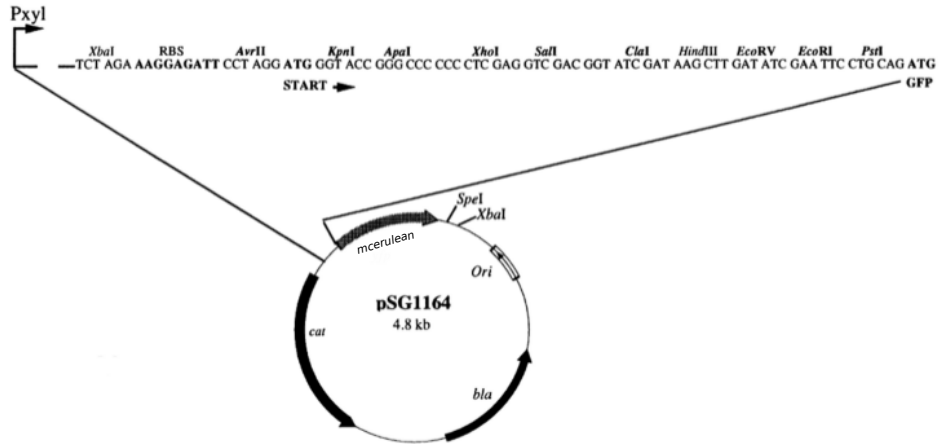

Figure 7: Schematic overview of the plasmid pSG1164*cerulean* (adapted after[89])

legend: P_{xyl}: xylose inducible promoter for downstream genes; *ori*: origin of replication; *bla*: encodes the ampicillin resistance; *cat*: encodes the chloramphenicol resistance; *mcerulean*: encodes the blue fluorescing protein mCerulean); *RBS*: ribosomal binding site; the other abbreviations represent names of restriction enzymes.

- **pSG1729**

  The plasmid pSG1729[89] carries homologies to the *amyE* site of the *B. subtilis* chromosome. This homologies result, once *B. subtilis* is transformed with the plasmid, in a double cross

over event that recombines the construct stable into the chromosome. Screening for double cross over integration capitalizes on the effect that upon successful integration the *amyE* gene is disrupted and starch can no longer be degraded. The pSG1729 is commonly used to create an ectopic N-terminal fluorescent protein fusion which is under the control of the xylose promoter present. It encodes for a spectinomycin resistance for selection in *B. subtilis* as well as an ampicillin resistance for propagation in *E. coli*.

2.1.5.2. pDP150

The plasmid pDP150 is a derivate of pDR111 and commonly used to integrate a construct under IPTG control ($P_{hyper\text{-}spank}$) at the *threonine* site of the *B. subtilis* chromosome. The plasmid carries two resistance markers for selection in *B. subtilis*, spectinomycin and erythromycin. Successful integration with a double cross over results in the loss of spectinomycin resistance gene.

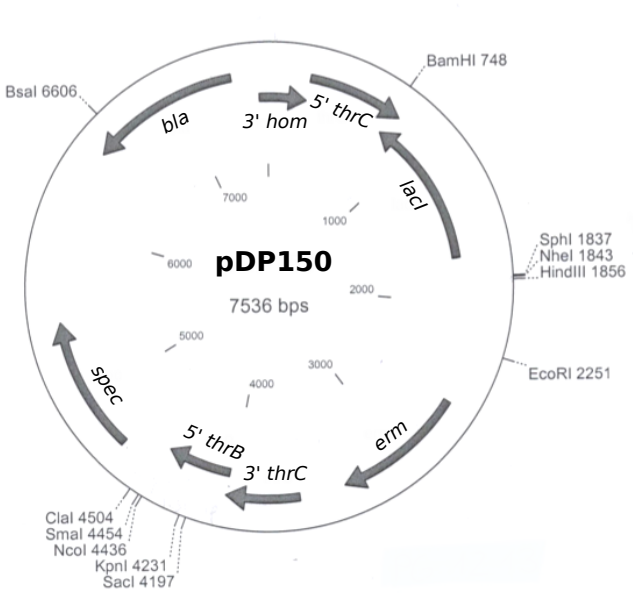

Figure 8: Schematic overview of the pDP150 plasmid.

legend: *bla*: encodes the ampicillin resistance; *spec*: encodes for the spectinomycin resistance; *erm*: encodes for the erythromycin resistance; *thrC*: encodes for the threonine synthase; *5′ thrB*: encodes for the 5′ part of the homoserine kinase; *3′ hom*: encodes for the 3′ end of the homoserine dehydrogenase; *lacI*: encodes for the lac repressor; the other abbreviations represent restriction enzymes and their cut sites. The $P_{hyper-spank}$ promoter and the lac operator (*lacO*) regulatory DNA sequence can be found between the restriction sites of *Eco*RI and *Hind*III.

2.1.5.3. pHJDS

This plasmid is a combination of the backbone of pSG1164 and the multiple cloning site of pSG1729[90]. It is used to construct N-terminal fusions at the original locus which are under the

control of the xylose inducible promoter. It carries a chloramphenicol resistance for selection in *B. subtilis*.

2.1.5.4. pDR111

This plasmid carries homologies for integration at the *amyE* site of the *B. subtilis* chromosome. It has a multiple cloning site and an IPTG inducible $P_{hyper-spank}$ promoter. For selection in *B. subtilis* the plasmid carries a spectinomycin resistance. A successful double cross over event in the *B. subtilis* chromosome results in the loss of the ability to degrade starch. The plasmid was provided by David Rudner (Harvard Medical School, Boston, Massachusetts, USA).

2.1.5.5. pCm::Tet

The plasmid pCm::tet[92] is used to exchange a chloramphenicol resistance for a tetracycline resistance.

2.2. Molecular biological methods

2.2.1. Polymerase chain reaction (PCR)

Amplification of specific DNA fragments was achieved using the polymerase chain reaction (PCR)[93].

This method can be subdivided into three principle steps: The denaturing step, in which high temperatures are applied to melt a double stranded DNA template. Followed by the annealing part, in which short oligonucleotides (primers), that define the target DNA sequence, anneal to the template. And finally the elongation round, in which the DNA polymerase amplifies the DNA fragment that lies in between the primer pairs. The described steps are repeated for several rounds and the newly amplified sequences can serve as additional templates.

Reaction mix: 10 µl 5x PCR buffer (5x Phusion high fidelity reaction buffer, NEB), 0.32 mM dNTP-Mix (NEB), 0.4 mM primer, 0.5 µl Phusion DNA Polymerase (NEB) and $_{dd}H_20$ *ad* 50 µl.

As template DNA 1 µl of a 1:100 diluted *B. subtilis* chromosomal DNA was used (ref. section 2.2.6.).

The PCR reaction was performed using a thermocycler (Biometra) applying the program shown in table 8.

Table 8: PCR program to amplify specific DNA fragments

Denaturing	2 min	95 °C	
Annealing	30 s	***x*** °C	
Elongation	***z*** min	72 °C	10 cycles
Denaturing	30 s	95 °C	
Annealing	30 s	***y*** °C	
Elongation	***z*** min	72 °C	25 cycles
Denaturing	30 s	95 °C	
Annealing	30 s	60 °C	
Elongation	***z*** min	72 °C	
Hold	∞	16 °C	

The time **(*z*)** for the elongation step depends on the synthesis rate of the phusion DNA polymerase (1000 bp per min) and the length of the amplified DNA fragment. The annealing temperature **(*x*)** and **(*y*)** can be calculated dependent on the length of the primer and the binding affinity to the template DNA. To this end the "2 + 4" rule applies: [2·n(A/T)+ 2·n(G/C)].

2.2.2. Purification of DNA fragments

To purify DNA fragments from enzymes, nucleotides and salts the *QIAquick® PCR Purification Kit* (Qiagen) was used. The *QIAquick® PCR Purification Kit* was utilized following the manufacturer's instructions. DNA was eluted in 40 µl $_{dd}H_2O$ and stored at -20 °C.

2.2.3. Agarose gel electrophoresis

Plasmids and DNA fragments were separated using horizontal agarose gel electrophoresis. To this end 1% agarose (w/v) was dissolved in 1x TAE buffer using a microwave. To stain the DNA 0.01% (v/v) Midori Green (Nippon Genetics Europe GmbH) was added to the fluid agarose mixture. The separation was achieved by applying 120 V.

Before loading the DNA sample on the agarose gel, the sample was mixed with 6x DNA loading buffer. As DNA standard the 1 kb or the 100 bp ladder (NEB) was used. Visualization of the separated DNA signals was achieved using a UV screen.

10x TB buffer	Tris-HCl pH 8.0	0.9 M
	Boric acid	0.9 M
50x TAE buffer	Tris-Acetat pH 8.2 –8.4	2 M
	Ethylenediaminetetraacetic acid disodium salt dihydrate (EDTA)	0.05 M
6x DNA loading buffer	Glycerol	20% (v/v)
	10x TB-buffer	60% (v/v)
	Bromophenol blue	0.05% (w/v)
	${}_{dd}H_2O$ *ad* 30 ml	

2.2.4. Gel extraction

To purify DNA out of an agarose gel, the signal of interest was cut out on a UV screen. Then following the manufacturer's instructions of the *QIAquick® Gel Extraction Kit* (Qiagen) the DNA can be purified. Finally the DNA was eluted in 40 µl ${}_{dd}H_2O$ and stored at -20 °C.

2.2.5. Plasmid extraction

2.2.5.1. Plasmid extraction with "quick and dirty protocol"

In a first step 2 ml of an overnight culture were pelleted at room temperature (RT) using a centrifuge (Eppendorf 5424) at 13000 rpm for 2 min.

Then the supernatant was discarded and the pellet was resuspended in 300 µl buffer 1. After addition of 300 µl buffer 2 the tubes were inverted 5–6 times. Subsequently 300 µl buffer 3 were added and mixed by inversion followed by an incubation time of 5 min on ice. In a next step the samples were pelleted for 15 min at 13000 rpm and 4 °C (Eppendorf, 5424R).

The supernatant was carefully transferred into a new reaction tube. Then 600 µl isopropanol were added and the samples were precipitated (13000 rpm, 45 min, RT; Eppendorf 5424R).

The DNA pellet was washed in 500 µl of 70% ethanol (v/v) and pelleted at 13000 rpm and RT for 10 min. As soon as the ethanol was completely evaporated, 40 µl ${}_{dd}H_2O$ was added. The DNA was stored at -20 °C.

Buffer 1	Tris-HCl (pH 8.0)	50 mM
	EDTA	10 mM
	RNase A	100 µg/ml
Buffer 2	NaOH	200 mM
	Sodium dodecyl sulfate (SDS)	1% (w/v)
Buffer 3	Potassium acetat	3 M
	Acetic acid	11.5% (v/v)

2.2.5.2. Plasmid extraction for sequencing

To extract a plasmid with higher purity, for example for sequencing, a plasmid prep kit was used. The following kits were used to this end: Zymo Research (Freiburg) *ZR Plasmid Miniprep^{TM}-Classic*, PEQ-lab (Erlangen) *peqGOLD Plasmid Miniprep Kit I* and VWR (Darmstadt) Omega *E.Z.N.A ® Plasmid DNA Mini Kit I*. Manufacturer's protocols were followed. To measure DNA concentrations a NanoDrop Lite (Thermo Scientific) was used.

2.2.6. Chromosomal DNA extraction out of *B. subtilis* cells

First, 2 ml of an over night *B. subtilis* culture were pelleted (1 min, 13000 rpm) using a table centrifuge (Eppendorf 5424).

Then the pellet was resuspended in 500 µl lysis buffer (50 mM EDTA, 100 mM NaCl, pH 7.5). Afterwards 10 µl lysozyme (stock: 100 mg/ml) was added to the sample followed by an incubation step at 37 °C for 15–30 min.

After a successful lysis of the cell wall 20 µl of 15% (w/v) sodium lauroyl sarcosinate solution was added followed by an incubation step of 5 min on ice.

After addition of 500 µl phenol (Roti-Phenol, Roth), the samples were mixed followed by a centrifugation step of 5 min at 13000 rpm at RT. The watery phase was carefully transferred into a fresh 2 ml reaction tube. Then 500 µl phenol:chloroform:isoamyl alcohol (25:24:1 (v/v/v), Roth) was added, well mixed and finally centrifuged (13000 rpm, 5 min, RT).

The upper phase was transferred into a fresh 1.5 ml Eppendorf tube containing 40 µl of 3 M sodium acetate. Afterwards 1 ml of ethanol was carefully added (99,8% p.a., Roth). Then the reaction tube was cautiously inverted until the DNA started to precipitate.

Using a custom made hook the DNA could be retrieved. In a next step the DNA was washed in 70% ethanol (v/v) and air dried. As soon as the ethanol has evaporated the DNA was eluted in 40 µl $_{dd}H_2O$. The chromosomal DNA was stored at -20 °C.

2.2.7. Restriction digest

Using endonucleases, double stranded DNA can be specifically cut. They are enzymes that hydrolyze the sugar-phosphate backbone of the DNA.

An analytical restriction digest contains 1 µl Cut smart buffer (NEB), 2 µl plasmid DNA, 4–10 U of the enzyme in a total volume of 10 µl filled up with ${}_{dd}H_2O$. Then the samples were incubated for 1 h at 37 °C.

For a preparative restriction digest 5 µl of Cut smart buffer (10 ×, NEB), 20 µl plasmid DNA (ref. section 2.2.4.) or 20 µl PCR product (ref. section 2.2.2.) and 20–50 U of the appropriate enzyme (NEB) were mixed and adjusted with ${}_{dd}H_2O$ to a final volume of 50 µl. In a next step the sample was incubated at 37 °C for 2 h. To remove free phosphate 5'-ends 10 U CIP (*calf intestinal phosphatase*, NEB) were added 30 min prior to end of incubation.

PCR fragments were purified using the *QIAquick® PCR Purification Kit* (Qiagen). Digested plasmids and fragments cut out of plasmids were purified using an agarose gel with subsequent gel extraction (ref. section 2.2.4.) with the *QIAquick® Gel Extraction Kit* (Qiagen).

2.2.8. Ligation

Using DNA ligation two DNA fragments can be linked. Here, the DNA fragments align to form a double strand and the DNA ligase closes the break in the sugar phosphate backbone.

To this end plasmid and insert were mixed in a ratio of 1:3 or 1:5, 2 µl of T4 DNA ligase buffer (NEB), 1 µl T4 DNA Ligase (NEB) and supplemented with ${}_{dd}H_2O$ to a total volume of 20 µl. The samples were incubated over night at 16 °C or at 23 °C for 10 min. Ligation reactions were stored at -20 °C.

2.2.9. Preparation of chemical competent *E. coli* cells

A preculture of 2–5 ml LB media with DH5α-cells was diluted to a final OD_{600nm} of 0.005 in 125 ml SOB media and incubated at 18 °C and 200 rpm for 48 h until an OD_{600nm} of 0.6 was reached. From now on all steps were performed at 4 °C.

In a next step the culture was incubated on ice for 10 min. This was followed by a centrifugation step of 10 min at 3000 rpm and 4 °C (rotor: JLA-16.250, centrifuge: Avanti® J-E, Beckman Coulter). The supernatant was discarded and the pellet was resuspended in 80 ml cold TB buffer. After another 10 min on ice another centrifugation of 10 min at 3000 rpm and 4 °C (Beckman Coulter, Allegra®X-15R, rotor:SX4750) was performed.

The supernatant was discarded and the pellet resuspended in 20 ml of TB complemented with 7% (v/v) dimethyl sulfoxide (DMSO). After another 10 min on ice 100 µl aliquots were shock frozen in liquid nitrogen. The competent cells can be stored at -80 °C.

TB medium	Hepes	10 mM
	$CaCl_2$	15 mM
	KCl	250 mM
adjust pH to 6.7 with KOH or HCl		
	$MnCl_2$	55 mM

2.2.10. Transformation of chemical competent *E. coli* cells

One aliquot of chemical competent *E. coli* cells was thawed on ice. Then 20 µl of either a ligation reaction or 0,5–1 µl of a plasmid were added.

The cells were incubated for 10 min on ice. Afterwards a 2 min heat shock at 42 °C was applied followed by another incubation of 5 min on ice. Finally 900 µl of SOC medium were added and the cells were incubated for one hour at 37 °C. Then 100 µl of the cells were spread on LB agar plates containing the appropriate antibiotics to select for the uptake of the plasmid.

SOC medium	Trypton	2% (w/v)
	Yeast extract	0.5% (w/v)
	NaCl	0.05% (w/v)
	KCl	2.5 mM
	adjust pH to 7.0	
complement sterile after autoclaving:		
	$MgCl_2$	10 mM
	Glucose	20 mM

2.2.11. DNA sequencing

To verify cloned constructs, DNA sequencing was used[94]. To this end plasmids were purified as described in section 2.2.5.2..

Sequencing was performed by the following companies: GATC Biotech (Konstanz) or Eurofins Genomics (Ebersberg). Plasmids and oligo nucleotides were diluted as described by the companies' instructions.

2.2.12. Cultivation of natural competent *B. subtilis* cells

10×T-Base	$(NH_4)_2SO_4$	150 mM
	K_2HPO_4	1 M
	KH_2PO_4	440 mM
	Tri-sodium citrate	39 mM
SpC medium	T-Base (10 ×)	1 ×
	D-Glucose monohydrate	0.5% (w/v)
	$MgSO_4$	0.018% (w/v)
	Casamino acids	0.025% (w/v)
	Yeast extract	0.2% (w/v)
SpII medium	T-Base (10 ×)	1 ×
	D-Glucose monohydrate	1% (w/v)
	$MgSO_4$	0.084% (w/v)
	Casamino acids	0.01% (w/v)
	Yeast extract	0.1% (w/v)
	$CaCl_2$	0.5 mM

Enrichment of natural competent *Bacillus* cells was accomplished by inoculating 20 ml of SpC medium with cells from a fresh overnight agar plate. The SpC medium was supplemented with the appropriate antibiotics and inducers prior to incubation at 37 °C. After an incubation time of 3 h the absorbance at 600 nm was measured until the optical density (OD) reached a stable value.

Then the sample was diluted into 100 ml of SpII medium and incubated for 90 min at 37 °C.

In a last step the cells were pelleted (10 min, 4000 rpm, Beckman Coulter, Allegra®X-15R, rotor:SX4750) and resuspendend in 9 ml supernatant and 1 ml 50% glyerol (v/v). Finally aliquots were made and stored at -80 °C.

2.2.13. Transformation of competent *B. subtilis* cells

To transform competent *Bacillus* cells with chromosomal DNA or plasmids, 125 µl of competent cells were mixed with 3–7 µl plasmid DNA or 0.3–0.7 µl chromosomal DNA. After an incubation time of 30 min at 37 °C the cells were spread on LB agar plates containing the appropriate antibiotics. The plates were incubated at 30 °C until transformants arose.

2.3. Microbiological methods

2.3.1. Glycerol stocks

To store strains for a longer time period, glycerol stocks were prepared. For that purpose 600 µl of an overnight culture was mixed with 400 µl glycerol (50% (v/v)). The glycerol stocks can be stored at -80 °C.

2.3.2. Determination of optical density

To determine the optical density of a culture the $OD_{600\ nm}$ was measured (Ultrospec 10 cell density meter, Amersham Pharmacia Biotech). The cuvettes used had a diameter of 1 cm (plastic cuvettes REF67.742, Sarstedt).

2.3.3. Growth curve

In order to determine the doubling time of a strain, growth assays were performed. For this purpose the strains of interest were plated on agar plates with the appropriate antibiotics and incubated at 30 °C over night. The next day LB medium was inoculated with cells from the mentioned LB agar plates and incubated at 30 °C for 1–2 h. The optical density of the culture was measured and adjusted to an OD of 0.01–0.05 in a final volume of 20 ml LB medium. Then the cultures were incubated at 30 °C and the optical density was determine every 30–60 minutes. The doubling time (t_D) was calculated using the following equation, with t representing the time, λ the growth coefficient and $N(t)$ the measured OD at timepoint t:

$$t_D = \frac{\ln 2}{\lambda} \qquad \lambda = \frac{\ln\left(\frac{N(t)}{N(t_0)}\right)}{\delta t}$$

2.4. Biochemical methods

2.4.1. SDS-Polyacrylamide gel electrophoresis (SDS-PAGE)

Table 9: Composition of SDS gels and buffers

	Components	**Concentration**
Running gel 8%	Rotiphorese Gel 30* (Roth)	4 ml
	Tris-HCl pH 8.8	3.75 ml
	10% SDS (w/v)	150 µl
	$_{dd}H_2O$	7 ml
Running gel 10%	Rotiphorese Gel 30 (Roth)	5 ml
	Tris-HCl pH 8.8	3.75 ml
	10% SDS (w/v)	150 µl
	$_{dd}H_2O$	6 ml
Running gel 12%	Rotiphorese Gel 30 (Roth)	6 ml
	Tris-HCl pH 8.8	3.75 ml
	10% SDS (w/v)	150 µl
	$_{dd}H_2O$	5 ml
Stacking gel	Rotiphorese Gel 30 (Roth)	990 µl
	Tris-HCl pH 6.8	1.875 ml
	10% SDS (w/v)	75 µl
	$_{dd}H_2O$	4.5 ml
4 × SDS sample buffer	Tris-HCl pH 6.8	50 mM
	SDS	8% (w/v)
	Glycerol	40% (v/v)
	β-Mercaptoethanol	20% (v/v)
	Bromphenol blue	0.01% (w/v)
10× running buffer	Tris	3.03% (w/v)
	Glycin	14.4% (w/v)
	SDS	1% (w/v)
	$_{dd}H_2O$ *ad* 1l	

*Rotiphorese gel 30: 30% Acrylamide (w/v), 0.8% N-N'-Methylenbisacrylamide

To separate proteins according to their size, SDS-polyacrylamid gelelectrophoresis was performed. The separation was realized under denaturating conditions[95]. Depending on the size of the protein of interest, 8%, 10% or 12% running gels were casted.
In order to cast the gels, the components for stacking and running gels were mixed and the polymerization was started by the addition of 75 µl 10% (w/v) ammonium peroxodisulfate (APS) and 7.5 µl Tetramethylenethylendiamine (TEMED) (ref. table 9).
The gels were casted using the *Mini-Protean* system (BIO-RAD, Hercules, USA).
Samples were mixed with 4 × SDS sample buffer and denatured at 95 °C for 10 min. A well was loaded with 10 to 15 µl of a sample. Electrophoresis was performed in 1×running buffer at 80 V until a separation of the signals could be observed. Then the Voltage was increased to 120 V (Electrophoresis power supply, Consort EV243). *PageRuler^{TM} Plus* from Thermo Scientific (Schwerte) was used as protein ladder.

2.4.2. Western Blot

Using the *Trans-Blot®-Turbo^{TM}*(BIO-RAD) the through prior SDS-PAGE separated proteins were transferred from a polyacrylamide gel onto a nitrocellulose membrane (Protran BA-83, Whatman^{TM}, GE). Therefor three layers of Rotilabo®-Blotting paper (Roth, 0.35 mm thick) soaked in transfer buffer, one in $_{dd}H_2O$ activated nitrocellulose membrane, the SDS-gel and another three layers of blotting paper soaked in transfer buffer were placed on top of each other inside the blotting cassette. For the transfer the standard program of the blotting machine was applied (30 min, 25 V and 1 mA).

Transfer buffer:	Tris	0.58% (w/v)
pH 9.8	Glycine	0.3% (w/v)
	SDS	0.035% (w/v)
	Ethanol	20% (v/v)

2.4.3. Indirect immuno detection of proteins

The proteins that were covalently bound to the nitrocellulose membrane were detected using specific antisera.
To reduce unspecific antibody binding due to free protein binding sites on the membrane, the nitrocellulose membrane was incubated in 5% milk (w/v) in PBST for 1 h to over night.
Then the nitrocellulose membrane was incubated for 1 h with the primary antibody in 5% milk (w/v) in PBST (for a list of antibodies and their concentration refer to table 10) followed by 3 × 10 min washes with PBST. Afterwards the membrane was incubated for another hour with the secondary antibody in 5% milk (w/v) in PBST. The secondary antibody is a HRP-conjugated

Table 10: Antibodies used during this study

Primary antibody		
α-GFP	1:500	Gramsch laboratories (Schwabhausen)
α-DnaA	1:500	Gramsch laboratories (Schwabhausen)
Secondary antibody		
mouse-α-rabbit-HRP*	1:10,000	Sigma (München)

*HRP: Horseradish peroxidase

antibody. After 3 $\times$ 10 min of washing the membrane with PBST it was incubated for 1 min in solution 1 and solution 2 prior to signal detection using the *ChemiDoc® MP System* (BIO-RAD).

PBST	Na_2HPO_4	0.00115% (w/v)
	NaH_2PO_4	0.0029% (w/v)
	NaCl	0.00584% (w/v)
	Tween 20	0.1% (v/v)
solution 1	Luminol	2.5 mM
	Coumaric acid	396 µM
	Tris-HCl (pH 8.5)	100 mM
solution 2	H_2O_2	0.00018% (v/v)
	Tris-HCl (pH 8.5)	100 mM

2.5. Fluorescence microscopy

2.5.1. Sample preparation

Cells were grown in minimal medium (ref. table 2 and 3) until they reached exponential phase. Then 3 µl of the culture was mounted on a glass cover slip. To ensure continuous nutrition supply and to immobilize the cells they were covered with a pad consisting of $S7_{50}$ minimal medium and 1% (w/v) agarose.

2.5.2. Fluorescence dyes and proteins

Using fluorescence dyes the DNA and membrane of bacterial cells were visualized (ref. table 11). The DNA was stained using DAPI (4',6-diamidino-2-phenylindole, 0.2 µg/ml, Roth). The fluorescence stain binds to AT rich sequences and increases its fluorescence intensity upon DNA binding[96].

The membrane was stained using the lipophilic dye FM4-64 ([N-(3-triethylammoniumpropyl)-4-(p-diethylaminophenylhexatrienyl) pyridinium dibromide], 2.5 µg/ml, life technologies). It binds to the outer layer of the cell membrane but is not able to pass it[97].
Various variants of the green fluorescent protein (gfp) from *Aequoria victoria* were used to localize proteins inside bacterial cells[98].
To generate a fluorescent variant of an investigated protein the pSGvectors were used (ref. section 2.1.5.1.).

Table 11: Characteristics of dyes and fluorescence markers

	Excitation wavelength	**Emission wavelength**	**Concentration**
Dyes:			
DAPI	358 nm	461 nm	0.2 µg/ml
FM4-64	515 nm	640 nm	2.5 µg/ml
Fluorescence markers:			
YFP	513 nm	527 nm	
CFP	433 nm	475 nm	
mCherry	587 nm	610 nm	

2.5.3. Microscopy

For microscopy a Olympus *BX51* microscope with an Olympus objective (100x, immersion oil, numerical aperture (NA): 1.40) and a Hg/Xe lamp (Olympus) was used. The images were acquired using a digital CCD camera (Cool Snap EZ, Photometrics) controlled by the *Metamorph 6.3-Software* (Meta Imaging Software). Appropriate filter sets (Chroma) were used.
Alternatively a Zeis Axio Imager microscope with a Zeiss objective (100x, immersion oil, NA: 1.45) and a digital CCD camera (CoolSNAP HQ, Photometrics) was used.

2.6. FRAP microscopy

2.6.1. Microscope setup

For FRAP experiments a Zeiss Axio Observer A1 with a TRIF objective (100x, immersion oil, NA: 1.45, Zeiss) and an automated stage (Visitron Systems, Munich) was used. Images were acquired using a digital EMCCD camera (Evolve, Photometrics). A 515 nm laser (Visitron Systems, Munich) was used to excite and bleach the sample. Acquisition was controlled using the VisiView 2.1.4 software (Visitron Systems, Munich). A custom made macro was applied for acquiring the FRAP sequences.

2.6.2. FRAP analysis

Analysis of FRAP data was performed using Fiji ImageJ[99] and as described by Kleine Borgmann[100]. Acquired streams were aligned using the StackReg plugin[101].
Fluorescence intensities of the region of interest were measured and background fluorescence subtracted. To normalize for acquisition bleaching the fluorescence of a control cell was measured. To normalize for different bleach depths and cluster intensities full scale normalization was applied. Fits to the data points were obtained using the nonlinear regression algorithm from Wolfram Mathematica 8.0. As a model the function $f(t) = A \cdot (1 - e^{-t/t_0})$, with the recovery time constant t_0 and the maximum amplitude A was used. For each experiment the fits were applied and the recovery half time calculated. Then the mean and the standard deviation of the recovery half times were computed. In plots, one single experiment is visualized together with the applied fit.

2.7. Single molecule microscopy

2.7.1. Microscope setup

For single molecule microscopy an Olympus IX71 with an Olympus TRIF objective (100x, ApoN, NA: 1.7, immersion oil) was used. Image acquisition was accomplished using a back-illuminated EMCCD camera (Andor, iXon Ultra, BFi Optilas). A 50 mW multiline argon laser (JDS Uniphase, laser head: 2219-G5MLS) was focused on the back-focal plane and operated during image acquisition with 17 mW. An appropriate YFP filter-set was used. For image acquisition the program Andor Solis 4.21 was applied. Streams of 1500 frames of 40.1 msec or 24.5 Hz were acquired. For faster image acquisition only a subset of 128×128 pixel of the chip was read out.

2.7.2. Sample preparation

High refractive index glass cover slips (n=1.78) for the Olympus objective were used. To clean the cover slips they were first sonicated in a 2% (v/v) Hellmanex®III (Hellma®) solution for 15 min. Afterwards the cover slips were rinsed thoroughly with ${}_{dd}H_2O$. Prior to use residual water was removed using compressed air (Elix®Clean 720) and the cover slips were transferred to a custom made holder. Then 3 µl of the culture were mounted and covered with a 1% (w/v) $S7_{50}$ agarose pad.

2.7.3. Data analysis

2.7.3.1. Tracking of single molecules

Acquired streams were loaded into Fiji ImageJ[99] and pixel sizes (100 nm) and time increments (41 msec) were calibrated. Tracking of single molecules was achieved using the ImageJ plugin MTrackJ[102].

2.7.3.2. SDFFS program

Obtained tracks were loaded into the SDFFS program and parameters like the apparent diffusion constant and the mean square displacement were calculated. The program is also capable of graphically displaying single tracks in a Cartesian plane with an implemented heat map function. Furthermore the amount of stopped molecules per time increment can be read out. A stopping molecule is in this case defined as a molecule remaining inside an area with a diameter of 230 nm. This is based on the resolution limit of the microscope setup.
The program was developed by Prof. Dr. Bernhard Schmitt, a member of the AG Dahlke in the mathematics department of the Philipps-University Marburg based on suggestions and experiments performed by Stephan Altenburger and Sandra Fries (AG Graumann, Synmikro, Philipps-University Marburg).

2.7.3.3. Diffusion constant

Using the SDFFS program, diffusion constants for the tracked molecules can be calculated based on the following formula:

$$D = \frac{MSD}{4 \cdot \tau}$$

With D being the diffusion constant, MSD the mean square displacement and τ the time increment.

2.8. Software

During this work several programs were used to analyze and obtain data.
To obtain DNA and protein sequences of *B. subtilis* the SubtiList server was used `http://genolist.pasteur.fr/SubtiList/`.
Sequencing results and cloning strategies were analyzed utilizing the *Clone Manager 7* (Scientific & Educational Software). Microscope images were analyzed using Fiji ImageJ[99] or *Metamorph 6.3-Software* (Meta Imaging Software). For statistical analysis and to visualize experimental data, *Mathematica 8* (Wolfram) and *Excel 2007* (Microsoft) was used. To assemble and draw figures *Inkscape* (Free Software Foundation, Inc.) was utilized.

3. Results

3.1. YFP-DnaA localizes in a cell-cycle-dependent manner

Localization of the initiator of DNA replication, DnaA, was reported to follow a cell-cycle-dependent pattern[2]. Colocalization of YFP-DnaA with the origin of replication was observed to occur usually in very early and late stages of the cell cycle, whereas most of the time YFP-DnaA was colocalizing with the replication machinery at the cell center[2]. These results were based on images acquired of many cells throughout the cell cycle, not on time lapse observations of single cells. I performed time lapse microscopy to investigate the localization of YFP-DnaA with respect to the origin of replication during the cell cycle of an individual cell.

In figure 9 the result of a time lapse experiment is visualized. Cells from a strain harboring an inducible ectopic copy of YFP-DnaA as well as a CFP-labeled origin of replication (tagged with LacI-CFP which binds to a *lacO* array in the origin region, ME15) were grown whilst images were acquired with respect to the cell cycle.

The images presented in figure 9 display overlays of YFP-DnaA signals in green and the CFP-labeled origin in red, during a complete cell cycle. Triangles indicate the position of YFP-DnaA signals. White triangles represent foci that are not colocalizing with the origin of replication whereas yellow triangles highlight signals that do colocalize.

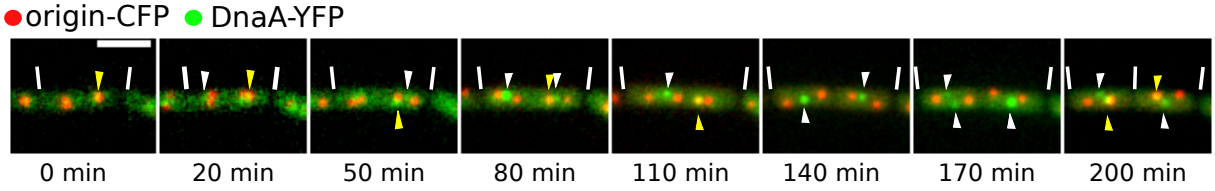

Figure 9: Time lapse of YFP-DnaA localization with respect to the position of the origin of replication. Image sequence displaying overlays of YFP-DnaA signals (green) with the origin of replication (red) over a time course of 200 min. Triangles indicate the position of YFP-DnaA signals, with yellow triangles reporting for colocalization and white triangles for no colocalization of both signals. White line, cell borders; scale bar, 2 µm. Cells were grown in $S7_{50}$ minimal medium at 30 °C until the early exponential phase. Then the expression of YFP-DnaA was induced with 0.1 % xylose (w/v) for 15 min.

In the first 50 min, until the newly duplicated origins of replication move apart, YFP-DnaA mostly colocalizes with one of the origins. Then, for a time period of around 90 min the YFP-DnaA signal preferentially locates in between the two separating origins, probably colocalizing with the replication machinery. In the last image (figure 9), cell division has occured and in each cell two YFP-DnaA foci are visible, whereof one is colocalizing with one origin of replication.

These experiments show that DnaA can transiently colocalize with origin regions, after they have been moved away from the cell center. Therefore, DnaA is able to interact with *oriC* throughout the cell cycle, even though a large fraction is recruited to the replication machinery.

3.2. YFP-YabA follows the localization pattern of YFP-DnaA

YabA, which has previously been reported to be a negative regulator of replication initiation, is able to bind to DnaA and DnaN, the sliding clamp of the DNA polymerase[73,82,83]. Presumably, due to these interactions YabA administrates its regulatory function through tethering DnaA to the replication machinery and therefore keeping it away from the origin of replication[2]. Localization studies so far reported a colocalization of YabA with the replication machinery in late cell stages[82]. In total, 51% of all cells displayed colocalization with DnaX, the τ subunit of DNA polymerase III, in 16% of all cells only one out of two YFP-YabA foci was colocalizing with DnaX and in 33% no colocalization could be detected[82].
In order to analyze the localization behavior of YabA with respect to the origin of replication and the replication machinery, a strain combining a CFP-labeled origin with DnaX-mCherry and an inducible ectopic copy from which YFP-YabA could be expressed were generated (KS140). A direct colocalization of DnaA and YabA results in sick cells where both fluorescence signals are always colocalizing (data not shown). Cells were grown in $S7_{50}$ minimal medium at 25 °C and induced for 30 min with 0.1% (w/v) xylose.
Four different localization patterns were observed (figure 10). Images displaying overlays of YFP-YabA (green) with the CFP-labeled origin (red) are shown in the upper panels whereas images displaying overlays of YFP-YabA (green) with DnaX-mCherry (red) are shown in the bottom panels.

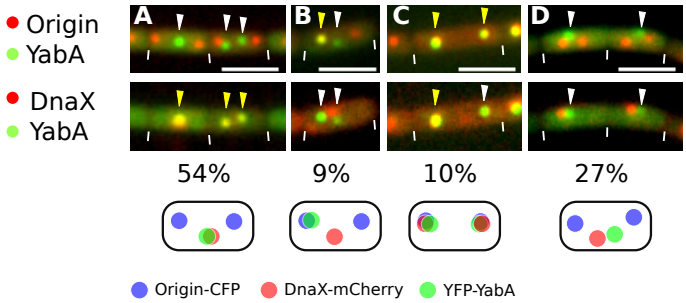

Figure 10: Overview of YFP-YabA localization pattern.
Overlays of YFP-YabA signals (green) with origin-CFP (red) in the upper panel and with DnaX-mCherry (red) in the lower panel, are shown. Triangles indicate positions of YFP-YabA foci. White triangle, no colocalization; yellow triangle, colocalization. White lines, cell borders; scale bars, 2 µm. Numbers represent percentage of observed pattern. The small cartoons in the bottom of the figure visualise the four different localization pattern described.
A–D Different pattern of YFP-YabA localization. YFP-YabA colocalizes with DnaX-mCherry in 54 % of all cases (A), with the origin of replication in 9% of all cases (B) and all three signals colocalize in 10% of all cells observed (C). In 26% of all cells no colocalization of YFP-YabA with any of the two other signals could be observed (D).

In 54% of all cases (total of 208 cells analyzed) the YFP-YabA signal was colocalizing with the replication machinery (figure 10 A). These findings are in accordance with the results reported by Hayashi *et al*[82]. A colocalization with the CFP-tagged origin of replication was witnessed in

9% of all cells (figure 10 B), whereas in 10% a colocalization of YFP-YabA with both signals, the origin of replication and the replication machinery, was observed (figure 10 C). In around 26% of all cases no colocalization of YFP-YabA with any of the other two signals was noticed (figure 10 D).

The previously mentioned results represent findings that don not take the cell cycle stage of the individual cells into account. To compare YFP-YabA to YFP-DnaA localization the localization patterns were analyzed depending on cell length. To this end, the cells were divided into three groups corresponding to different cell length: $\leq$ 2.25 µm, 2.25–3.2 µm and $\geq$ 3.2 µm. Then the localization patterns were analyzed separately for each group. These results are displayed in figure 11 B–H. Only the predominant localization patterns are displayed.

In small cells ($\leq$ 2.25 µm) the predominant pattern with 52% is a colocalization of YFP-YabA with the replication machinery. In 10% of all cells in this group YFP-YabA colocalizes with the origin of replication and in 33% no colocalization can be observed.

The medium sized cells (2.25–3.2 µm) show a colocalization with the replication machinery in 56% of all cases. In 25% no colocalization was observed and in 9% YFP-YabA colocalizes with the origin of replication. In 6% of all cells two YabA foci colocalize with two origins and one DnaX foci.

In the group with the longest cells ($\geq$ 3.2 µm) the colocalization of YFP-YabA with the replication machinery is the most abundant pattern (46%). With 21% of all cells showing no colocalization followed by colocalization of two origins and one DnaX foci with two YFP-YabA foci in 13% of all cells.

Only small differences were observed between the different groups. The predominant pattern is, as expected from the first analysis, a colocalization of YFP-YabA with the replication machinery. In small and medium sized cells the next most popular pattern, besides the none colocalization pattern, is the colocalization with the origin of replication. In medium-sized and long cells the mixed pattern of two YabA foci colocalizing with two origin of replication and one DnaX focus shows increasing occurrence.

To graphically display the localization results, the total cell length of the investigated cells was measured as well as the distance from each YFP-YabA focus to the closest cell pole and plotted against each other (figure 11 A). In that diagram filled circles represent single YFP-YabA foci whereas open triangles stand for cells with two YFP-YabA foci. For figure 11 A only cells in which YFP-YabA colocalized with either the CFP-labeled origin or the replication machinery were included. In cells containing a single YFP-YabA focus this resides mostly in the cell center (dashed line), where the replication machinery is positioned.

In figure 11 I the position of YFP-YabA foci (green) and origin-CFP foci (black) in correlation to the cell lengths is displayed.

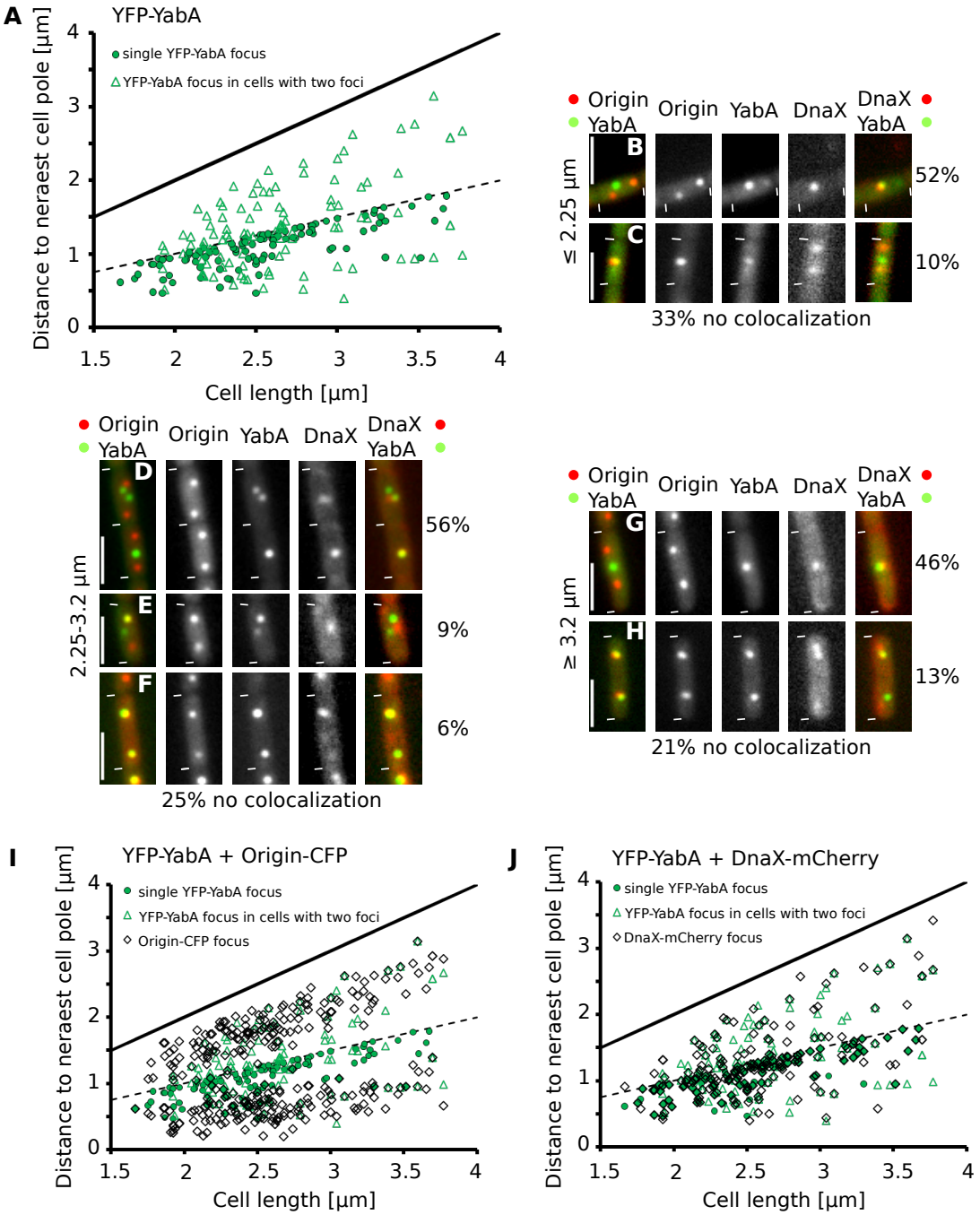

Figure 11: Cell-cycle dependent localization of YFP-YabA.
A Position of YFP-YabA foci to the nearest cell pole in correlation to total cell length. Green circles, single YFP-YabA foci; open triangle, YFP-YabA focus closest to measured cell pole in cells with two foci; open square, YFP-YabA focus further away from measured cell pole in cells with two foci. Dashed line, cell center; Black line, cell length.
B–H Different localization pattern of YFP-YabA, dependent on cell length. YFP-YabA (green) localization compared to the origin of replication (red, tagged with LacI-CFP which binds to a *lacO* array in origin region) and the replication machinery (red, DnaX, τ subunit of DNA polymerase III). White line, cell borders; scale bars, 2 µm.
I–J Position of origin regions (I) or DnaX-mCherry foci (J) and YFP-YabA foci to nearest cell pole, dependent on cell length. YFP-YabA symbols as described in A; Black open diamonds, origin-CFP foci (I) or DnaX-mCherry foci (J).

Figure 11 J displays the observed YFP-YabA signals (green) together with DnaX-mCherry signals (black). A colocalization of the replication machinery with YFP-YabA especially with cells containing a single focus can be observed.
YabA has been shown to influence DNA binding of DnaA. My analysis shows that YabA is also found at *oriC*, in a transient manner, during all times in the cell cycle.

3.3. Overexpression of DnaN results in an increased number of YFP-YabA and YFP-DnaA foci

The sliding clamp of the DNA polymerase III (DnaN) interacts with the negative regulator YabA. Previous reports suggest that an overproduction of DnaN stimulates replication initiation dependent on YabA[74]. Furthermore it was shown that an overproduction of DnaN caused a decreased association of YabA and increased association of DnaA with *oriC*[75]. To investigate the localization of YFP-DnaA and YFP-YabA upon overexpression of DnaN, strains harboring an ectopic copy of DnaN as well as an ectopic copy of YFP-DnaA (KS112) or YFP-YabA (KS131) were constructed.
Cells were grown in rich medium at 37 °C. In order to compare the effect of DnaN overproduction one culture was induced with 0.1% (w/v) xylose, which only induces the fusion protein, and another culture was additionally induced with 100 µM IPTG, which triggers expression of surplus DnaN. Cells were stained with FM4-64 and DAPI to stain the membrane and DNA, respectively.
The data is summarized in table 12 and figure 12.
In table 12 the number of foci per cell are displayed for each strain under two conditions. Upon induction of extra DnaN the average number of foci increases from 2.9 YFP-DnaA foci to 3.6 YFP-DnaA foci per cell. A similar situation arises for YFP-YabA upon overexpression of DnaN. Here the average number of foci rises from 1.1 YFP-YabA foci per cell to 2.3 YFP-YabA foci per cell. So in the case af YFP-YabA the number of foci doubles when extra DnaN is induced.

Table 12: Number of YFP-DnaA and YFP-YabA foci per cell

strain	extra DnaN	Number of foci counted [%] 0	1	2	3	4	>5	Cells	Average no. of foci
yfp-dnaA thrC::dnaN	–	0	6.3	45.3	10.9	24.2	13.3	128	2.9
	+	0	3.9	16.6	20.4	39.2	19.9	181	3.6
yfp-yabA thrC::dnaN	–	27.5	44.1	22.5	5.9	0	0	222	1.1
	+	4.5	18.4	36.1	30.3	8.5	2.2	402	2.3

Cells were grown in rich medium at 37°C and induced with 0.1% (w/v) xylose for 30 min to induce expression of YFP-DnaA and YFP-YabA, respectively. For overexpression of DnaN, 100 µM IPTG was added.

An example is displayed in figure 12. The YFP-DnaA strain is shown in figure 12 A and the YFP-YabA strain in figure 12 B. The upper panel displays the localization of the fusion protein without DnaN induction whereas the lower pannel shows the localization upon DnaN overexpression. The overlays show in red the membrane and in green the tagged protein fusions. A clear increase in the number of foci can be observed between the lower and upper panels for both fusions.

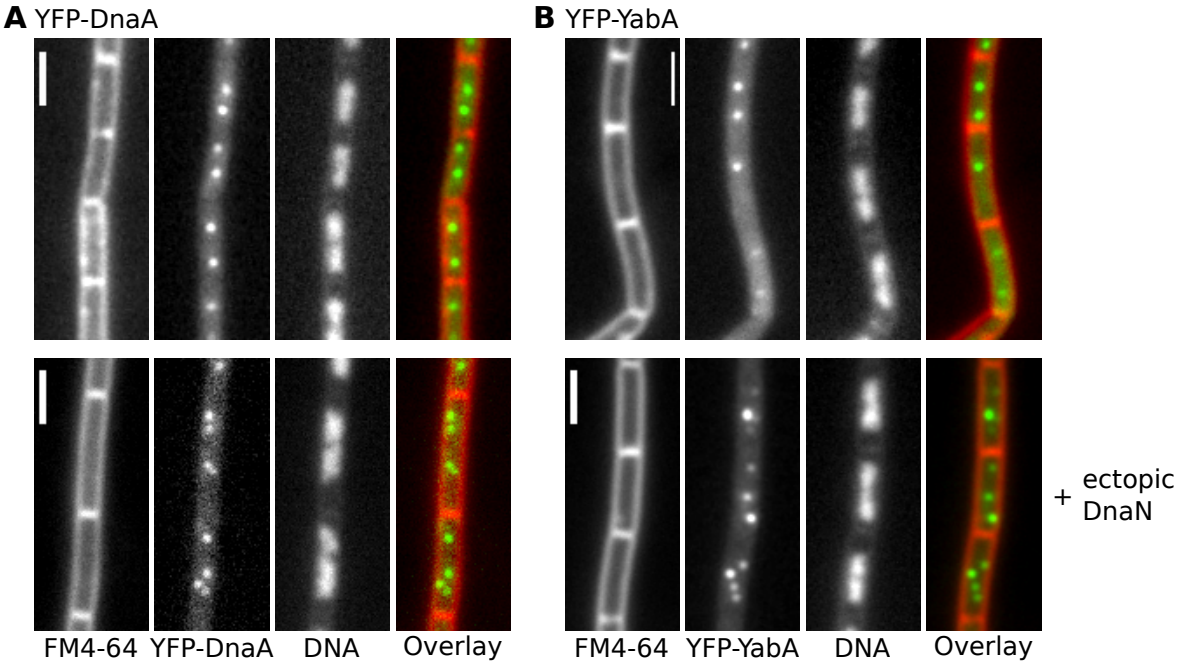

Figure 12: Localization of YFP-YabA and YFP-DnaA upon overexpression of DnaN.
Fluorescence microscopy images of cells expressing ectopic DnaN in addition to YFP-YabA or YFP-DnaA. Localization of YFP-DnaA (**A**) and YFP-YabA (**B**). Upper panels, xylose based induction of YFP-DnaA (A) and YFP-YabA (B); lower panel, co-induction of YFP-DnaA (A) or YFP-YabA (B) and of DnaN for 30 min. Scale bars, 2 µm.

Possibly, DnaN titrates YabA away from origin regions, such that DNA binding activity of DnaA is no longer counteracted by YabA at this subcellular region.

3.4. Triple deletion of *yabA*, *soj* and *spo0J* is not lethal

The initiation of replication is tightly regulated. The two best understood regulatory proteins in *B. subtilis* are the small protein YabA and the ParA homologue Soj.
YabA is thought to tether DnaA via DnaN to the replication machinery and thereby inhibiting binding of DnaA to *oriC*. A deletion of *yabA* results in a 2.5 times overinitiation of replication and in elongated cells that exhibit a growth defect compared to the wild type[73].
Soj is a weak ATPase that can be stimulated by the ParB homolog Spo0J[77]. In the ATP bound state Soj is a dimer and acts as a stimulator of DnaA activity at *oriC*. Upon ATP hydrolysis Soj disassembles into its monomeric state where it acts as an inhibitor of the cooperative binding

of DnaA to the origin region. Deleting the *soj-spo0J* operon results in a segregation phenotype leading to larger cells and a mild over initiation phenotype. Recently Murray and Koh[103] reported a Δ*soj* Δ*yabA* double mutant. This mutant overinitiates DNA replication and showed a decreased growth rate in rich media.
Geers reported that a triple deletion of *yabA* and *soj-spo0J* is lethal[104]. These results could not be confirmed. In contrast, a triple deletion strain was generated.

3.4.1. Construction of *PY79* Δ*yabA* Δ*soj-spo0J*

Competent cells harboring a *yabA* deletion were transformed with chromosomal DNA of a strain containing a deletion of the *soj-spo0J* operon. To verify the deletions, chromosomal DNA was extracted and test-PCRs were performed. In figure 13 the results of these experiments are depicted.

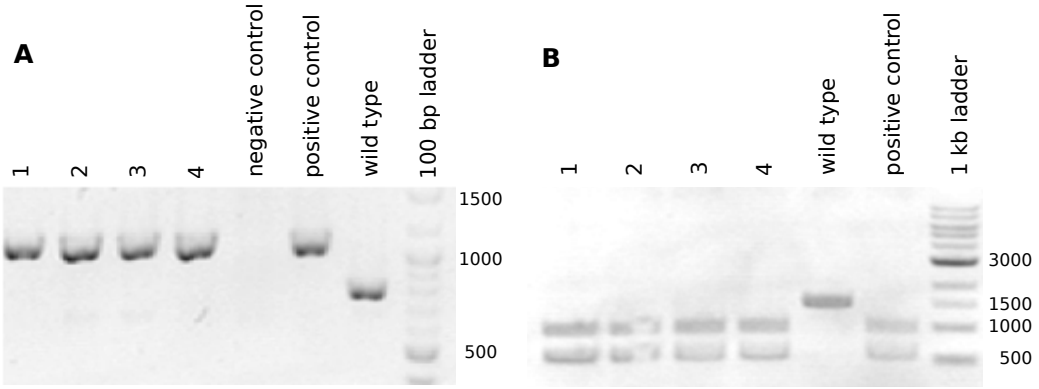

Figure 13: Agarose gels showing a test-PCR and a test-digest to verify successful deletion of *yabA* and *soj-spo0J*.
A Representative agarose gel showing a test-PCR to confirm successful deletion of *yabA* using primers 828/829. Numbers (1–4), four tested clones. The expected signal has a size of around 1100 bp compared to the wild type with 750 bp.
B Agarose gel with a *Kpn*I restricted test-digest of the purified PCR fragments obtained from a *soj-spo0J* test-PCR (test-PCR not shown). The first four lanes show the results of the four tested clones, followed by a wild type and a positive control. The last lane displays the DNA standard. The*Kpn*I restriction site resides within the spectinomycin resistance cassette used to select for the *soj-spo0J* deletion. Upon *Kpn*I restriction the 1500 bp fragment gets cut into a 1000 and 500 bp sized fragments.

In figure 13A the results of the test-PCR to verify the *yabA* deletion is shown. Four different clones were tested. In a wild type background a PCR performed with the primers used should give rise to a fragment of around 750 bp (figure 13A, lane: wild type). Upon successful generation of the deletion a phleomycin cassette disrupts the *yabA* gene and the expected size of the PCR fragment increases to 1100 bp (ref. figure 13A, lanes: 1–4 and positive control). All four tested clones still harbor the *yabA* deletion.
A second test PCR was performed to confirm the deletion of the *soj-spo0J* operon (data not shown). Here, the selected primer pair gives rise to a 1500 bp fragment for the wild type and the

deletion. Therefore the PCR fragments were purified (ref. section 2.2.2.) and then digested with the restriction enzyme *Kpn*I (figure 13 C). The spectinomycin cassette used for the deletion of the *soj-spo0J* operon contains a single *Kpn*I restriction site, which allows a differentiation between the wild type *soj-spo0J* operon and the deletion. All four tested clones shown in figure 13 C (lanes: 1–4) harbor the deletion as the PCR fragment of 1500 bp is cut in a 1000 bp and a 500 bp sized fragment.

3.4.2. Deleting *soj-spo0J* and *yabA* results in a mild growth defect and elongated cells

To investigate the effect of the single, double and triple deletions on cell growth, doubling times were determined. To this end the cells were grown in rich medium at 30 °C. The results of these experiments are depicted in table 13.

Single deletions of *yabA* or the *soj-spo0J* operon led to a mild growth defect. The doubling half times of the Δ*soj-spo0J* and Δ*yabA* strain are slightly increased (4 and 8%) compared to the doubling time of the wild type. A deletion of *yabA* and *soj-spo0J* showed a more severe effect on growth. The doubling time of the triple mutant is 30% higher than the one of the wild type.

Table 13: Doubling times of wild type and mutant cells

strain	**t_D* [min]**	**SD** [min]**
wild type	35.4	2.4
Δ*soj-spo0J*	36.7	2.9
Δ*yabA*	38.1	2.1
Δ*yabA* Δ*soj-spo0J*	46	3.2

Data was obtained from three independent experiments performed in two technical replicates.
* t_D: doubling time ** SD: standard deviation

To study the phenotypical effect of the deletions, fluorescence microscopy was performed. Using DAPI and FM4-64 to stain the DNA and membrane, respectively (figure 14) differences between the mutants were observed. For this analysis the cells were grown in rich medium at 30 °C.

Applying a membrane stain offered the opportunity to analyze the cell length of individual cells. Significant differences between the wild type and the mutant strains were observed. All data regarding measured cell length can be found in table 14.

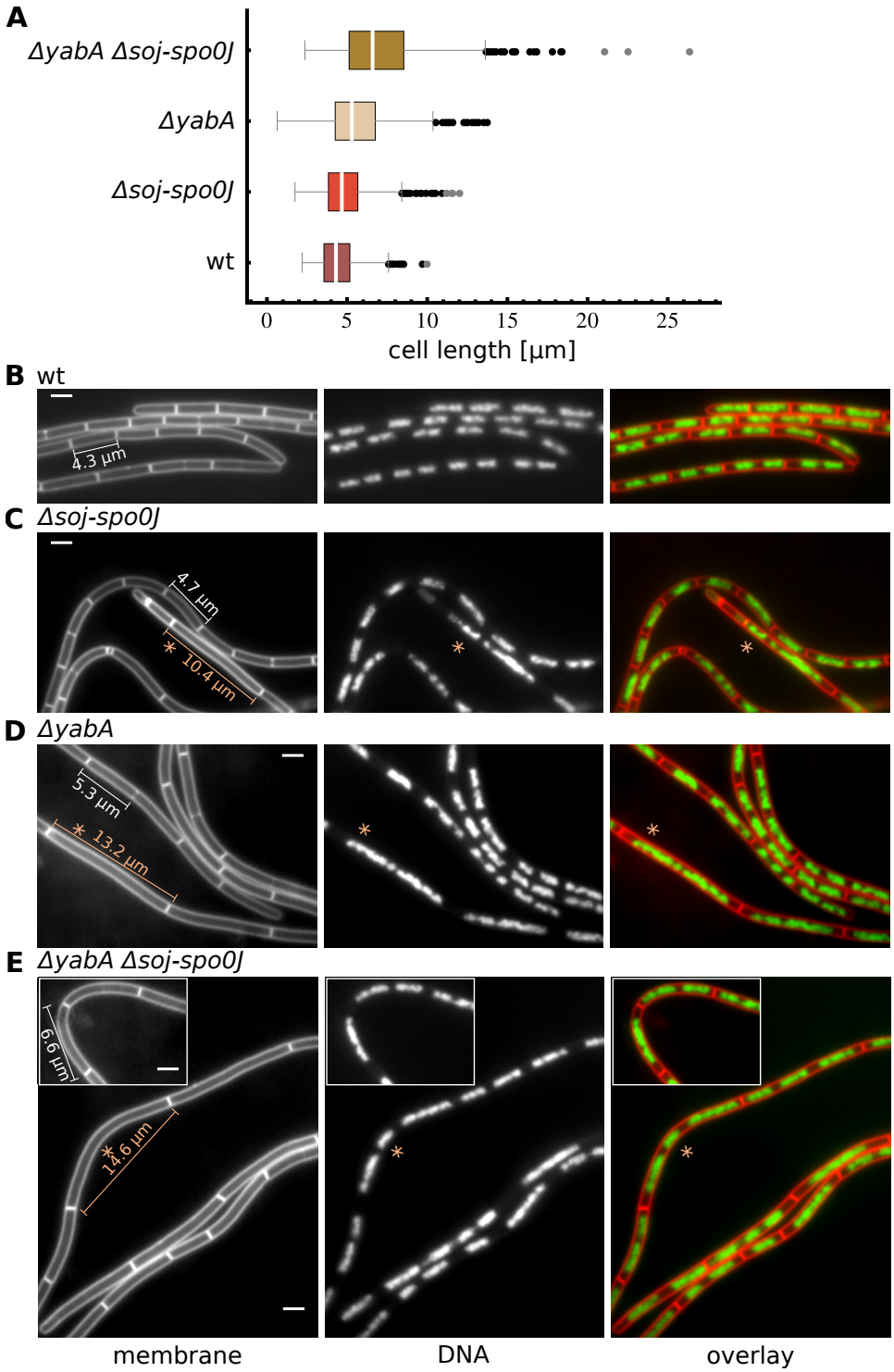

Figure 14: Cell length of wild type and mutant strains.
A Box plot showing measured cell length for wild type and deletion strains.
B–E Images of membrane and DNA stained cells as well as their overlays. Scale bars, 2 µm. White line segment, average cell length measured; orange line segment, example for an above-average elongated cell. Orange asterisk, highlights elongated cells in DAPI and overlay images. Wild type (B), Δ*soj-spo0J* (C), Δ*yabA* (D) and Δ*yabA*Δ*soj-spo0J* (E) cells.

A box-and-whisker diagram was used to illustrate the data obtained through cell length measurements (figure 14 A). Inside the box lies half of all data points measured, with the white line indicating the median of the data set. Whiskers extend until the last value inside the 1.5 interquartile range (ITR, length of the box). Points beyond are considered as outliers (back dots) or extreme values (3 ITR, grey dots).

Wild type cells were in average 4.3 µm in length (total of 1042 cells measured). Observed cells did not vary in length and showed a normal nucleoid distribution (figure 14 B).

Deletion of the *soj-spo0J* operon had an impact on the average cell length. Cells were around 4.7 µm in length and showed considerable segregation defects (figure 14 C, orange asterisk). Notably, the cells that displayed a segregation abnormality were also those which were considerably longer. This observations are in accordance with findings from Lee and Grossmann[86].

YabA is a negative regulator of DNA replication initiation. Deleting *yabA* resulted in an average cell length of 5.3 µm (total of 1032 cells measured). Similar to a *soj-spo0J* deletion an increasing number of largely elongated cells were observed. These cells contained several nucleoids probably due to overinitiation of replication (figure 14 D, orange asterisk).

Deletion of *yabA* and the *soj-spo0J* operon had the biggest impact on cell length (figure 14 E). The average cell length observed was increased to 6.6 µm (total of 1020 cells measured). Elongated cells contained several nucleoids and displayed segregation defects.

Table 14: Cell length of wild type and mutant strains

Strain	Median [μm]	Total no. of cells	Relative cell length
wild type	4.3	1042	1
Δ*soj-spo0J*	4.7	1013	1.1
Δ*yabA*	5.3	1032	1.2
Δ*yabA* Δ*soj-spo0J*	6.6	1020	1.5

Data was obtained from at least three independent experiments. Cells were grown in rich medium at 30 °C.

3.4.3. Deleting *soj-spo0J* and *yabA* results in an overinitiation phenotype

The investigation of the triple deletion *soj-spo0J yabA* displayed an increased cell length and a reduced doubling time. In order to investigate a possible overinitiation of replication, the origin was labeled using a repressor operator system. Essentially, the repressor of the lac operon, LacI, was labeled with a fluorophor and the operator sequence *lacO* was integrated near the *oriC* region. In doing so the origin of replication can be visualized.

Table 15: Number of origin foci per cell in wild type and mutant strains

strain	Average no. of foci per cell	SD*	Number of cells counted	Average no. of foci relative to wild type
wild type	2.07	0.62	882	1.0
Δ*soj-spo0J*	2.95	1.10	459	1.4
Δ*yabA*	5.76	2.90	494	2.8
Δ*yabA* Δ*soj-spo0J*	8.61	4.32	435	4.2

Data was obtained from at least two independent experiments performed in defined $S7_{50}$ minimal medium at 25 °C.
* SD: standard deviation of foci counted

To analyze whether Δ*soj-spo0J* Δ*yabA* cells overinitiate replication, a strain containing a CFP-labeled origin of replication together with a Δ*yabA* Δ*soj-spo0J* deletion was constructed (KS197). Cells were grown in $S7_{50}$ minimal medium at 25 °C and stained with FM4-64 to visualize the cell membrane and the number of CFP-signals per cell counted (figure 15). Analogously the number of CFP foci per cell in the single deletions and wild type cells were analyzed.

Wild type cells contained under the tested conditions in average two (2.07 ± 0.62) origins per cell (figure 15 A).

Cells with a Δ*soj-spo0J* deletion contained around three (2.95 ± 1.1) origin foci per cell (figure 15 B, orange asterisk). In relation to wild type cells a 1.4 times overinitiation was observed (table 15). This results are in accordance to previous findings reported by Lee and Grossmann[86].

Deleting *yabA* resulted in a 2.8 times overinitiation (table 15). In average six (5.76 ± 2.9) foci are visible per cell (figure 15 C).

A drastic overinitiation in a *yabA soj-spo0J* deletion strain was observed. Around nine (8.61 ± 4.32) origin of replication foci per cell were witnessed (figure 15 D). This corresponds to a 4.2 times overinitiation compared to wild type levels (table 15). So a deletion of two regulators of DNA replication initiation leads to an overinitiation.

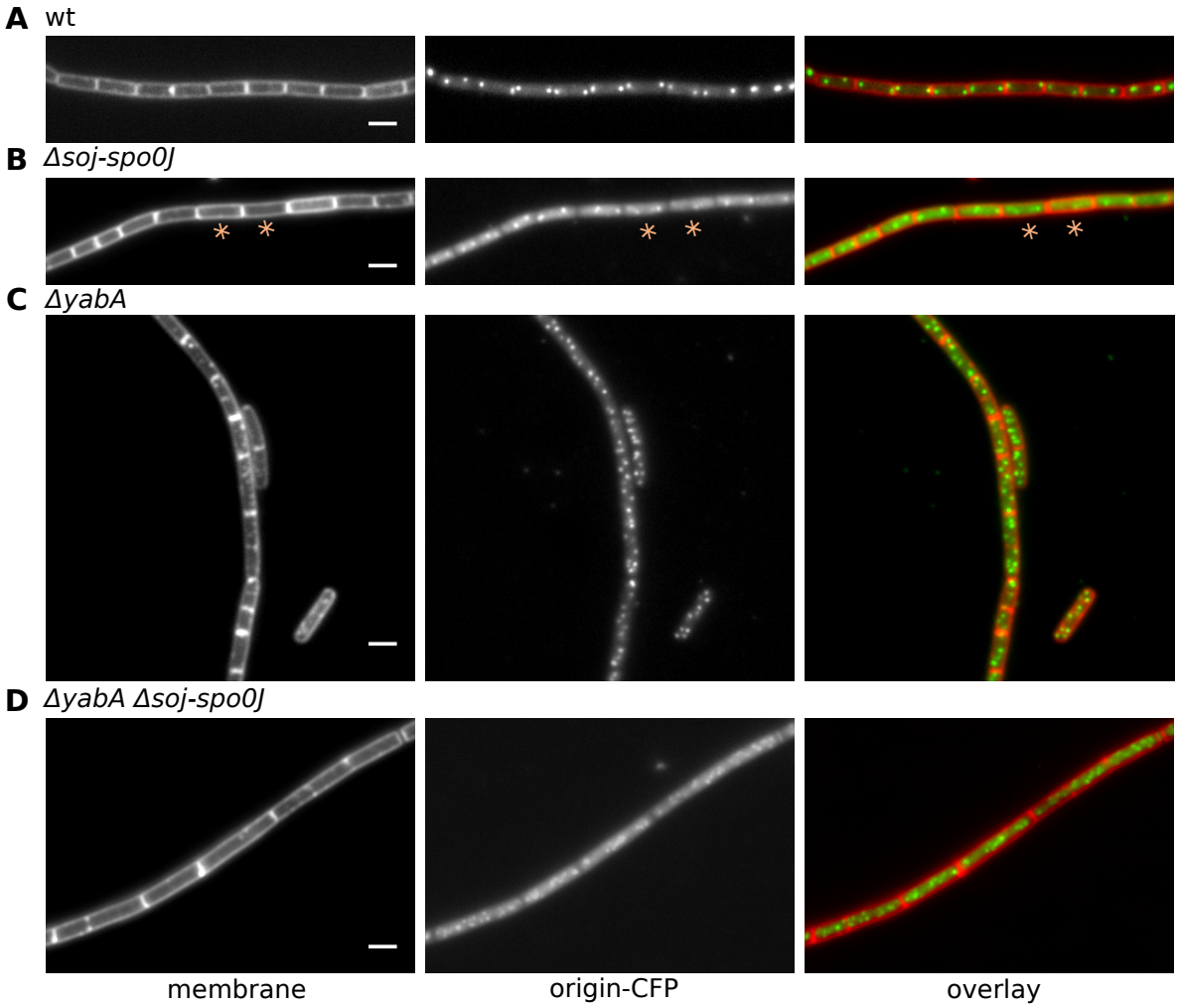

Figure 15: Localization of the CFP-labeled origin of replication in wild type and mutant strains.
Fluorescence microscopy images showing the CFP-signal of wild type and mutant cells. Overlays combine both signals, membrane stain (red) and CFP-labeled origin of replication (green).
Localization of the CFP-labeled origin signal in wild type (A), Δ*soj-spo0J* (B), Δ*yabA* (C) and Δ*soj-spo0J*Δ*yabA* cells (D).
Scale bars, 2 μm; orange asterisk, abnormal localization pattern.

3.5. FRAP analysis

FRAP, Fluorescence recovery after photobleaching, is a microscope technique that is commonly used to investigate the dynamic behavior of fluorescently labeled proteins. A focused laser beam is used to bleach an area of interest inside a cell and then fluorescence recovery over time is monitored. Background fluorescence is subtracted and fluorescence recovery is normalized for acquisition bleaching. To correct for different bleaching depths and intensities, the relative fluorescence before and after bleaching was normalized.
In the following experiments this technique was used to investigate the dynamics of YFP-DnaA in different deletion backgrounds and in functional YFP-DnaA single amino acid substitutions as well as for a YFP-YabA strain.

3.5.1. FRAP measurements of YFP-DnaA

DnaA, the highly conserved initiator of DNA replication in bacteria, is tightly regulated. In *B. subtilis* a spatially sequestration of DnaA mediated by YabA was described[2]. The initiator of DNA replication DnaA is thought to either bind tightly to specific DNA sequences (DnaA boxes) in the *oriC* region or to be tethered to the replication machinery via YabA. In a cell grown in minimal medium at low temperatures one to two YFP-DnaA foci can be observed. I was interested whether the YFP-DnaA molecules bound in this foci displayed any dynamic behavior. To this end FRAP experiments were performed.
In the following experiment FRAP analysis was used to determine the recovery half time, the average residence time and the existence and extend of a possible immobile fraction for YFP-DnaA. To this end a strain harboring an inducible copy of YFP-DnaA and a CFP-labeled origin (ME15), was grown in defined $S7_{50}$ minimal medium at 25 °C. Expression of YFP-DnaA was induced for 30 min with 0.1% xylose (w/v). Under this conditions YFP-DnaA preferentially colocalizes with the origin of replication. Note that in this strain an unlabeled wild type copy of DnaA exists. For results on a strain expressing YFP-DnaA from its original locus refer to the last passage of this section.
Upon bleaching the region of interest, a fast fluorescence recovery was observed (figure 16 A, white triangle). On the basis of normalized fluorescence recovery over time the recovery half-time for each experiment was calculated (figure 16 B). For YFP-DnaA a recovery half-time of 2.9 $\pm$ 0.2 s was observed (Mean $\pm$ standard error of the mean (SEM), standard deviation (SD)=1.7 s, n=61 experiments).
Based on the recovery half-time the average residence time of YFP-DnaA was determined ($t_{1/2}$/ln2). Over all the experiments conducted YFP-DnaA stayed for 4.2 $\pm$ 0.3 s inside the bleached area, the area of interest (figure 16 A, dashed circle).
If all molecules inside the cell analyzed are able to move freely, the relative fluorescence recovery, when normalized to the fluorescence intensity of the entire cell, should reach 100%. If this is

not the case, then the difference between the plateau reached by the recovery curve and the 100% define the extent of the immobile fraction of molecules. These molecules are firmly bound during the time course of the experiment and can therefore not move freely inside the cell. This does not imply that the mobile molecules are freely diffusing molecules. In this case only an unsubstantial amount of 10.3 ± 1.2% immobile molecules was detected.

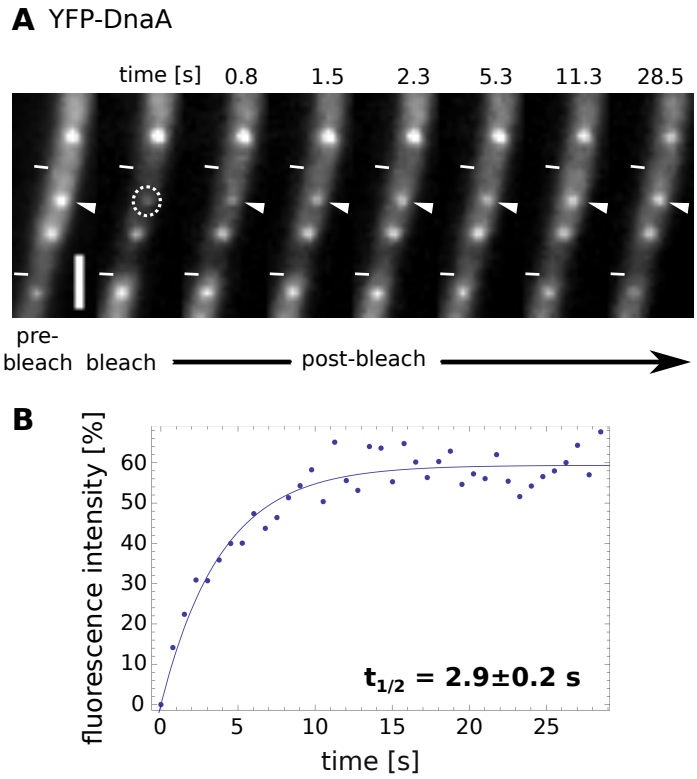

Figure 16: FRAP measurements of YFP-DnaA
A FRAP sequence of YFP-DnaA, showing recovery of the fluorescence signal in the region of interest over time. White triangle, region of interest. White dashed circle, area bleached. White lines, cell borders; scale bar, 2 µm. **B** Fluorescence intensity (%) plotted over time (s). Blue line represents fit used to calculate the recovery half-time. Diagram displays data obtained from a single experiment shown in (A). The calculated recovery half-time for YFP-DnaA determined from 61 experiments is 2.9 ± 0.2 s (Mean ± SEM).

FRAP measurements in a strain expressing a fully functional YFP-DnaA fusion from the original locus obtained similar results (CDS2[2]). In this case the observed recovery half-time was 2.5 ± 0.3 s (SD=1.5 s, n=32 experiments). In average the YFP-DnaA molecules stayed for 3.6 ± 0.4 s inside the observed area. The percentage of immobile molecules observed was 10.4 ± 1.2%, indicating that over all the experiments conducted the amount of immobile molecules are negligible.

3.5.2. FRAP measurements of YFP-DnaA in deletion strains

3.5.2.1. Deletion of *yabA* decelerates YFP-DnaA movement

Deletion of *yabA* results in an overinitiation of DNA replication[73]. YFP-DnaA displayed a high dynamic, presumably assembling and disassembling at *oriC*. I was interested whether the dynamic behavior of YFP-DnaA would change upon deletion of *yabA*.
A strain expressing YFP-DnaA from the original locus under xylose induction combined with a *yabA* deletion was generated (KS171). Cells were grown in $S7_{50}$ minimal medium containing 0.5% xylose (w/v) at 25 °C.

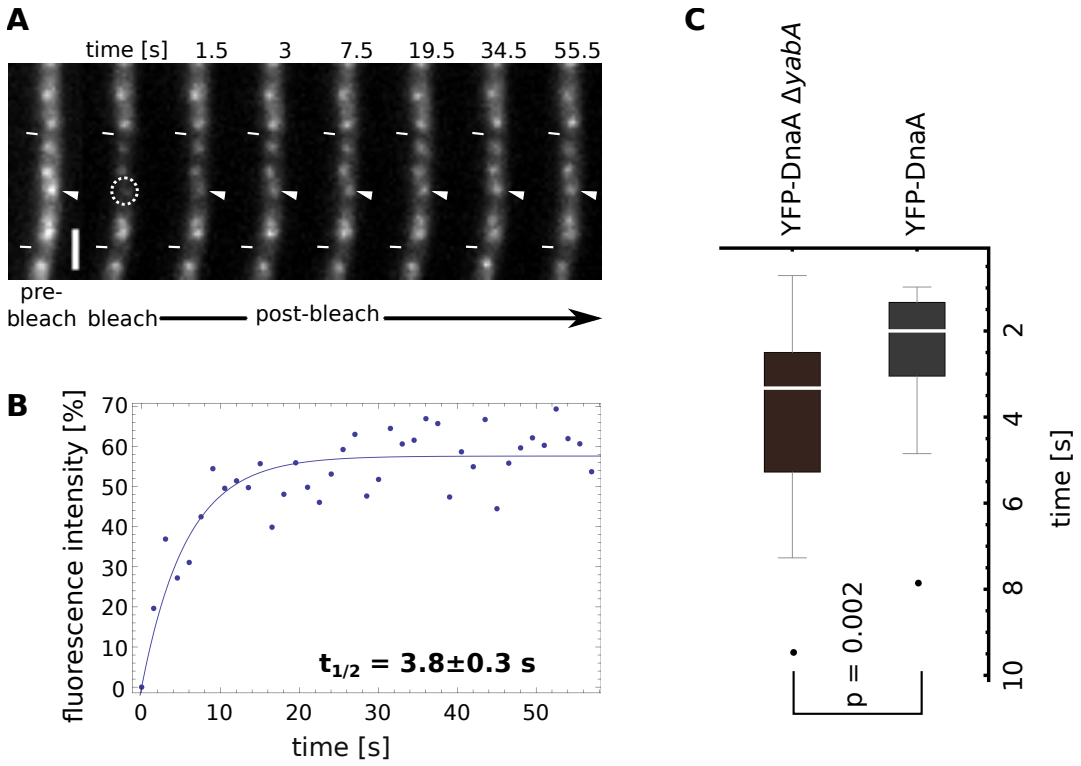

Figure 17: FRAP measurements of YFP-DnaA in a Δ*yabA* deletion strain.
A FRAP sequence showing the recovery of YFP-DnaA fluorescence signal after bleaching. White triangle, area of interest; white dashed circle, bleached area. White lines, cell borders; scale bar, 2 µm. **B** Fluorescence intensity plotted over time. Blue line, fit. Recovery half-time determined out of 42 experiments is 3.8 ± 0.3 s. **C** Box-plot showing the distribution of the calculated recovery half-times for YFP-DnaA (CDS2) and YFP-DnaA Δ*yabA* (KS171). Black dots are considered outliers (lie outside of 1.5 ITR). A significant differnce between both strain was observed (probability (p)=0.002, students t-test).

A FRAP image sequence and the corresponding recovery plot are shown in figure 17 A and B. As previously reported, a deletion of *yabA* has an impact on the localization pattern of YFP-DnaA[2]. In the cell displayed 5 YFP-DnaA foci are visible (figure 17 A), whereas in a wild type strain grown under the same conditions 1–2 foci were observed (figure 16 A).
The recovery half-time of YFP-DnaA in a *yabA* deletion strain (KS171) was significant lower

than in the wild type strain (CDS2, students t-test, probability (p)=0.003). The recovery half-time determined from 42 experiments was 3.8 ± 0.3 s (SD=2.0 s, n=42 experiments). A box-and-whisker diagram was used to visualize the recovery half-times obtained for the two strains tested. Black dots indicate outliers (outside 1.5 ITR). The average residence time of YFP-DnaA in a *yabA* deletion was 5.5 ± 0.4 s. Similar to the wild type strain, no substantial portion of immobile molecules was detected (10.8 ±1.2%).

3.5.2.2. YFP-DnaA dynamic slows down upon *soj-spo0J* deletion

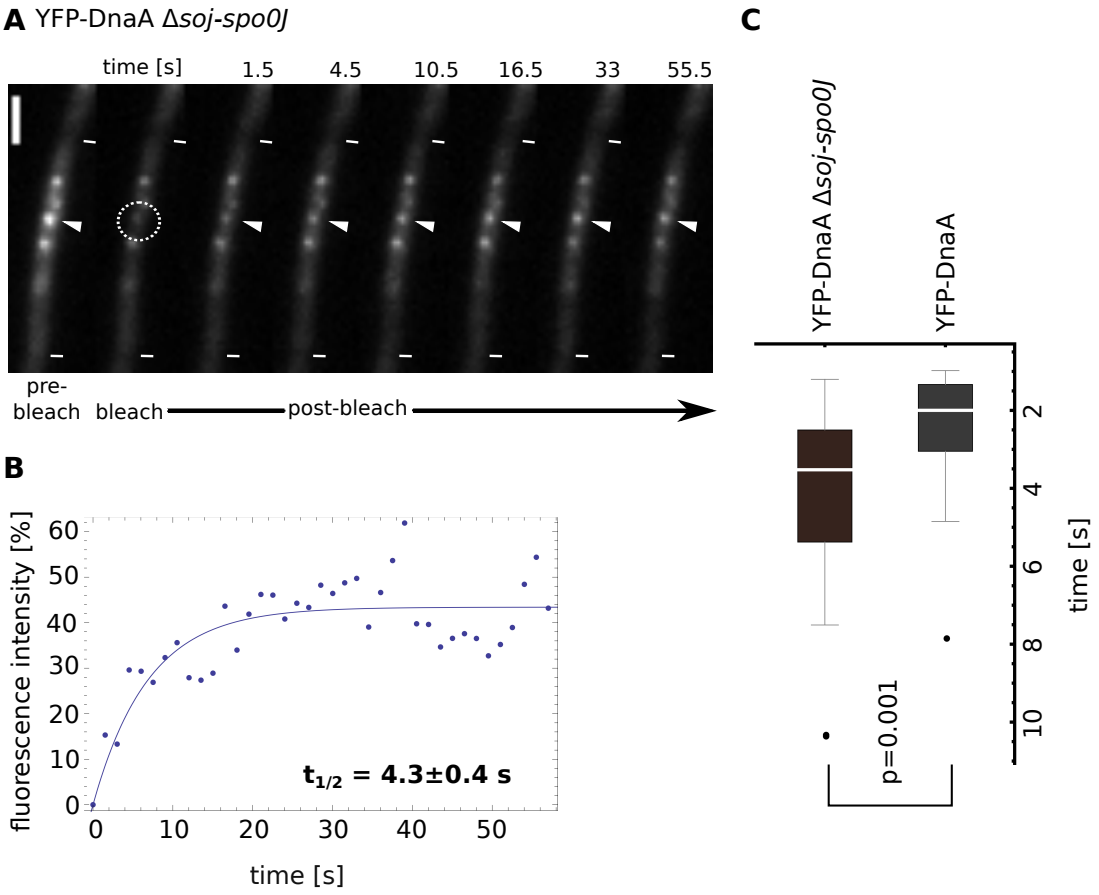

Figure 18: FRAP measurements of YFP-DnaA in a Δ*soj-spo0J* deletion strain.
A FRAP sequence showing the recovery of YFP-DnaA fluorescence signal after bleaching. White triangle, area of interest; white dashed circle, bleached area. White lines, cell borders; scale bar, 2 µm. **B** Fluorescence intensity plotted over time. Blue line, fit. Recovery half-time conducted from 32 experiments is 4.3 ± 0.4 s. **C** Box-plot showing the distribution of the calculated recovery half-times for YFP-DnaA (CDS2) and YFP-DnaA Δ*soj-spo0J* (KS175). Black dots are considered outliers (lie outside of 1.5 ITR). A significant difference between both strain was observed (p=0.001, students t-test).

A deletion of *soj-spo0J* is characterized by a mild overinitiation of replication combined with slightly elongated cells and segregation defects (section 3.4.)[86]. To study whether a deletion of the *soj-spo0J* operon would result in a similar alteration of YFP-DnaA behavior, as shown

for a *yabA* deletion, a strain with a xylose inducible copy of *yfp-dnaA* at the original locus was transformed with chromosomal DNA of a strain harboring a *soj-spo0J* deletion. The resultant strain (KS175) was grown in minimal medium with 0.5% xylose (w/v) at 25 °C.

Deletion of *soj-spo0J* alters the localization of YFP-DnaA (figure 18 A). Geers reported the presence of 5–7 YFP-DnaA foci in Δ*soj-spo0J* cells[104].

FRAP experiments showed that YFP-DnaA has a significant reduced recovery half-time compared to the wild type strain (p=0.001, figure 18 C). The recovery half time calculated for YFP-DnaA in a *soj-spo0J* deletion strain is 4.3 ± 0.4 s (SD=2.3 s, n=32 experiments, figure 18 B). In average the YFP-DnaA molecules stayed for 6.1 ± 0.6 s inside the area of interest.

Around 14.6 ± 1.4% of immobile molecules were detected. Compared to the amount of immobile molecules in the wild type strain no significant difference was observed (students t-test, p=0.1).

3.5.2.3. A fraction of YFP-DnaA molecules becomes increasingly static upon deletion of *soj-spo0J* and *yabA*

Deleting *yabA* or *soj-spo0J* resulted in an increased recovery half-time for YFP-DnaA compared to the wild type strain. To address this issue further, a triple deletion strain, harboring a *yabA* and a *soj-spo0J* deletion as well as expressing a YFP-DnaA fusion from the original locus was investigated (KS180). The cells were grown in minimal medium at 25 °C under xylose induction.

Deletion of *yabA* and *soj-spo0J* resulted in a strong overinitaition of replication and cell elongation as well as a substantial growth defect. As for the single deletions an altered localization pattern for YFP-DnaA was observed. The cell displayed in figure 19 A contains 5 YFP-DnaA foci, indicating an increase in YFP-DnaA foci compared to the wild type strain.

Image series from FRAP experiments as well as the corresponding fluorescence recovery curve are shown (figure 19 A, B). Surprisingly the YFP-DnaA molecules in the triple deletion strain displayed a similar recovery half-time as in the wild type. The measured recovery half-time is 2.9 ± 0.3 (SD=1.4 s, n=29 experiments), resulting in an average residence time of 4.1 ± 0.4 s.

The amount of immobile molecules was analyzed. Surprisingly, 23.4 ± 2.1% of immobile molecules were detected. This is a significant difference to the amount of immobile molecules observed in the wild type strain (students t-test, p=0.00001), indicating that an increased fraction of molecules are tightly bound during the time course of the experiment.

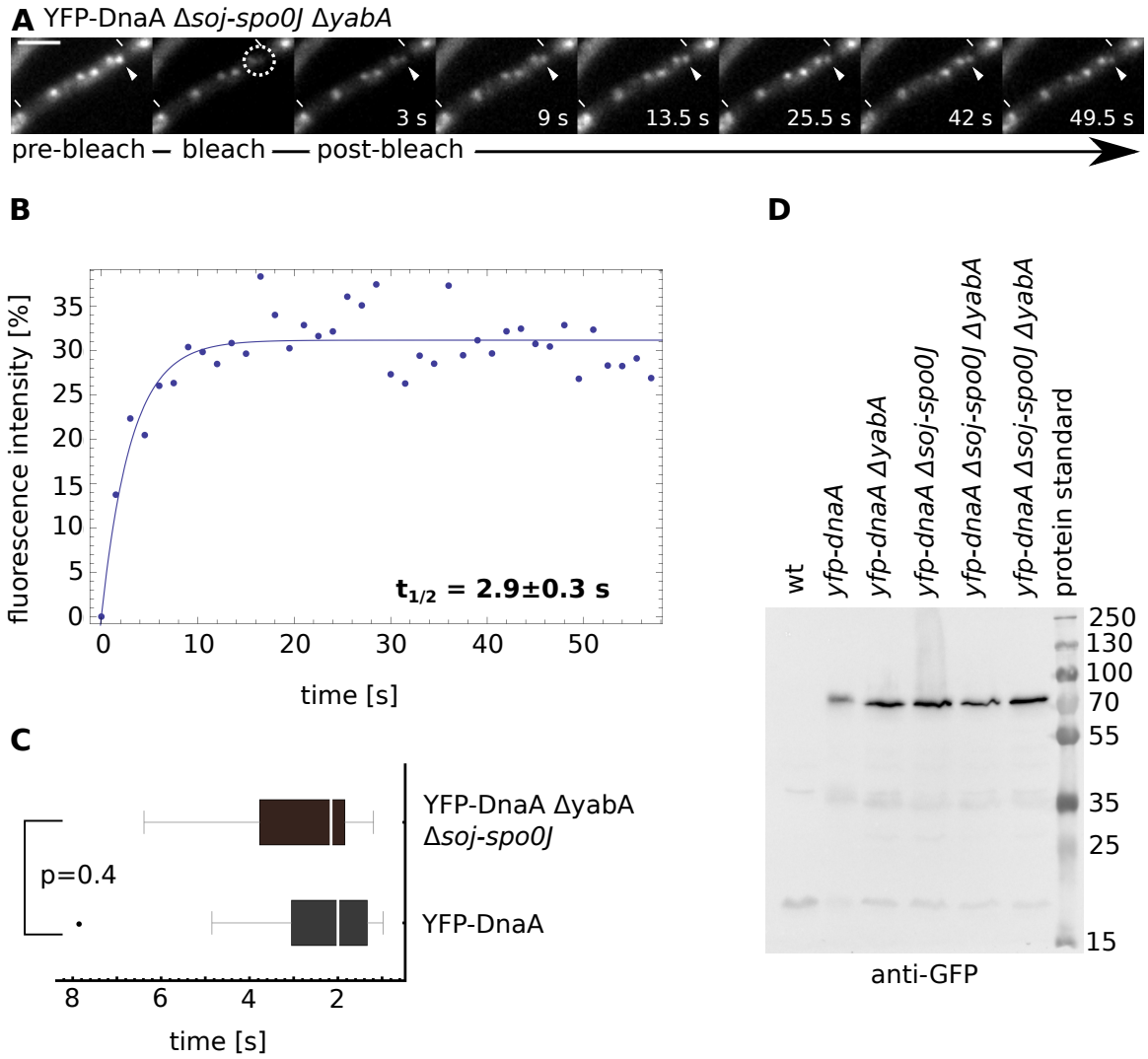

Figure 19: FRAP measurements of YFP-DnaA in a Δ*soj-spo0J* Δ *yabA* deletion strain.
A FRAP sequence showing the recovery of YFP-DnaA fluorescence signal after bleaching. White triangle, area of interest; white dashed circle, bleached area. White lines, cell borders; scale bar, 2 µm. **B** Fluorescence intensity plotted over time. Blue line, fit. Recovery half-time calculated from 29 experiments is 2.9 ± 0.3 s. **C** Box-plot showing distribution of calculated recovery half-times for YFP-DnaA (CDS2) and YFP-DnaA Δ*soj-spo0J*Δ *yabA* (KS180). Black dots are considered outliers (lie outside of 1.5 ITR). No significant difference between both half-times were detected (p=0.3, students t-test). **D** Western blot analysis of wild type and mutant cell extracts using *α*-GFP antiserum. The expected size for YFP-DnaA fusion protein is 78 kDa.

Data obtained from all FRAP experiments so far are summarized in table 16. A western blot was performed to verify that all strains in which a FRAP analysis was performed harbored a YFP-DnaA fusion (figure 19 D). The signal corresponding to the size of YFP-DnaA can be seen at 78 kDa.

Table 16: Data obtained from FRAP measurements of YFP-DnaA in deletion backgrounds.

Strain	Recovery half-time [s]	Average residence time [s]	Immobile fraction [%]	No. of experiments
YFP-DnaA (ME15)	2.9 ± 0.2	4.2 ± 0.3	10.3 ± 1.2	61
YFP-DnaA (CDS2)	2.4 ± 0.3	3.6 ± 0.4	10.4 ± 2.0	32
YFP-DnaA Δ*yabA* (KS171)	3.8 ± 0.3	5.5 ± 0.4	10.8 ± 1.2	42
YFP-DnaA Δ*soj-spo0J* (KS175)	4.3 ± 0.4	6.1 ± 0.6	14.6 ± 1.4	32
YFP-DnaA Δ*soj-spo0J*Δ*yabA* (KS180)	2.9 ± 0.3	4.1 ± 0.4	23.4 ± 2.1	29

Data represents means and SEM of FRAP experiments. Experiments were performed in defined $S7_{50}$ minimal medium at 25 °C.

3.5.3. FRAP measurements of YFP-DnaA carrying single amino acid substitutions

3.5.3.1. YFP-DnaA displays a high turnover rate at the replication machinery

In the following experiment a YFP-labeled single amino acid substitution of DnaA was investigated. The mutation R387C has been shown by Eisemann to be impaired in DNA binding and thus inactive in transcriptional autoregulation[33]. As this version of YFP-DnaA is unable to bind to DNA, no colocalizations with the origin of replication should occur.

In order to determine a possible difference in YFP-DnaA turnover between the *oriC* region and to the replication machinery, a strain expressing an inducible ectopic copy of YFP-DnaAR387C and a CFP-labeled origin was used (ME21). Cells were grown in minimal medium at 25 °C. Induction of the fusion protein was accomplished through incubation with 0.1% xylose (w/v) for 30 min.

A FRAP image sequence shows the recovery of the fluorescence signal (figure 20 A). Overlay displayed origin-CFP signal (red) combined with YFP-DnaAR260A signal (green) indicating that both signals are not colocalizing. The recovery half-time for YFP-DnaAR387C molecules is 2.5 ± 0.4 s (SD=2.2 s, total of 33 experiments performed), suggesting no significant difference to wild type molecules (p=0.4). Hence, no difference in the turnover rate between the *oriC* region and the replication machinery was found. The resulting average residence time is 3.6 ± 0.5 s. Around 9.1 ± 2.1% of the YFP-DnaAR387C molecules were immobile, which is similar to wild type YFP-DnaA molecules.

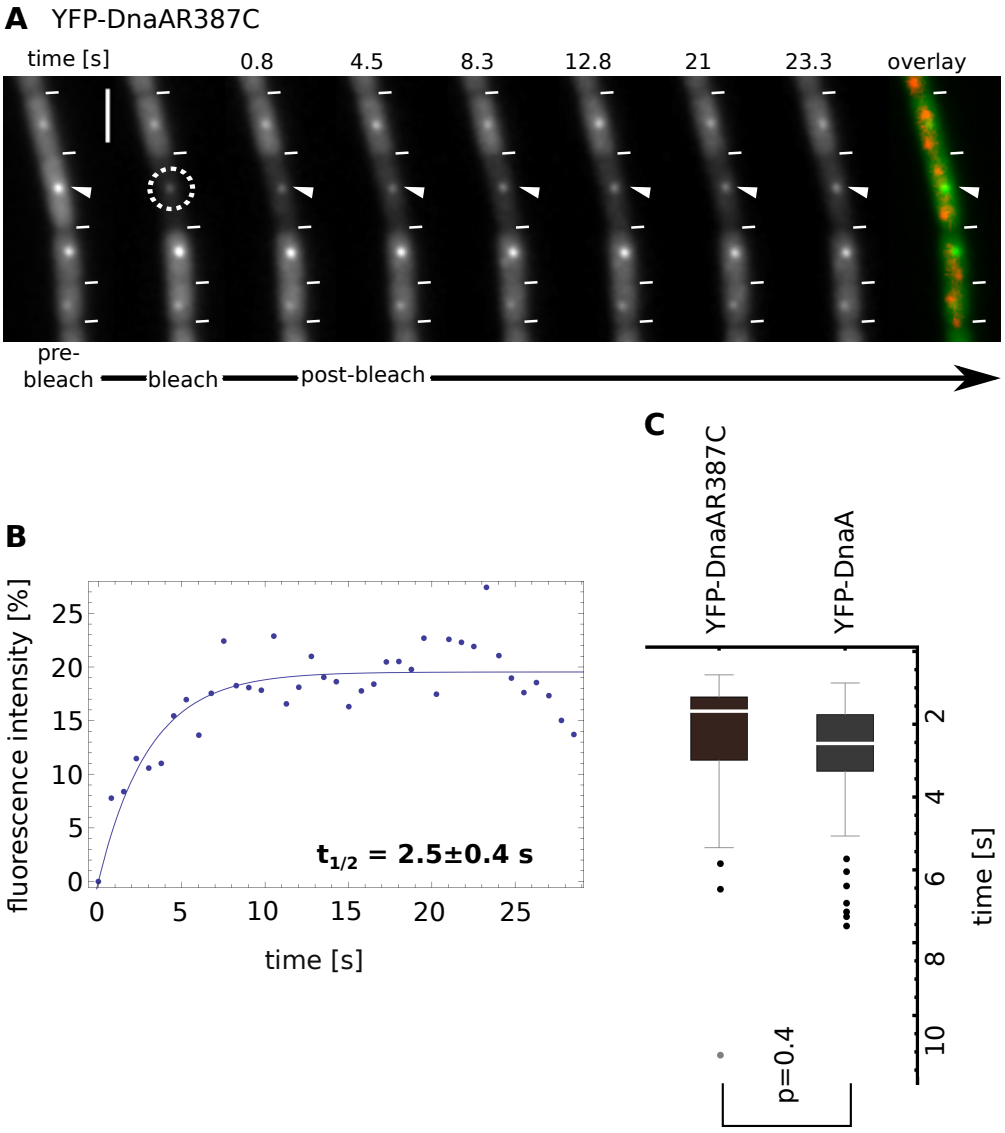

Figure 20: FRAP measurements of YFP-DnaAR387C.
A FRAP sequence showing the recovery of YFP-DnaAR387C fluorescence signal after bleaching. White triangle, area of interest; white dashed circle, bleached area. White lines, cell borders; scale bar, 2 µm. **B** Fluorescence intensity plotted over time. Blue line, fit. Recovery half-time is 2.5 ± 0.4 s. **C** Box-plot showing calculated recovery half-times for YFP-DnaA (ME15) and YFP-DnaAR387C (ME21). Black dots are considered outliers and grey dots extreme values (lie outside of 1.5 ITR or 3 ITR, respectively). No significant difference between both half-times could be detected (p=0.4, students t-test).

3.5.3.2. Impaired ATPase activity leads to longer residence time of YFP-DnaA

The R260A DnaA mutant was shown to have a 1.5 fold reduced ATP-binding and a 2 fold reduced ATPase activity (Eisemann, 2012). Furthermore cells were reported to be significantly smaller compared to wild type cells. The substituted arginin resides inside the box VII motif in domain III of the DnaA protein.
FRAP analysis of YFP-DnaAR260A mutants showed an increased half-time recovery compared

to wild type measurements (figure 21 A, p=0.0002). The calculated recovery half-time for YFP-DnaAR260A was 4.1 ± 0.2 s (SD=1.9 s, n=82 experiments), resulting in an average residence time of 5.9 ± 0.3 s. The amount of immobile molecules was similar to that observed in the wild type strain (10.4 ± 1.9%).

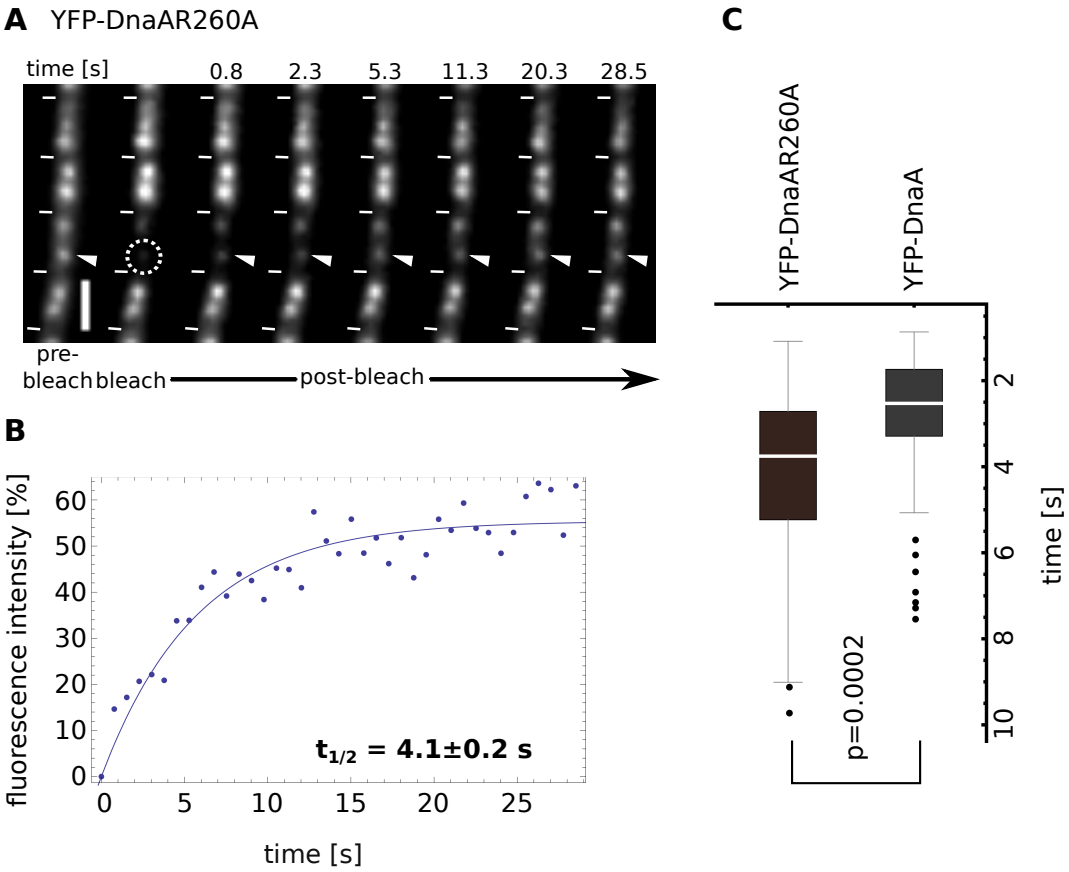

Figure 21: FRAP measurements of YFP-DnaAR260A.
A FRAP sequence showing the recovery of YFP-DnaAR260A fluorescence signal after bleaching. White triangle, area of interest; white dashed circle, bleached area. White lines, cell borders; scale bar, 2 µm.
B Fluorescence intensity plotted over time. Blue line, fit. Recovery half-time is 4.1 ± 0.2 s.
C Box-plot showing distribution of calculated recovery half-times for YFP-DnaA (ME15) and YFP-DnaAR260A (ME18). Black dots are considered outliers (lie outside of 1.5 ITR). A highly significant difference between both half-times was detected (p=0.0002).

3.5.4. YFP-YabA displays similar dynamics as YFP-DnaA

YabA is a negative regulator of initiation of DNA replication. As YFP-DnaA showed a highly dynamic behavior I was interested how YFP-YabA would behave in a FRAP experiment. FRAP experiments were performed in a strain expressing an inducible ectopic copy of YFP-YabA in a *yabA* strain. The cells were grown in $S7_{50}$ minimal medium at 25 °C and YFP-YabA expression was induced by addition of 30 µM IPTG.
Like YFP-DnaA, YFP-YabA showed a fast recovery after bleaching (figure 22 A). The recovery

half-time calculated from 36 experiments was 2.3 ± 0.2 s (SD=1.5 s, n=36 experiments), which is similar to the recovery half-time measured for YFP-DnaA (CDS2, p=0.6). Furthermore the average residence time was determined (3.3 ± 0.3 s).
In the YFP-YabA strain a higher amount of immobile molecules than in the YFP-DnaA strain were detected. A total of 19.7 ± 2.1% of all molecules were immobile (p=0.002, figure 22 C).

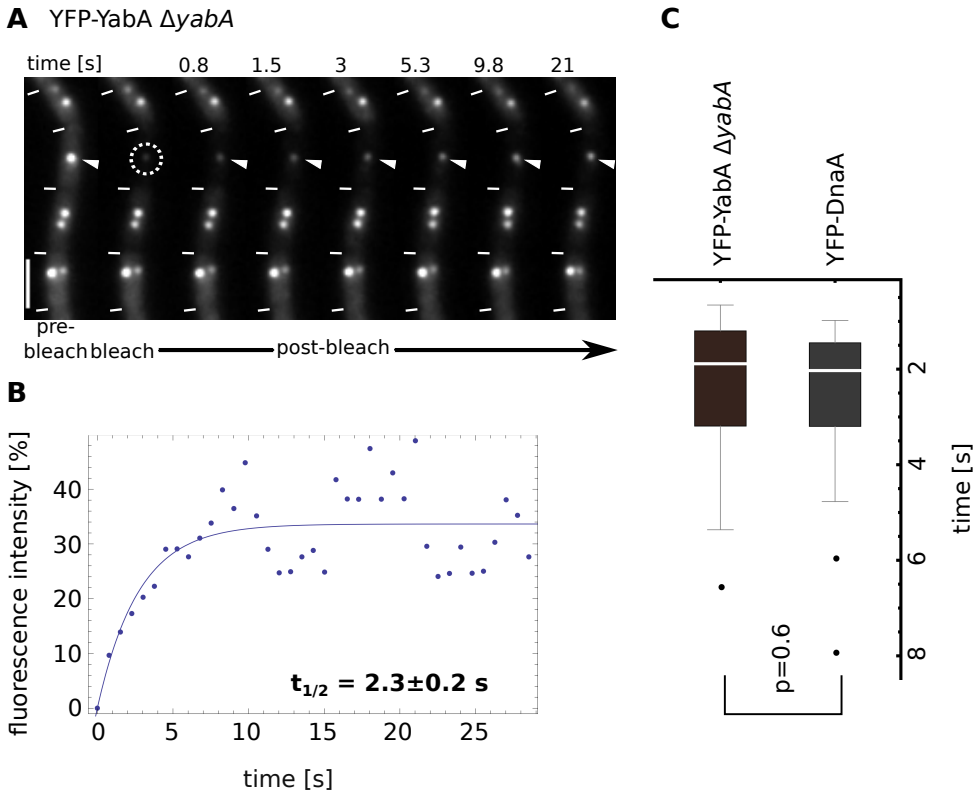

Figure 22: FRAP measurements of YFP-YabA.
A FRAP sequence showing the recovery of YFP-YabA fluorescence signal after bleaching. White triangle, area of interest; white dashed circle, bleached area. White lines, cell borders; scale bar, 2 µm. **B** Fluorescence intensity plotted over time. Blue line, fit. Recovery half-time is 2.3 ±0.2 s (SD=1.5 s). **C** Box-plot showing distribution of calculated recovery half-times for YFP-DnaA (CDS2) and YFP-YabA (KS173). Black dots are considered outliers (lie outside of 1.5 ITR). YFP-YabA and YFP-DnaA displayed a similar dynamic behavior (p=0.6).

3.6. *E. coli* DnaA-eYFP oscillates between cell halves

So far localization studies of DnaA in *E. coli* reported DnaA to either localize as discrete foci colocalizing with the *oriC* or the *datA* region or in a helical pattern along the long axis of the cell, similar but locally distinct from MreB helices[24,25].
I used a functional chromosomal DnaA-eYFP sandwich fusion (gift of Hironori Niki, National Institute of Genetics (NIG), Japan) to perform FRAP experiments in order to compare these results to the ones obtained for *B. subtilis* YFP-DnaA (section 3.5.1.). As the fluorescence signal

seemed to be oscillating between the two cell halves, it was impossible to follow the fluorescence recovery over time.
Instead of performing FRAP experiments, 200 ms streams were acquired using a 515 nm laser. The images of the cells acquired contained depending on the cell length up to four DnaA signals per cell. For the following analysis only small cells containing two foci, probably colocalizing with the origin of replication (personal communication Shingo Nozaki, NIG, Japan), were used. In these cells the fluorescence intensity inside the areas around the two foci was measured, the background subtracted and the fluorescence intensity normalized to the total fluorescence of the whole cell. Then the fluorescence intensity of both areas over time was plotted (figure 23 A). An alternation of fluorescence intensities in area 1 (black) and area 2 (green) was observed. The fluorescence images displayed above correspond to fluorescence intensity maxima, showing the oscillation of the DnaA-eYFP signal between the two measured areas. The brightfield image contains two colored circles indicating which area belongs to which fluorescence signal.
From the previous analysis a negative correlation between the two foci in the two cell halves was suspected. To investigate the extend of the correlation the Pearson product correlation coefficient (Pearson's r) was calculated. The coefficient can adopt a value between +1 and -1, with -1 being a perfect negative correlation, 0 no correlation and +1 for a perfect positive correlation. Comparing the fluorescence intensity of area 1 to area 2 a coefficient of $r = -0.79$ was calculated, supporting the hypothesis of a negative correlation between the two regions (figure 23 D).
DnaA is able to bind to *dnaA* boxes inside the *oriC* region. This area is also highly transcribed. To investigate weather the DNA-dependent RNA polymerase is responsible for the oscillating behavior of DnaA-eYFP, cells were grown until early exponential phase before adding 200 µg/ml rifampicin. Rifampicin inhibits transcription by binding to the DNA-dependent RNA polymerase. Samples were analyzed every 30 min for 3 h. Investigation of the oscillation behavior of a sample treated with rifampicin for 30 min showed no significant difference to untreated samples (figure 23 B and E). Still a very strong negative correlation ($r = -0.73$) was observed, indicating that the oscillating behavior is not due to DNA-dependent RNA polymerase removing DnaA from its binding sites. This was also seen in samples treated longer with rifampicin (data not shown).
As a control strain a *B. subtilis* strain expressing TetR-YFP binding to a *tetO* array near the origin of replication (KS188) was used. It served as an example for a strain containing two fluorescence signals per cell but without having a correlation between the two regions (figure 23 C & F). The 100 ms stream using a 515 nm laser was acquired by Nina El Najjar (Synmikro, Philipps University Marburg). No correlation between the two areas surrounding the two foci was observed ($r = -0.002$).

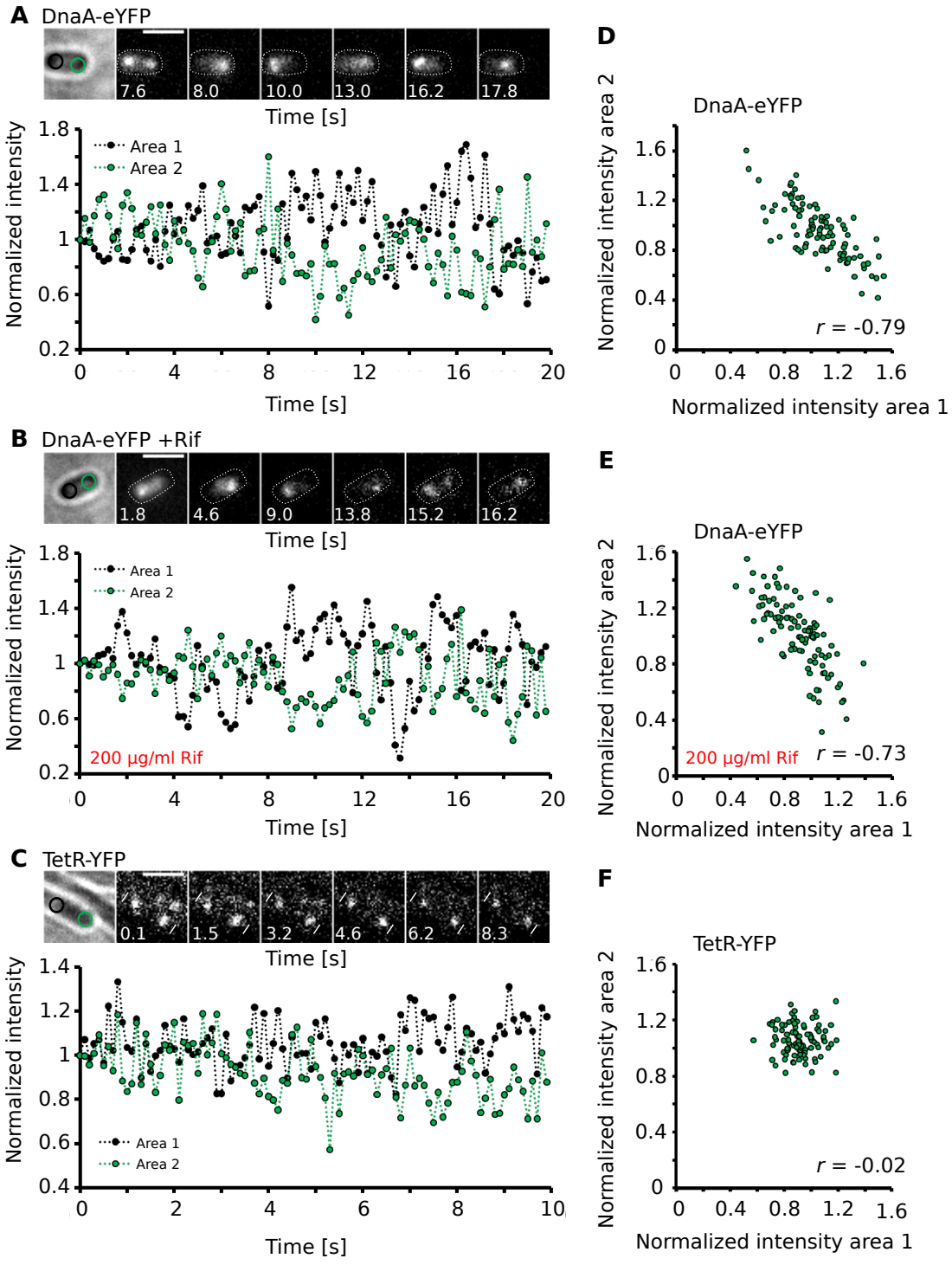

Figure 23: Oscillation of DnaA-eYFP in *E. coli*.
Fluorescence microscopy images of *E. coli* cells expressing DnaA-eYFP (A) with 200 µg/ml rifampicin (B) and *B. subtilis* cells expressing TetR-YFP binding to a *tetO* array near *oriC* (C). Fluorescence intensities of two areas, each containing one fluorescence signal, were measured and normalized to the total fluorescence intensity of the cell. Intensities of both areas were plotted over time. Area 1 (green) and area 2 (black). Image sequences displaying the oscillation of DnaA-eYFP (A–B) and the static TetR-YFP (C) are shown. White lines, cell borders; scale bars, 2 µm; white dashed lines, cell outlines; black open circle, area 1; green open circle; area 2. To visualize the correlation between the two measured areas they were plotted against each other (D–F). Correlation coefficients (r) were determined.

3.7. Single molecule (SM) microscopy

To follow up the results obtained by FRAP experiments, single molecule (SM) microscopy was performed.
This microscopy technique uses a focused laser beam to highly illuminate a small part of the specimen. Photobleaching of the specimen in this area occurs fast and single molecules can be detected. To analyze the movement of single molecules, 2000 frames of 41 ms streams were acquired. Once most molecules had been bleached, single molecules were observed and manually tracked using the MTrackJ plugin from Fiji ImageJ[102,99]. To further investigate the trajectories obtained, the SDFFS program (section 2.7.3.2., program version 15/12/2014) was used. This program was generated by Prof. Bernhard Schmitt from the mathematics department of the Philipps-University Marburg, Germany. Only those tracks, whose signal was detectable for at least 4 frames were analyzed.

3.7.1. YFP-DnaA is highly dynamic at the single molecule level

For single molecule experiments a strain expressing an ectopic copy of YFP-DnaA (ME15) was used. The cells were grown at 25 °C in M9 minimal medium until early exponential phase. The expression of YFP-DnaA was repressed by addition of 0.5% glucose (w/v) to the medium. This was necessary to reach the single molecule level. Note, that in this strain wild type DnaA is expressed from its native site.
In FRAP experiments a dynamic behavior for YFP-DnaA was observed (section 3.5.1.). Analysis of YFP-DnaA at the single molecule level revealed the existence of static and dynamic single molecules (figure 24, 25).
The image sequence in figure 24 A shows a dynamic YFP-DnaA molecule over a time period of 0.45 s. The movement of this molecule was visualized in a dynamic heat map using the SDFFS program (figure 24 B). The start point of the track was normalized to the point of origin. The movement of the single molecule is indicated by a blue line. The red color surrounding the track intensifies if the single molecule remains inside a defined area. Another way to visualize the observed movement of a single molecule is displayed in figure 24 C. In this diagram the black line represents the distance from the start point of the track (µm) over time (s). The total increment over the time steps is displayed with a red line and the defined stopping area by a green line. A molecule is defined as static when the total increment remains under the defined stopping distance of 0.23 µm. The stopping area was defined based on the resolution limit of the microscope setup (section 2.7.3.2.).
An example for a static YFP-DnaA molecule can be seen in figure 25 A. The heat map depicted in figure 25 B clearly shows that the observed molecule is static. An analysis of the increment over time revealed that the distance covered remained below the stopping threshold of 0.23 µm (figure 25 C).

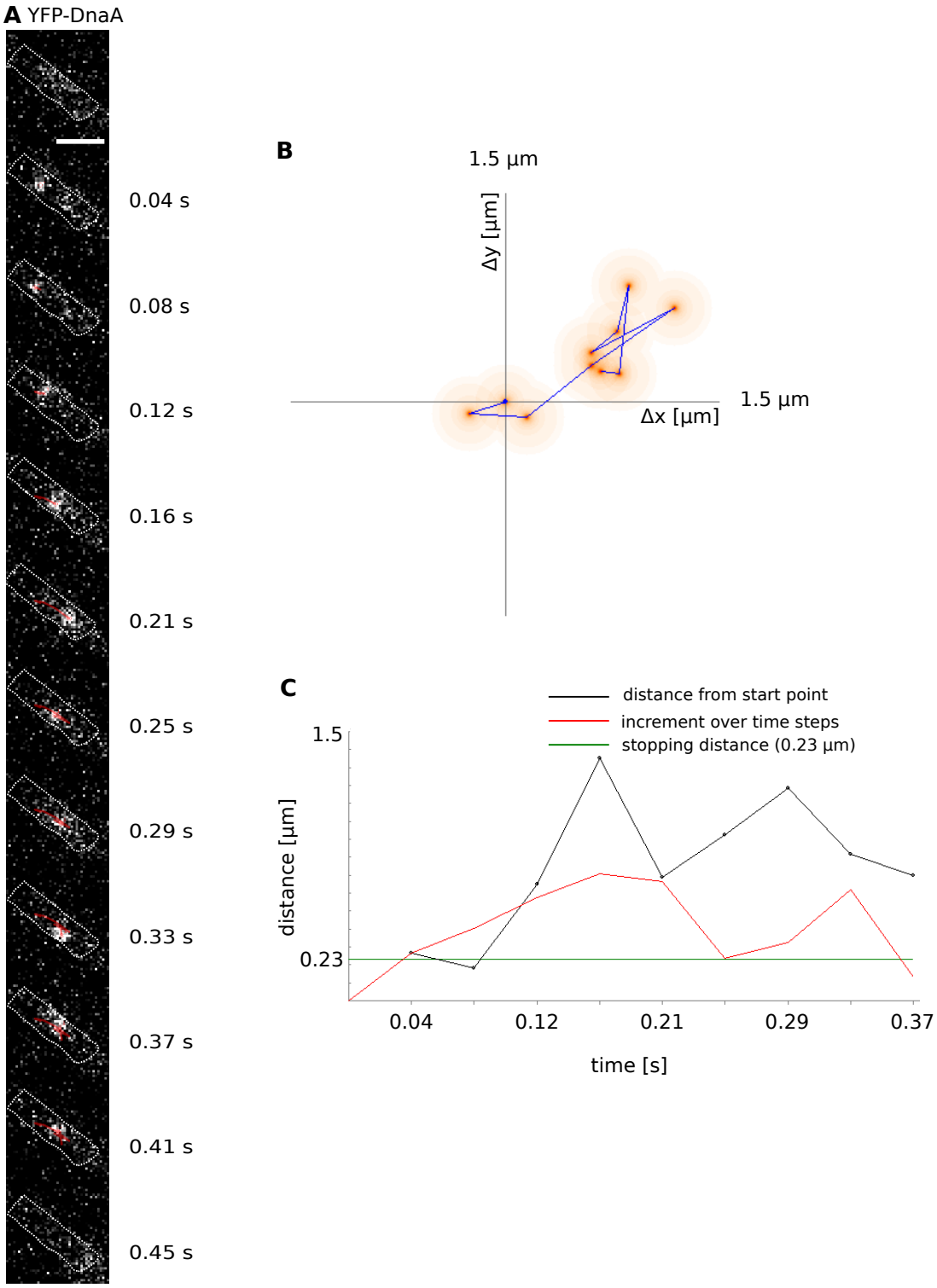

Figure 24: Mobile YFP-DnaA molecule
A Image sequence showing a single YFP-DnaA molecule. Each frame corresponds to a time interval of 41 ms. White line, cell outline; scale bar, 2 µm.
B Dynamic heat map of the YFP-DnaA trajectory shown in (A). Coordinate plane corresponds to a length of 1.5 µm. The beginning of the track starts at the point of origin.
C Diagram visualizing the distance from the origin (black) over time, the increment over time (red) and the defined stopping area (0.23 µm, green).

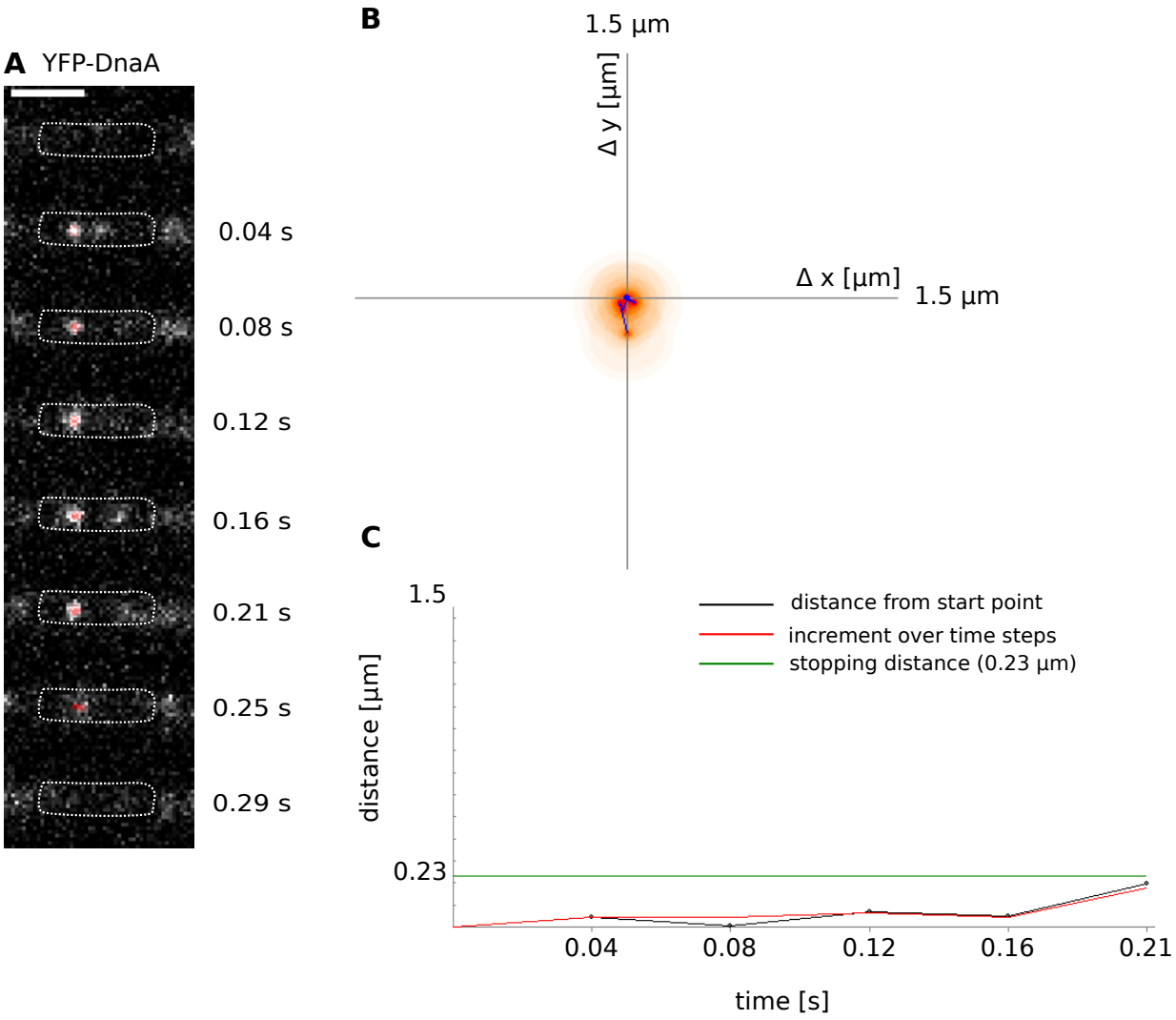

Figure 25: Static YFP-DnaA molecule
A Image sequence showing a YFP-DnaA molecules. Each frame corresponds to a time interval of 41 ms. White dashed line, cell outline; scale bar, 2 µm.
B Dynamic heat map of the YFP-DnaA trajectory shown in (A). Coordinate plane corresponds to a length of 1.5 µm. The beginning of the track starts at the point of origin.
C Diagram visualizing the distance from the origin (black) over time, the increment over time (red) and the defined stopping area (0.23 µm, green).

A total of 185 trajectories consisting of 5.7 time points in average were investigated. Mobile as well as static tracks were observed raising the question on the proportion of mobile to static molecules.

The percentage of stopped molecules for subsequent time intervals (time interval = 41 ms) was analyzed using the SDFFS program. The histogram shows the fraction of trajectories considered static for $\geq$3 time points (figure 26 A). Around 34% of all molecules remained inside the defined stopping area for 3 or more time intervals. Only 18% of the trajectories stayed for four or more

time intervals, whereas for ≥5 and ≥6 time points 9% and 6% of all molecules were defined as static, respectively.

In the cumulative distribution function (CDF) the normalized number of track points over time leaving the stopping area are visualized (figure 26 B). The more stopping molecules were observed and the longer they stopped, the longer the CDF needs to reach 1. In this analysis the stopping area was permanently repositioned after each time step. Based on this results an expected average stopping time for YFP-DnaA molecules of 101 ms was calculated. Although this time is likely higher due to the underestimation of track length caused by the stochastic bleaching of YFP molecules, which was not corrected for.

Only a minority of YFP-DnaA molecules stopped for longer than 3 time intervals in the defined area, indicating that DnaA is rather dynamic at single molecule level.

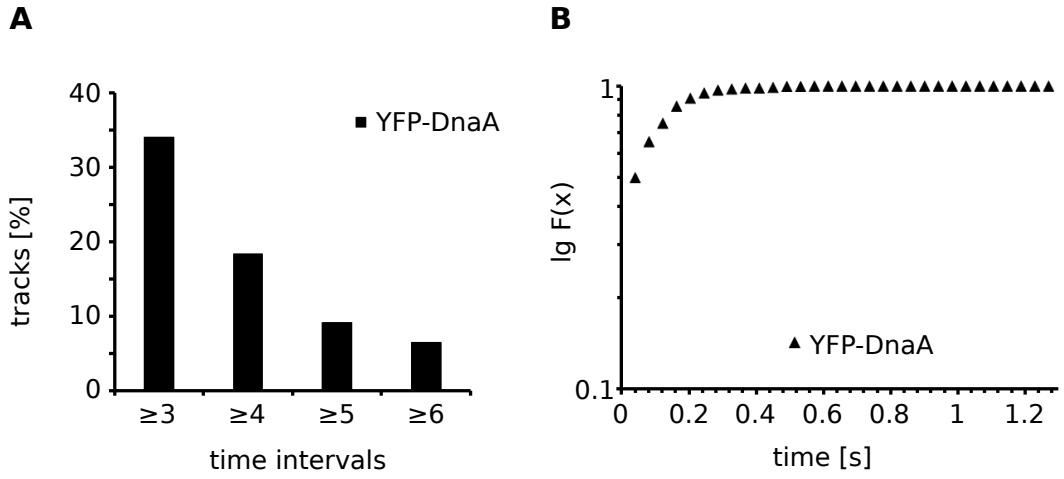

Figure 26: Analysis of YFP-DnaA molecules
A Histogram showing percentage of molecules stopping for 3, 4, 5 and 6 time steps. One time step corresponds to 0.041 s. A total of 185 molecules were analyzed. Note, that tracks stopping for 6 time steps will be included in the 3–5 time points as well. **B** Cumulative distribution function (CDF) showing the normalized number of molecules leaving the defined stopping area over time. The area is specified as a circle with the diameter of 230 nm.

Figure 27 A displays the mean square distribution (MSD) over time using a double logarithmic scaling. The slope of the regression line (green line) α is 0.201 $\mu m^2/s$. For free diffusion $\alpha = 1$, whereas for $\alpha < 1$ a subdiffusion is assumed. This is only true if the increments in x- and y-direction follow a Gaussian distribution, as is the case for YFP-DnaA (figure 27 B).

The diffusion constant (D) was determined using the following equation:

$$D = \frac{MSD}{2 \cdot x \cdot \tau}$$

,

with x beeing the number of dimensions analyzed, τ the time interval and MSD the mean square

distribution.

A diffusion constant of 0.676 $\pm$ 0.061 $\mu m^2/s$ (Mean $\pm$ standard error of the mean (SEM)) was calculated for YFP-DnaA single molecules based on the analyzed trajectories.

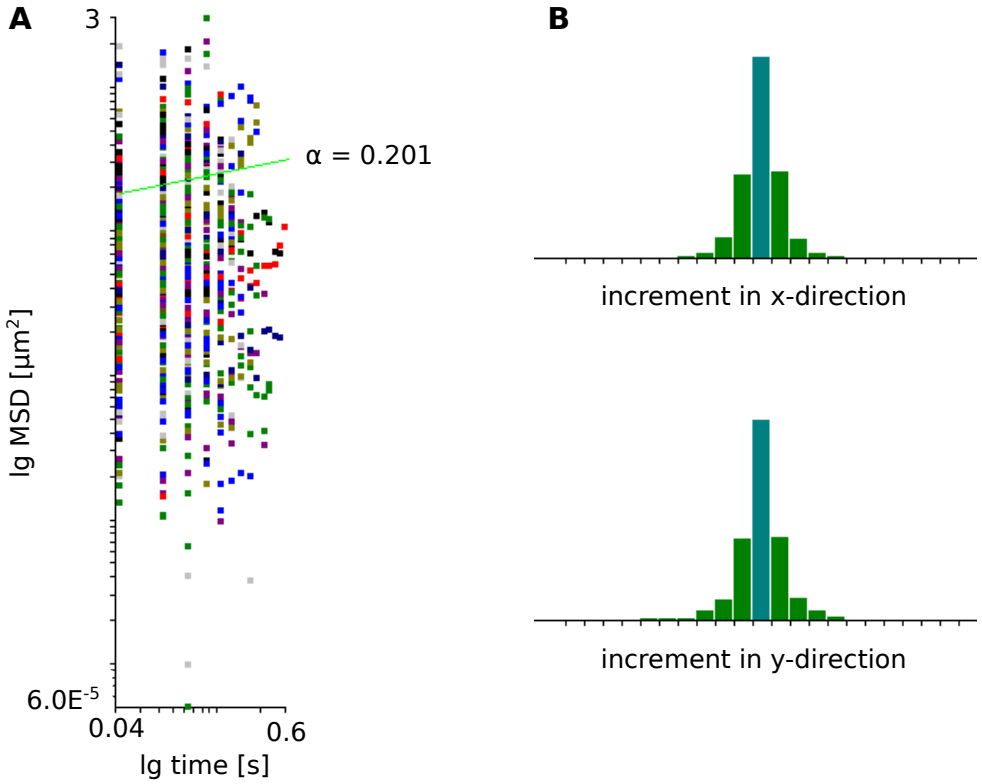

Figure 27: Mean square deviation of YFP-DnaA molecules
A Diagram shows the mean square deviation (MSD) [μm^2] of all trajectories obtained for YFP-DnaA over time [s]. The slope of the regression line (green line) is 0.201 $\mu m^2/s$. **B** Histograms show increment in x- and y-direction, which display a Gaussian distribution.
The SDFFS program developed by Prof. Bernhard Schmitt (AG Dahlke, Phillips-University Marburg, Germany) was used to analyze and display the single molecule data.

3.7.2. *E. coli* DnaA single molecules are more static than *B. subtilis* DnaA molecules

Analysis of the *E. coli* DnaA-eYFP fusion revealed an oscillation between the two cell halves. Single molecule microscopy was performed to further investigate the behavior of DnaA-eYFP and compare it with the results obtained for *B. subtilis* YFP-DnaA. Therefore the *E. coli* strain MG1655 was grown in M9 minimal medium at 30 °C[24].

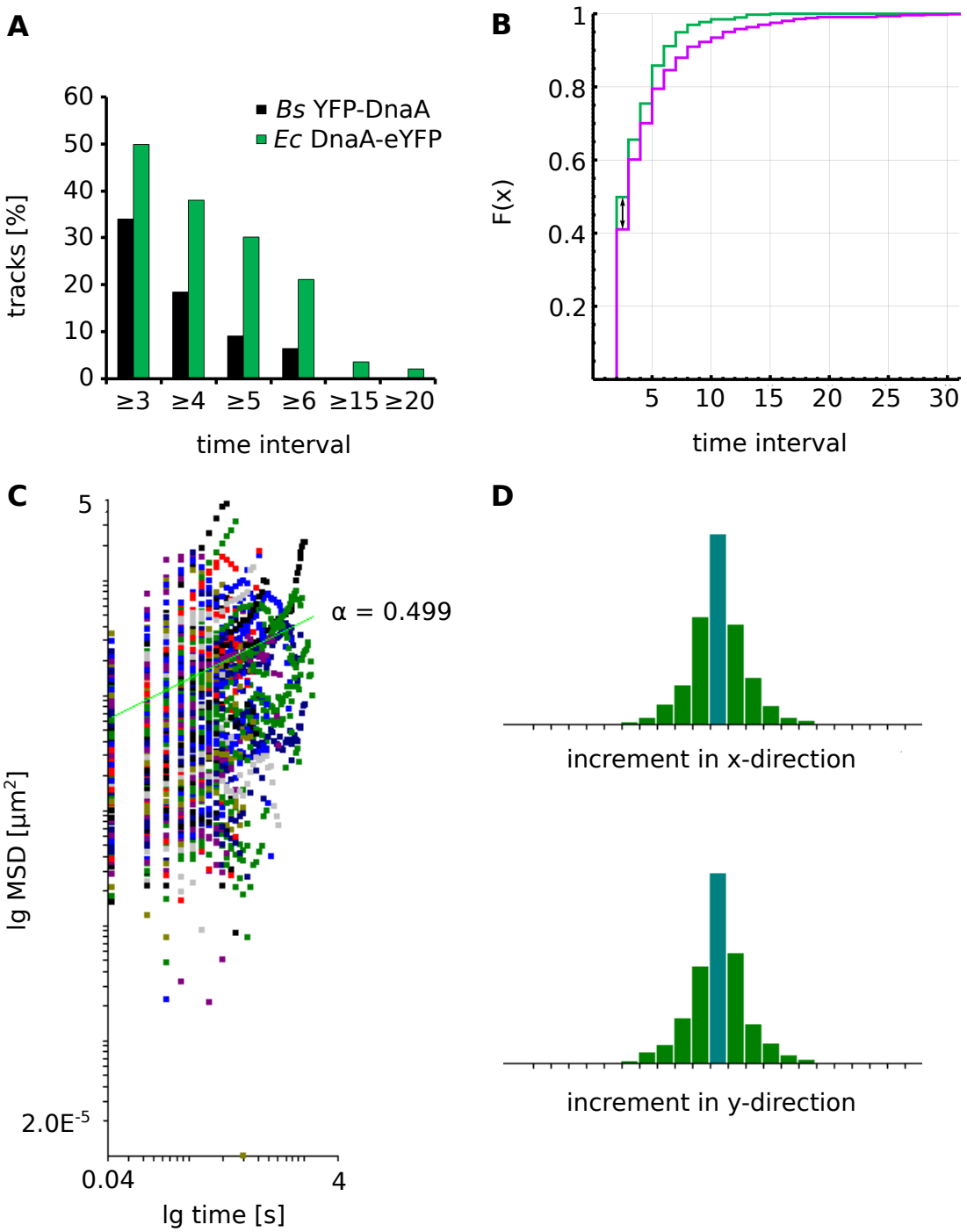

Figure 28: Analysis of *E. coli* DnaA-eYFP single molecules
A Histogram showing percentage of molecules stopping for 3–6, 15 and 20 time steps. One time step corresponds to 0.041 s. A total of 279 molecules were analyzed. Black colored columns represent *B. subtilis* YFP-DnaA whereas the green colored columns represent *E. coli* DnaA-eYFP.
B Diagram displaying the cumulative distribution function (CDF) of the normalized number of molecules leaving the defined stopping area over time. The area is specified as a circle with a diameter of 230 nm. Green line, *B. subtilis* YFP-DnaA; purple line, *E. coli* DnaA-eYFP. Black arrow indicates the largest difference between the two curves, which is used for the Kolmogorow-Smirnow test. **C** Diagram shows the mean square deviation (MSD) [μm^2] of all trajectories obtained for YFP-DnaA over time [s]. The slope of the regression line (green line) is 0.499 $\mu m^2/s$. **D** Histograms show increment in x- and y-direction, which exhibit a Gaussian distribution.

A total of 279 trajectories with an average length of 9.6 points were analyzed. The histogram displayed in figure 28 A shows the fraction of stopped molecules of *E. coli* (*Ec*, green) and *B. subtilis* (*Bs*, black) DnaA. Around 50% of all molecules observed stopped for 3 or more time intervals. This is 16% more than for *Bs* YFP-DnaA. For the time intervals $\geq$4, $\geq$5 and $\geq$6, 38%, 30% and 21% of stopping molecules were observed, respectively. Analysis of *Ec* DnaA-eYFP molecules revealed that 4% and 2% of stopped molecules remained inside the stopping area for more than 15 or 20 time frames, respectively. The*Ec* DnaA-eYFP molecules analyzed tend to be more static than the *Bs* YFP-DnaA molecules observed.
Using the CDF the stopping behavior of molecules from different strains can be compared. A statistical test was used to estimate the probability that the two functions are equal (Kolmogorow-Smirnow test). With a probability of 5% the CDF of *Bs* YFP-DnaA and *Ec* DnaA-eYFP are identical ($p = 0.05$), indicating a significant difference in the average residence time between the YFP-labeled DnaA proteins of both species (figure 28 B). The average stopping time of an *Ec* DnaA-eYFP molecule is 135 ms.
Figure 28 C displays the mean square deviation over time for *Ec* DnaA-eYFP molecules. The slope of the regression line is 0.499 $\mu m^2/s$, indicating a subdiffusion. Histograms show increment in x- and y-direction, which display a Gaussian distribution (figure 28 D). The diffusion constant calculated for *Ec* DnaA-eYFP is 0.335 ± 0.012 $\mu m^2/s$. This is about half as fast as the diffusion constant determined for *Bs* YFP-DnaA.

3.7.3. YFP-YabA single molecules are more static compared to YFP-DnaA molecules

YFP-YabA molecules displayed a similar localization behavior as that observed for YFP-DnaA (section 3.2.) and the recovery half-time matched that of YFP-DnaA in FRAP experiments (section 3.5.4.). To further characterize the connection between this two proteins, single molecule microscopy was performed, using a strain expressing an ectopic copy of YFP-YabA in a *yabA* deletion strain (KS167). Cells were grown in M9 minimal medium at 25 °C.
An example for a static single YFP-YabA molecule is displayed in figure 30 A. Analysis of this trajectory on a heat map supported the notion of a static behavior (figure 30 B). The increment over time stayed below the defined stopping distance of 230 nm (figure 30 C) further indicating that the analyzed molecule is not mobile.

Further investigation of YFP-YabA single molecules showed a strong increase of static molecules when compared to YFP-DnaA (figure 29). Overall 171 trajectories with an average length of 6.7 points were analyzed. Around 67% of all molecules observed remained inside the stopping area for 3 or more time frames. This is 33% more compared to YFP-DnaA. Similar results were obtained upon investigating the percentage of molecules stopping for $\geq$4–$\geq$6 time intervals (44%, 34% and 27% to 18%, 9% and 6% in YFP-DnaA). A small fraction of YFP-YabA molecules remained static for $\geq$15 time frames.

A comparison of the CDFs from both strains indicates that YFP-YabA tends to be more static than YFP-DnaA. The difference between the two curves is significant ($p = 10^{-22}$). The estimated average residence time for YFP-YabA is 209 ms. This is twice as long as was observed for YFP-DnaA.

The slope of the regression line for the MSD over time for YFP-YabA molecules $\alpha = 0.151$ $\mu m^2/s$ (data not shown). As $\alpha > 1$ a subdiffusion is expected. The diffusion constant determined is 0.158 ± 0.016 $\mu m^2/s$, indicating YFP-YabA to be four times slower than YFP-DnaA.

However, it should be noted that freely diffusing YabA molecules would not be detectable in the 41 ms stream acquisitions, so the lower diffusion rate may simply be due to the fact that one can only see the static YabA fraction, and not the dynamic molecules.

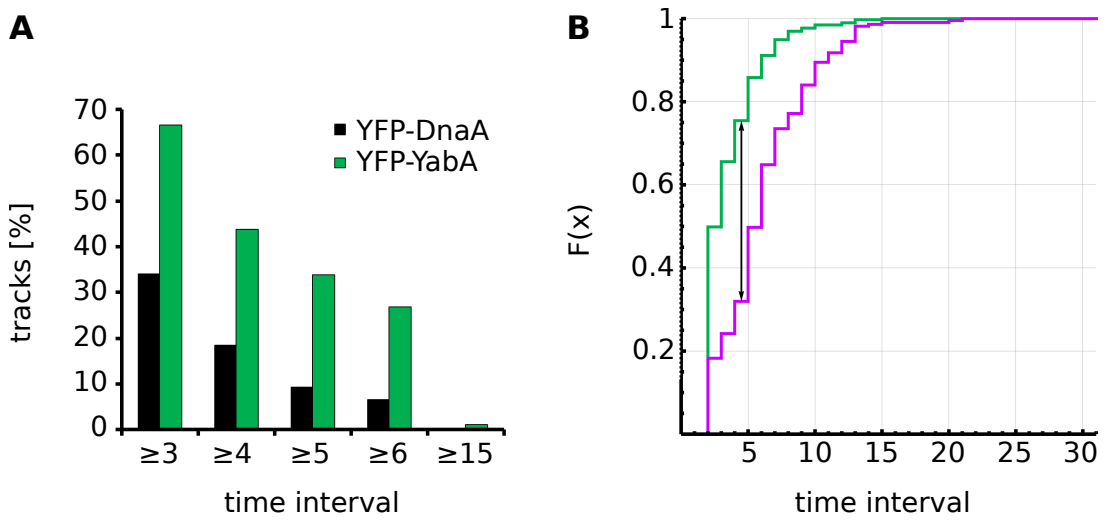

Figure 29: Analysis of YFP-YabA single molecules
A Histogram showing percentage of molecules stopping for more than 3–6 and 15 time steps. One time interval corresponds to 0.041 s. A total of 171 molecules were analyzed. Black colored columns represent YFP-DnaA whereas the green colored columns represent YFP-YabA.
B Diagram displaying the CDF of the normalized number of molecules leaving the defined stopping area over time. The area is specified as a circle with a diameter of 230 nm. Green line, YFP-DnaA; purple line, YFP-YabA. Black arrow indicates the largest difference between the two curves, which is used for the Kolmogorow-Smirnow test.

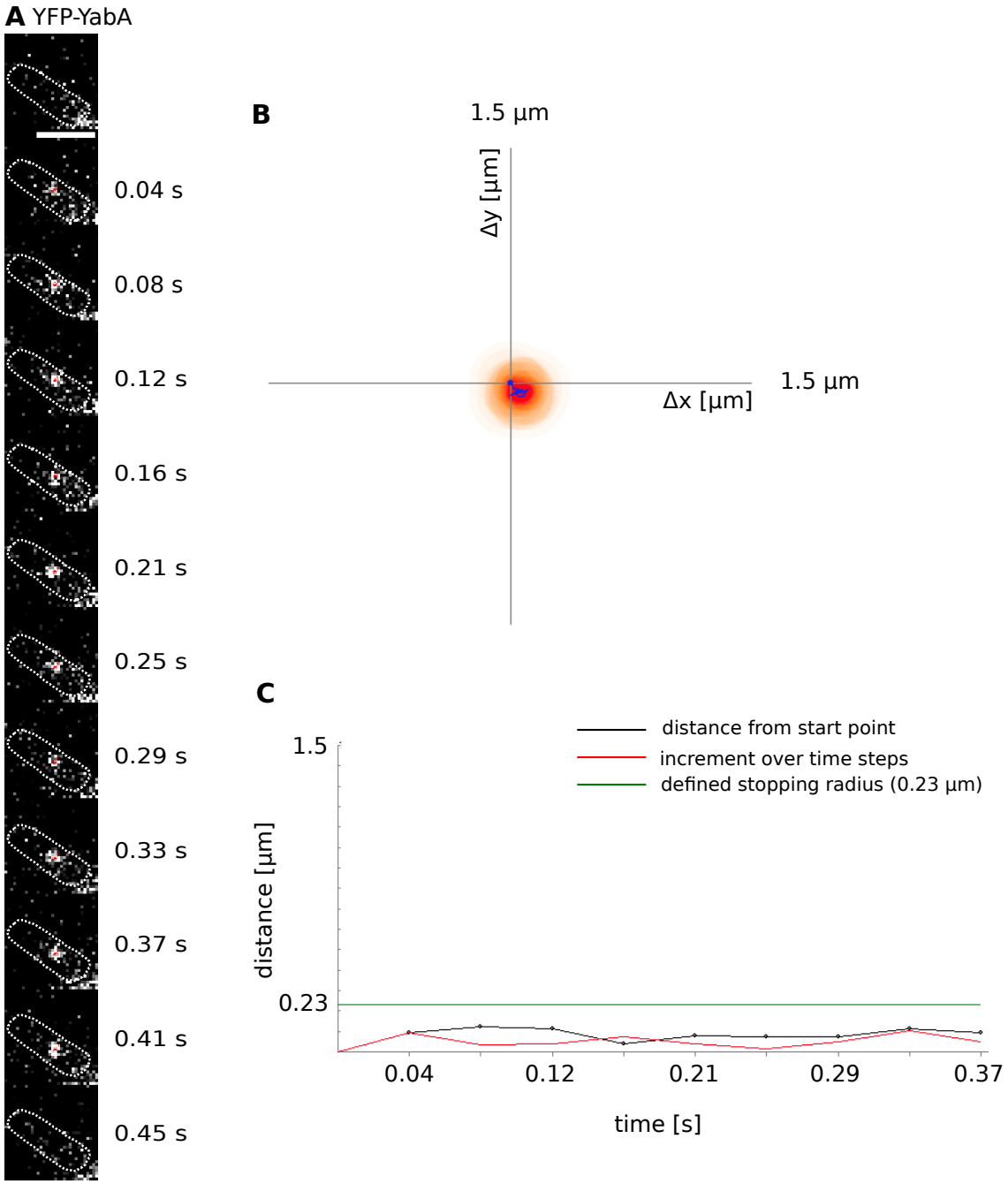

Figure 30: Example for a static YFP-YabA single molecule
A Image sequence showing single YFP-YabA molecules. Each frame corresponds to a time interval of 41 ms. White dashed line, cell outline; scale bar, 2 µm. **B** Dynamic heat map of of the YFP-YabA single molecule trajectory shown in (A). Coordinate plane corresponds to a length of 1.5 µm. The beginning of the track starts at the point of origin. **C** Diagram visualizing the distance from the origin (black) over time, the increment over time (red) and the defined stopping area (0.23 µm, green)

3.7.4. Deletion of *soj-spo0J* has a decelerating impact on YFP-DnaA at the single molecule level

In FRAP experiments a deletion of the *soj-spo0J* operon resulted in an increased recovery half-time of YFP-DnaA compared to YFP-DnaA in a wild type strain (section 3.5.2.2.). For SM microscopy a strain expressing an ectopic YFP-DnaA fusion in a *soj-spo0J* deletion strain (KS192) was used. Cells were grown in M9 minimal medium with 0.5% glucose (w/v) at 25 °C.

A total of 125 trajectories with an average length of 6.7 points were analyzed. Overall YFP-DnaA in a *soj-spo0J* deletion strain showed a strong tendency to remain inside the defined stopping area, meaning that YFP-DnaA upon deletion of *soj-spo0J* becomes more static than in a wild type strain. The percentage of molecules remaining static for ≥3–≥6 time intervals were 54%, 33%, 21% and 15%, respectively (figure 31 A). A small fraction of YFP-DnaA molecules in the *soj-spo0J* deletion strain remained static for ≥15 time frames.

A significant difference between the two cumulative distribution functions was observed ($p = 0.001$), further supporting the observation that YFP-DnaA upon deletion of *soj-spo0J* adopts a more static behavior. The estimated average residence time for YFP-DnaA in a *soj-spo0J* deletion strain is 142 ms.

The slope of the regression line for the MSD over time for YFP-DnaA molecules in a *soj-spo0J* deletion strain $\alpha = 0.258$ μm^2/s (data not shown). As $\alpha > 1$, a subdiffusion is assumed. The diffusion constant for YFP-DnaA molecules in a *soj-spo0J* deletion strain is 0.313 ± 0.020 μm^2/s, indicating that the diffusion constant of YFP-DnaA halves upon deletion of *soj-spo0J*.

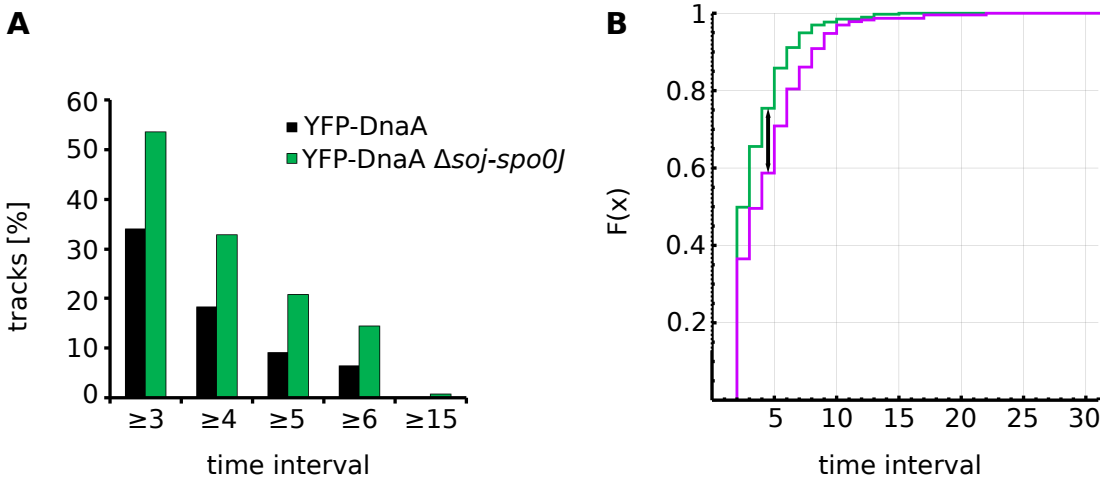

Figure 31: Analysis of YFP-DnaA single molecules in a *soj-spo0J* deletion
A Histogram showing percentage of molecules stopping for 3–6 and 15 time steps. One time interval corresponds to 0.041 s. A total of 125 molecules were analyzed. Black colored columns represent YFP-DnaA whereas the green colored columns represent YFP-DnaA in a *soj-spo0J* deletion strain.
B Cumulative distribution function (CDF) showing the number of normalized molecules leaving the defined stopping area over time. The area is specified as a circle with the diameter of 230 nm.

3.7.5. Analysis of YFP-DnaA amino acid substitutions at the single molecule level

Biochemical analysis of the DnaA amino acids substitution E183Q revealed a twofold decreased ATP-binding and a 6–7-fold reduced ATPase activity as well as a reduced oligomerization capacity (Eisemann, 2012). To analyze YFP-DnaAE183Q at the single molecule level, a strain expressing an inducible copy of YFP-DnaAE183Q (ME20) was grown in M9 minimal medium supplemented with 0.5% glucose (w/v) at 25 °C. Wild type DnaA was still expressed from its original promotor.

A total of 144 trajectories consisting of 5.7 points on average were analyzed. Investigation of the fraction of static molecules stopping inside the defined stopping area for 3–6 time intervals revealed that YFP-DnaAE183Q is more dynamic than wild type YFP-DnaA (figure 32 A). A percentage of 19%, 12%, 3% and 1% of stopping molecules was observed for ≥3–≥6 time points, respectively (24%, 18%, 9% and 6% for wild type).

Analysis of the CDF of both strains revealed a significant difference between the two functions ($p = 0.01$). The estimated average residence time for YFP-DnaAE183Q molecules is 79 ms. The diffusion constant calculated (0.983 ± 0.070 µm^2/s) was 1.5 times faster than the one measured for the YFP-DnaA wild type strain.

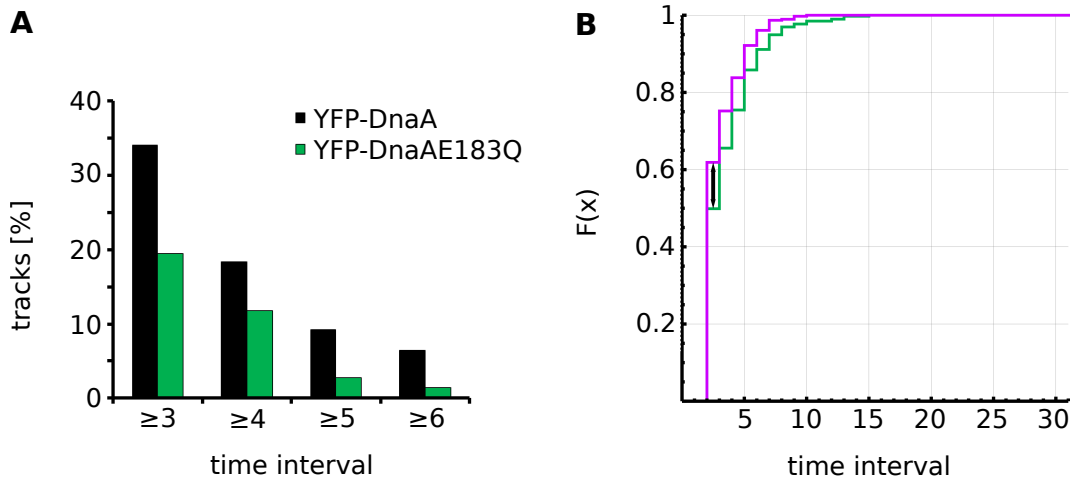

Figure 32: Analysis of YFP-DnaAE183Q single molecules
A Histogram showing percentage of molecules stopping for more than 3–6 time steps. One time interval corresponds to 0.041 s. A total of 144 molecules were analyzed. Black colored columns represent YFP-DnaA whereas the green colored columns represent YFP-DnaAE183Q.
B Cumulative distribution function (CDF) showing the normalized number of molecules leaving the defined stopping area over time. The area is specified as a circle with diameter of 230 nm.

Two further YFP-DnaA single amino acids substitutions were analyzed, the A163V substitution, leading to the formation of constitutive multimers and the R260A substitution described in section 3.5.3.2. No significant difference concerning the stopping behavior of this YFP-DnaA point mutations to wild type YFP-DnaA was observed (data not shown).

The estimated average residence time for YFP-DnaAR260A is 106 ms, which equals the one observed for YFP-DnaA. The diffusion constant calculated for YFP-DnaAR260A is 0.493 $\pm$ 0.030 $\mu m^2/s$, which is 30% slower than wild type YFP-DnaA. The slower diffusion constant is in concordance with the observed increased recovery half-time during FRAP experiments.

The average residence time of YFP-DnaAA163V is 87 ms, which is 10% shorter than for wild type YFP-DnaA. For the YFP-DnaAA163V mutant a diffusion constant of 0.725 $\pm$ 0.037 $\mu m^2/s$ was determined. This diffusion constant is 10% faster than the one of wild type YFP-DnaA.

3.8. Cellular localization of the GTPase Era in *B. subtilis*

Era is a small GTP-binding protein that belongs to the Era/Obg family of GTPases[105]. It was reported as an essential protein for cell growth in *E. coli* and some *B. subtilis* strains[106,107].

The Era protein contains two functional domains, a GTPase and a KH domain. The C-terminal KH domain is capable of RNA binding and mediates the interaction of Era with the 16SrRNA and the 30S ribosomal subunit[108,109].

Besides its role in ribosome maturation an involvement of Era in cell cycle regulation was implied. A reduction in the GTPase activity caused by a point mutation (P17R) in the GTP-binding domain led to a growth arrest in the predivisional two-cell stage[110]. These results led to the hypothesis that Era might function as a cell cycle checkpoint.

In the *B. subtilis* chromosome the Era protein is encoded downstream of *cdd* and upstream of *recO*. RecO is involved is DNA recombination, a function unrelated to that of Era, while Cdd is a cytidine deaminase.

In a tandem affinity purification experiment (TAP-tag) Era was pulled down by YabA, a negative regulator of DnaA, the initiator of DNA replication in *B. subtilis* (Marc Eisemann, unpublished results).

To analyze the localization of Era in *B. subtilis*, wild type cells were transformed with the plasmid pPG2393 resulting in a strain expressing Era-mVenus under its original promotor (KS144). The cells were grown in rich media at 37 °C supplemented with 0.5% xylose (w/v) for downstream gene expression.

Fluorescence images displayed in figure 33 A show examples for the four different localization patterns, which were observed in stationary cells. A total of 710 cells were analyzed. Around 86% of all cells observed, displayed a weak homogenous cytoplasmic distribution of the fluorescence signal (green asterisk). In 5% of all cases, a single fluorescence foci was observed (figure 33 A, button panel), whereas in another 5% of all cells several foci of Era-mVenus were visible (figure 33 A, left upper panel). A strong fluorescence signal, showing a cytoplasmic distribution was observed in 4% of all cases (orange asterisk).

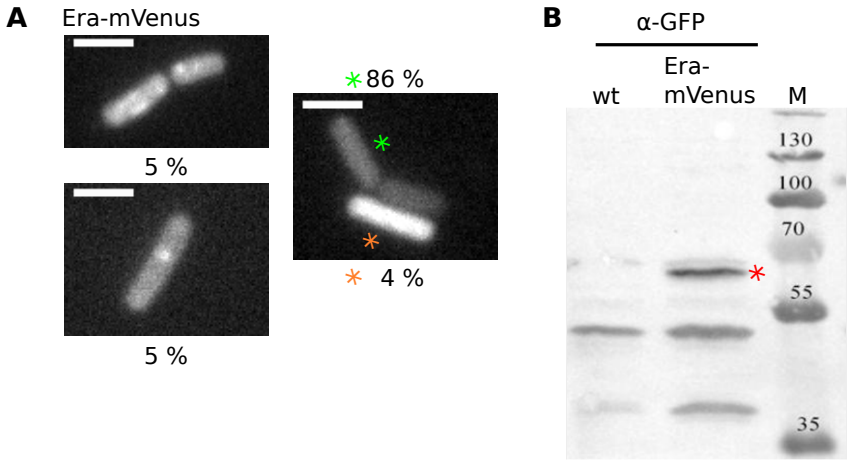

Figure 33: Localization of Era-mVenus in stationary cells
A Epifluorescence images showing the localization of Era-mVenus in stationary cells. Examples for four different localization patterns and their occurrence in percent are displayed. Orange asterisk and green asterisk, mark localization patterns and their occurrence in percent. Scale bars, 2 µm. **B** Western blot analysis of wild type and KS144 cell extracts using α-GFP antiserum. The expected size of the Era-mVenus fusion protein is 60 kD. Red asterisk, signal corresponding to Era-mVenus; M, protein standard.

A Western blot analysis of wild type and Era-mVenus cell lysate using α-GFP antiserum was performed to verify the expression of the fusion protein (figure 33 B). The signal detected around 60 kD corresponds to the expected size for the Era-mVenus protein (red asterisk).

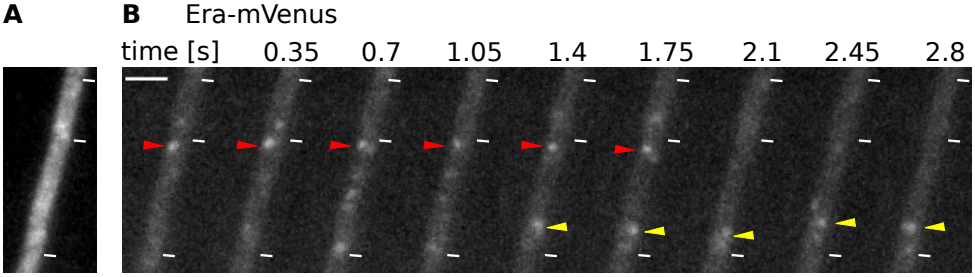

Figure 34: Localization of Era-mVenus in exponentially growing cells
A First image of the stream shown in (B), displaying the localization of Era-mVenus in exponentially growing cells. **B** Stream sequence of Era-mVenus showing mobile (yellow arrow) and static (red arrow) foci. Images were acquired every 350 ms. Scale bar, 2 µm; white lines, cell borders.

The observed fluorescence signal of Era-mVenus in exponentially growing cells was faint (figure 34 A). Era-mVenus localized homogenous all over the cell with small patch-like structures close to the cell pole. Stream acquisition (350 ms time frame) using a 515 nm laser revealed, after bleaching of the dispersed fluorescence signal, small static (figure 34, red arrow) and mobile (figure 34, yellow arrow) Era-mVenus foci. Notably, the foci detectable over several time

frames are located close to the cell pole, which corresponds to the position where ribosomes are predominantly present.

4. Discussion

A key aspect of this work was the analysis of the dynamics of DnaA, the initiator of DNA replication, in *B. subtilis*. Using different microscopical techniques I could show that DnaA is a highly dynamic protein and that deletion of *yabA* or *soj-spo0J* had a decelerating impact on its turnover at the replisome and *oriC*, presumably causing an overinitiation of replication. An amino acid substitution in DnaA was further shown to lead to an increased turnover rate of DnaA at its binding sites and presumably causing underinitiation.
YabA is a negative regulator of the initiation of replication in *B. subtilis*. My work shows that YFP-YabA follows the localization pattern of YFP-DnaA and exhibits a high turnover rate at its individual binding sites but behaves very differently at the single molecule level. These findings indicate that DnaA and YabA do not move together over the chromosome.
Furthermore, I could demonstrate that *E. coli* DnaA is also a very dynamic protein, indicating that the fast turnover rates of DnaA might be a general feature of DnaA.

4.1. YFP-DnaA localizes in a cell-cycle-dependent manner

In *B. subtilis*, the localization of the fluorescently labeled protein DnaA was reported to follow a cell-cycle-dependent manner[2]. During early and late stages of the cell cycle, YFP-DnaA colocalizes mainly with the origin region, whilst during ongoing replication YFP-DnaA was found predominantly localizing with the replication machinery[2].
Based on these findings a model was proposed, in which DnaA, after initiation of replication, is spatially sequestered to the replication machinery via YabA[2]. Once the replisome disassembles, DnaA is free to bind to *oriC* to initiate a new round of replication[2].
Time lapse microscopy was applied to further analyze the localization of YFP-DnaA with respect to the origin of replication. This microscope technique allows the pursuit of labeled proteins over the whole cell cycle of a single bacterium.
Data obtained from these experiments show that even during ongoing replication YFP-DnaA may transiently localize to the origin region, indicating that DnaA is able to bind to the *oriC* during the whole cell cycle, although a large fraction of DnaA is still recruited to the replication machinery (figure 9). Hence, DnaA localization does not strictly follow the proposed pattern, when observed during a whole cell cycle. It might be more dynamic than previously thought. The underlying dynamics of DnaA will be further substantiated using data from FRAP and single molecule microscopy.

4.2. YFP-YabA follows the localization pattern of YFP-DnaA

YabA is a negative regulator of replication initiation in *B. subtilis*, which interacts with DnaA and DnaN, the β-clamp of DNA polymerase III[73,82,83]. YFP-YabA localizes as distinct foci and

was previously reported to colocalize with the replisome during ongoing replication[82,83,111]. Formation of these foci largely depends on the interaction between YabA and DnaN[74]. Furthermore ,YabA was reported to be essential for the association of DnaA with the replisome[2]. Recently, YabA was shown to associate with the *oriC* region in a DnaA-dependent manner, using a combined technique of Chromatin immunoprecipitation and quantitative PCR (ChIP-qPCR)[75]. In addition, *in vitro* experiments revealed that YabA functions as an anti-cooperativity factor for DNA binding of DnaA and inhibits DnaA helix formation[75,76].

These findings indicate that YabA localizes with the replication machinery and the *oriC* region, which is similar to what was reported for YFP-DnaA[2].

To investigate the behavior of YFP-YabA throughout the cell cycle, I used a strain in which the localization of YFP-YabA can be followed with respect to the replication machinery (DnaX) and the origin region. It is noteworthy that a direct tagging of YabA and DnaA results in a growth defect and a perfect colocalization of both fluorescence proteins[2]. I observed in 54% of all cells investigated a colocalization with the replication machinery (figure 10 A), which is in accordance with previously published results[82]. Furthermore in 9% of all analyzed cells YFP-YabA colocalized with the origin region, in 10% with the replication machinery and *oriC* and in 27% no colocalization of YFP-YabA with any of the two other fluorescence markers was observed (figure 10 B–D). Analysis of the localization patterns according to cell length, revealed that YFP-YabA associates with the origin region throughout the cell cycle with a slight preference for colocalization with the origin regions during early and late stages of the cell cycle, which is the time when presumably, under the growth conditions utilized, the initiation of replication occurs (figure 11 I).

Overall the localization pattern of YFP-YabA largely resembles that observed for YFP-DnaA, which could indicate that YabA and DnaA move through the cell together as a complex. Alternatively they could interact with a third component, which acts as a scaffold and is thus responsible for the similar localization pattern. A good candidate for this linker part would be DnaN, which was already shown to be responsible for YabA localization to the replisome[74], whereas YabA was reported to mediate DnaA localization to the replication machinery[2].

I was able to show a colocalization of YFP-YabA with the origin of replication throughout the cell cycle, albeit in a small number of cells, which is in accordance to findings reporting YabA to inhibit cooperative binding of DnaA to *oriC* DNA and DnaA helix formation[75,76]. In most cells YFP-YabA was observed at the cell center colocalizing with the replication machinery, which is in accordance to the sequestration model described by Soufo *et al.*[2]. Combining the two observations is still somewhat puzzling because if YabA inhibits helix formation of DnaA at *oriC*, why would it localize at the replication machinery during ongoing replication? Unless YabA is a dynamic protein that moves back and forth between the origin and the replication machinery.

4.3. Overexpression of DnaN results in an increased number of YFP-YabA and YFP-DnaA foci

DnaN is the β-clamp of the DNA polymerase III and capable of interacting with YabA[73,83,111]. Overexpression of DnaN results in a YabA-dependent overinitiation of replication whereas depletion of DnaN leads to a decreased replication initiation and the induction of the SOS response[74,75,32].

As DnaN plays a crucial role during the spatial sequestration of DnaA to the replication machinery, I was interested if the localization pattern of YFP-DnaA and YFP-YabA changes upon overexpression of DnaN.

Analysis of a strain harboring YFP-YabA while overexpressing DnaN from an ectopic site revealed an increase from 1.1 YFP-YabA foci to 2.3 foci per cell, whereas a strain harboring YFP-DnaA showed an increase in YFP-DnaA foci from 2.9 foci per cell to 3.6 (table 12).

Previous investigations report that upon overexpression of DnaN a decreased association of YabA and an increased association of DnaA with the *oriC* region occur[75]. If this is the case, then the YFP-YabA foci observed probably colocalize mainly with the replication machinery, while the YFP-DnaA foci colocalize with the *oriC* region. Whether these foci in fact represent colocalizations with the origin of replication or the replication machinery remains to be explored. Furthermore an overexpression of DnaN was shown to result in an overinitiation of replication, while YabA inhibits cooperative binding of DnaA to *oriC* DNA[74,75]. An increase in DnaN could thus titrate YabA away from the *oriC* region thereby enabling DnaA to bind to *oriC* and initiate replication.

4.4. Triple deletion of *yabA*, *soj* and *spo0J* is not lethal but exhibits a strong overinitiation phenotype

Soj was shown to modulate DnaA activity depending on its nucleotide-bound state, while Spo0J stimulates its weak intrinsic ATPase activity, which influences the multimerization state of Soj (see introduction 1.5.8.)[77]. Furthermore Soj and Spo0J are members of the ParA and ParB family of proteins, respectively, and an involvement in chromosome partitioning was observed[112,88]. Murray and Koh recently reported that the deletion of *yabA* and *soj* led to a growth defect in rich medium and to an increase in origin to terminus ratio[103].

In this study I could show that a deletion of *yabA*, *soj* and *spo0J* is not lethal, as was previously reported by Geers[104]. These findings indicate that YabA and Soj/Spo0J are not the only proteins regulating DnaA function at *oriC*, assuming that an unregulated initiation process leads to cell death.

Furthermore, by comparing wild type, *yabA* and *soj-spo0J* mutants to the triple mutant, I could show that the triple deletion has a 30% increased doubling time compared to the wild type strain in rich media (table 13) and that the cell length in the triple mutant is drastically elongated in

comparison to wild type cells (table 14, figure 14). These findings show that although the triple deletion is not lethal, it has an significant impact on cell growth and cell length.
In addition, investigating the chromosome duplication of the triple mutant revealed a fourfold increase in replication initiation compared to the wild type strain (figure 15, table 15), indicating that deletion of *yabA* and *soj-spo0J* results in a severe but not lethal defect in controlling the initiation of replication, which might be due to other regulators. Two possible candidates could be the essential primosomal proteins DnaB and DnaD, which together with DnaI are responsible for helicase loading in *B. subtilis*[113]. Both proteins were reported to bind to double- and single-stranded DNA and might play a role in the opening of the *oriC* region[114,115,116]. For DnaD an inhibition of the cooperative binding of DnaA to DNA as well as of DnaA helix assembly was observed[76,117].

4.5. YFP-DnaA is highly dynamic at *oriC* and at the replication machinery

During time lapse experiments I observed a changing localizaton of YFP-DnaA with the replication machinery and the *oriC* region throughout the cell cycle, indicating a possible dynamic behavior of DnaA. Hence, I was interested in the turnover rate of DnaA binding to *oriC* and to the replication machinery. To this end I performed FRAP experiments in live cells expressing YFP-DnaA as the only copy of DnaA. Surprisingly, the half-time recovery for YFP-DnaA was 2.5 ± 0.3 *s*, which is fast compared to e.g. the recovery half-time observed for binding of the Lac-repressor to its operator sequence (around 4 min)[118].
Analysis of turnover rates with respect to the origin of replication were performed in a merodiploid strain expressing an ectopic YFP-DnaA fusion combined with a LacI/*lacO* tagged origin of replication. Under the conditions used YFP-DnaA colocalized with the origin region in around 90% of all cells. Hence, the turnover rate for YFP-DnaA at the origin region is 2.9 ± 0.2 *s* (figure 16).
The recovery half-time of YFP-DnaA at the replication machinery was measured in a merodiploid strain expressing a YFP-DnaA fusion carrying a single amino acid substitution (R387C) rendering it unable to bind to DNA[33]. This strain still formed foci, which were not colocalizing with the origin region (figure 20 A, overlay) and thus presumably colocalizing with the replisome. The recovery half-time at the replication machinery (2.5 ± 0.4 s, figure 20 C) showed no significant difference to the one measured at the *oriC* region, indicating no difference in YFP-DnaA dynamics at these two sites.
Notably, no difference in half-time recovery rates was observed between the strain expressing YFP-DnaA from the original site and the strains expressing YFP-DnaA ectopically with wild type DnaA present. Furthermore transcription of *dnaA* is downregulated in a strain expressing YFP-DnaA ectopically, as YFP-DnaA is active in autoregulation[32,33].
In FRAP experiments the turnover of a fluorescently labeled protein between a bleached region and the entire cell is analyzed. If all molecules that were bleached inside the spot are free to

exchange with the cytoplasmic pool of molecules, then a full normalized fluorescence recovery during the time of the experiment should be observed. If this is not the case and the fluorescence recovery still reaches a plateau, then an immobile fraction inside the bleached spot is assumed. For all three strains investigated so far around 10% of immobile molecules (with a standard deviation of around 9%) were observed (table 16). A high heterogeneity throughout the different cells measured was observed, probably due to the different cell cycle stages the cells resided in.

These findings indicate that YFP-DnaA binds no longer than a few seconds to the replication machinery and the *oriC* region and that there is no substantial subfraction of YFP-DnaA molecules permanently bound to the *oriC* region. Although one could speculate that in cells that initiate during the time period of a FRAP experiment an increase in immobile molecules might be observed.

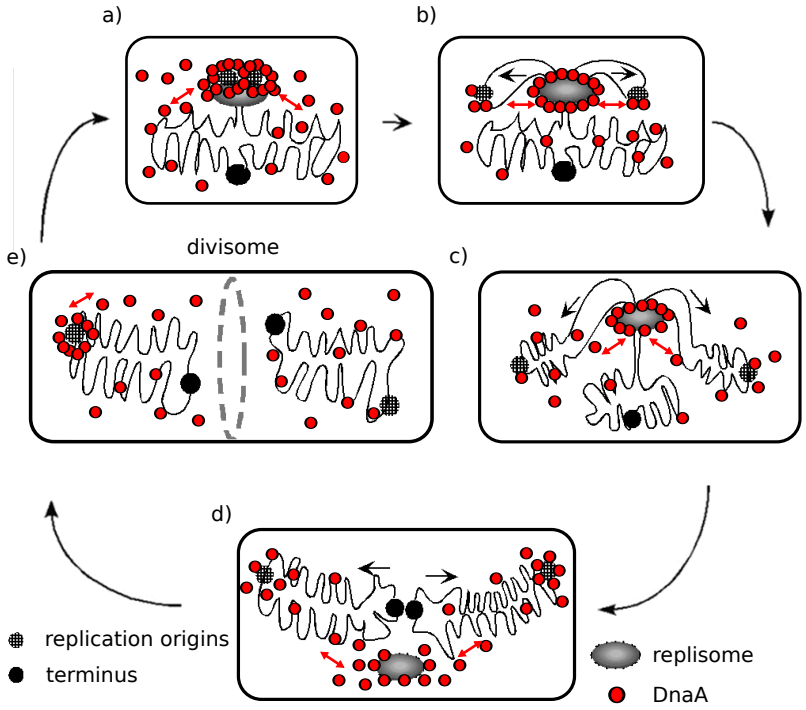

Figure 35: Model of DnaA localization in *B. subtilis* throughout the cell cycle.

Schematic display of the localization of DnaA over the whole cell cycle. (a) During initiation of replication DnaA, which is bound in the nucleoprotein complex, binds tightly to the origin region. Free DnaA is able to associate to and dissociate from DnaA binding sites. (b–c) Once the initiation has occurred, DNA replication proceeds in a bidirectional manner and most of DnaA is retained at the replication machinery via YabA. DnaA bound exchanges with the cytoplasmatic pool of DnaA molecules in the seconds range. Association of DnaA might be possible in a transiently manner. (d–e) Once replication is terminated, the replisome disassembles and DnaA is released. Although the binding is not permanent as previously expected, recruitment of DnaA to the replisome might work as a kind of sink for DnaA molecules. With the replisome gone DnaA primary target site is the origin of replication, where it can initiate a new round of replication, once cell division has occured. Figure modified after Soufo *et al.*[2]

4.6. Single molecule microscopy revealed high dynamics of YFP-DnaA

FRAP experiments indicated that DnaA is a highly dynamic protein. To further investigate this characteristic, I used a second method to analyze the dynamics of YFP-DnaA in live cells, called single molecule (SM) microscopy. After bleaching of most of the molecules, the movement of single YFP-DnaA molecules can be observed and tracked. Using the SDFFS program the trajectories can be analyzed. For SM microscopy a merodiploid strain expressing YFP-DnaA from an ectopic site was used. Expression of YFP-DnaA was not induced to facilitate the acquisition at the single molecule level. Notably, similar results were obtained in a strain expressing YFP-DnaA from the original site.

I could observe dynamic and static YFP-DnaA molecules (figure 24, figure 25), albeit less than 10% of all trajectories analyzed are static for more than 200 ms (figure 26 A). In this analysis a molecule is defined as static if the increment of movement over time remains below 230 nm, which is the resolution limit of the microscope setup.

Based on the mean square displacement (MSD) over time of all observed trajectories an average diffusion constant for YFP-DnaA molecules of 0.68 $\mu m^2/s$ was calculated. Free diffusing GFP molecules were reported to have an average diffusion constant of around 7 $\mu m^2/s$[119,120], indicating that YFP-DnaA molecules are not freely diffusing through the cell but might be interacting with the nucleoid, as DnaA also functions as a transcription factor (section 1.3.). The expected residence time, based on the cumulative distribution of observed static molecules, is 101 ms for YFP-DnaA. These results are in accordance with the FRAP data obtained for YFP-DnaA (section 3.5.1.). Interestingly, these finding indicate that DnaA binds only for around 100 ms to individual sites.

4.7. Deletion of *yabA* or *soj-spo0J* reduces the turnover of YFP-DnaA at individual sites

YabA and Soj are known regulators of the *B. subtilis* replication initiation. They both interact directly with DnaA and *in vitro* they inhibit the ability of DnaA to multimerize at *oriC*[75,80,76]. Furthermore a deletion of either of them results in a slight overinitiation[86,73]. I was interested whether a deletion of *yabA* or *soj-spo0J* would alter the dynamic behavior of YFP-DnaA.

In FRAP experiments performed in a *yabA* deletion strain, a significantly increased recovery half-time for YFP-DnaA molecules compared to the wild type was observed (3.8 $\pm$ 0.3 s, figure 17, table 16). The amount of immobile molecules remained unchanged.

For a deletion of *soj-spo0J* similar results were observed. The recovery-half time for YFP-DnaA molecules increased to 4.3 $\pm$0.4 s, albeit no significant difference in the amount of immobile molecules compared to the wild type was found (figure 18, table 16).

SM microscopy in a merodiploid strain ectopically expressing YFP-DnaA in a strain harboring a *soj-spo0J* deletion confirmed the results obtained by FRAP experiments. YFP-DnaA had an

expected average residence time of 141 ms compared to 100 ms in the wild type.
A deletion of *yabA* or *soj-spo0J* increased the residence time of YFP-DnaA at DnaA binding sites. As both deletions lead to an overinitiation of replication, one could conclude that the longer residence time of YFP-DnaA might be responsible for the observed overinitiation. This would mean that both YabA and Soj/Spo0J would both act in reducing the binding time of DnaA at *oriC*.

4.8. YFP-DnaA carrying a single amino acid substitution has a reduced binding time to *oriC*

Single amino acid substitutions, which change the biochemical or physiological properties of DnaA were analyzed (section 1.3.). DnaA protein carrying the E183Q substitution is impaired in ATP binding (2-fold compared to wt) and ATP hydrolysis (6–7-fold compared to wt)[33]. Notably, DnaAE183Q showed an decreased self-multimerization capacity[33]. Ectopic expression of YFP-DnaAE183Q leads to filamentous cells, even when the expression is repressed, suggesting a dominant negative effect over wild type DnaA[33]. Only small amounts of YFP-DnaAE183Q molecules per cell were observed, which allowed no FRAP analysis.
Using SM microscopy I could show a reduced estimated residence time of 79 ms for YFP-DnaAE183Q molecules compared to YFP-DnaA, indicating that DnaA molecules impaired in ATPase activity and self-multimerization capacity have a shorter residence time at DnaA binding sites than wild type DnaA. The average diffusion constant determined for YFP-DnaAE183Q molecules was 0.98 $\mu m^2/s$ and faster than the one determined for YFP-DnaA.
Does an reduced YFP-DnaA residence time result in underinitiation of replication? A previous analysis reported wild type-like origin numbers, albeit in significantly elongated cells[33]. So one could argue that this is a kind of underinitiation.
Several reports indicate that the oligomerization of the DnaA protein is the regulating step during initiation of replication in *B. subtilis*[75,33,76]. All three regulators, YabA, Soj and DnaD, were reported to interfere with DnaA multimerization at *oriC*[80,76,75,117]. Deletion of *yabA* or *soj-spo0J* resulted in longer residence times of YFP-DnaA, hence DnaA multimerization might be facilitated due to the absence of an anti-cooperativity factor. This stabilization of DnaA at *oriC* could in turn lead to the observed overinitiation of replication. The YFP-DnaAE183Q amino acid substitution on the contrary exhibits shorter residence times and is impaired in self-multimerization, thus its binding to *oriC* is not stable, which presumably leads to an underinitiation. These findings support a model in which DnaA favors to multimerize and several regulatory factors, like YabA, Soj and DnaD, inhibit DnaA in doing so. Failure to regulate the multimerization step, results in untimely and overinitiation of replication.
Previous reports revealed that the DnaAR260A mutant displays a reduced ATP binding (1.7-fold compared to wt) and ATPase activity (2-fold compared to wt)[33]. Furthermore the DNA binding activity of DnaAR260A in the presence of ATP was reduced[33]. Microscopic analysis of *B. subtilis*

cells expressing YFP-R260A in a merodiploid strain showed a considerable decrease in cell length, indicating a premature initiation[33].
FRAP analysis of YFP-R260A showed a significantly increased half-time recovery compared to YFP-DnaA (4.1 $\pm$ 0.2 s), indicating that the impaired ATP-dependent DNA binding capacity results in a slower tunrover of YFP-R260A at DnaA binding sites. The SM microscopy results are somewhat puzzling. They show no difference between the expected residence time for YFP-DnaAR260 and wild type molecules (106 vs 101 ms). Hence, YFP-R260A shows a slower turnover rate at DnaA binding sites but does not stop longer than wild type DnaA molecules. The average diffusion constant for YFP-DnaAR260A molecules, calculated from the MSD over time, is 0.49 $\mu m^2/s$, which is 30% slower than for the wild type. The average diffusion of YFP-R260A molecules is reduced but the stopping times remain wild type-like. The reduced average diffusion constant for YFP-DnaAR260A could be due to a change in the native constitution of the protein. Purified wild type DnaA forms a dimer in solution, DnaAR260A could for instance form a trimer. But biochemical data does not support this notion[33].
The amino acid subsitution A163V in the DnaA protein leads to the formation of a constitutive multimer, which is deficient in ATP binding and hydrolysis[33]. Expression of YFP-DnaAA163V led to a stong overinitaition of replication and to elongated cells even under uninduced conditions, which led to the hypothesis that YFP-DnaAA163V has a dominant negative effect over wild type DnaA[33]. This amino acid substitution was furthermore reported by Scholefiel and Murray to be resistant to YabA inhibition and to have in contrast to our findings a wild type-rate of initiation[76].
SM analysis of YFP-DnaAA163V revealed a slightly decreased residence time (87 ms vs 101 ms for wt) and an average diffusion constant of 0.73 $\mu m^2/s$, which is similar to wild type.
As DnaAA163V was reported to form a constitutive multimer I expected longer residence times. On the other hand, its conformation as a multimer could enable DnaAA163V to start the inititation process even faster, as it has a high binding affinity for *oriC* DnaA independent of ATP[33].

4.9. YFP-YabA has a similar turnover rate as DnaA but resides longer at the single molecule level

YabA is a negative regulator of initiation, which inhibits cooperative DnaA binding at *oriC* and tethers DnaA to the replisome via interaction with DnaN[2,75,76]. Furthermore during this study I could show that YFP-YabA follows a similar localization pattern as YFP-DnaA (section 3.2.). Therefore I was interested whether YFP-YabA would show a similar dynamics as YFP-DnaA. Interestingly, YFP-YabA molecules have a similar recovery-half time as YFP-DnaA (2.3 $\pm$ 0.24 s, figure 22). Hence, YFP-YabA molecules display a high tunrover at *oriC* and the replication machinery, albeit 20% of the YFP-YabA molecules are part of an immobile fraction, representing a significant increase compared to YFP-DnaA. Furthermore SM microscopy revealed a significant

increase in residence time (208 vs 101 ms in wt) and an average diffusion constant of 0.16 $\mu m^2/s$, which is 4-fold slower than the one measured for YFP-DnaA. These findings show that YFP-YabA, although it has a similar turnover rate as YFP-DnaA, behaves very differently at the single molecule level, as around 27% of all observed trajectories stop for 5 or more time frames (figure 29 A). These results further indicate that YabA does not move alongside DnaA over the chromosome but rather stays bound at sites where DnaA or DnaN are present. Only few mobile YFP-YabA were observed, indicating that the mobile fraction might be free diffusing. These molecules are not detectable with our experimental setup due to a stream acquisition time of 41 ms, which is not fast enough for free diffusing molecules.

4.10. Deletion of *yabA* and *soj-spo0J* do not alter YFP-DnaA dynamics

In this work I could show that a deletion of *yabA* and *soj-spo0J* resulted in a strong overinitiation of replication (section 3.4.3.). Previous results in *yabA* or *soj-spo0J* deletion strains revealed an increased recovery half-time for YFP-DnaA, which presumably caused the overinitiation of replication observed in these deletion strains.

I was interested in what respect the dynamics of YFP-DnaA would change upon deletion of *yabA* and *soj-spo0J*. Surprisingly, the half-time recovery of YFP-DnaA was similar to the one observed in the wild type strain (2.8 ± 0.27 s, figure 19). This finding was somewhat puzzling as from the previous analyzed experiments a further increased half-time recovery of YFP-DnaA was suspected. Notably, the subfraction of YFP-DnaA immobile molecules in this strain was 23%, which is significantly higher than in the wild type.

Based on these finding I would suspect that the increased fraction of immobile molecules might be the ones currently active in initiation of replication and their increase could be the reason for the observed overinitiation. On the other hand, in a *yabA soj-spo0J* deletion cell more YFP-DnaA foci are visible per cell (figure 19), so the increase of the immobile fraction could be due to an increase in DnaA foci and also *oriC* regions in general.

But how to explain the wild type-like dynamic of YFP-DnaA in this strain? Soj and YabA are both regulators capable of interacting with DnaA. Soj was shown to have a positive (as a dimer) and a negative (as a monomer) effect on initiation of replication[77,80]. For YabA, so far, only a negative regulatory effect on the initiation of replication was reported[73,2,75,76]. In *E. coli* the DnaA interacting protein DiaA forms tetramers and supports DnaA multimerization[9]. YabA also forms tetramers[83] and could potentially bind several DnaA molecules and thus might play a similar role as DiaA in *E. coli*. This notion is highly speculative but could award YabA a positive function in the initiation of replication process. These are two regulators that both have a positive and a negative influence on DnaA. If one is deleted, the other can still partially replace its function, as can be concluded from the degree of overinitation witnessed in the single deletions. Upon deletion of both regulators none of the two can modulate DnaA function and it is free to either multimerize and initiate or dissociate according to its intrinsic properties or as

regulated by other regulators, e.g. DnaD.

4.11. *E. coli* DnaA oscillates between cell halves

Localization studies on DnaA in *E. coli* report two diverse localization patterns for DnaA-YFP. One indicating DnaA to form a helical structure, similar to the one of MreB, along the long axis of the cell and the other describing DnaA to form discrete foci colocalizing with the origin of replication or the *datA* site[25,24]. As *B. subtilis* DnaA also localizes in discrete foci, I choose to use the *E. coli* strain reported by Nozaki *et al* for my analysis using cells that displayed two DnaA foci[2,24].

During stream acquisition a clear movement of the *Ec*DnaA-YFP fluorescence signal from one cell half to the other was observed. To further investigate this notion the fluorescence intensities inside two spots (two fluorescence foci) on the different cell halves were compared (after normalization to the fluorescence of the entire cell, section 3.6.). When plotted against each other a clear inverse correlation between the two areas was observed (figure 23 D). Hence, *Ec*DnaA-YFP reveals to be highly mobile and probably oscillates between two origin regions.

Notably, analysis of cells expressing TetR-YFP bound to a *tetO* array showed no correlation between the two areas measured (figure 23 F).

Transcription at the *oriC* region may be responsible for the oscillating behavior of *Ec*DnaA-YFP. The DNA-dependent RNA polymerase was shown to read into the *oriC* region due to the weak terminator sequence of the adjacent *mioC* gene[30]. Analysis of cells that were treated with rifampicin for 30 min showed no difference to non-treated cells with respect to the inverse correlation between the two cell halves (figure 23 E). Rifampicin inhibits transcription by binding to the DNA-dependent RNA polymerase. These results indicate that the DNA-dependent RNA polymerase is likely not responsible for dynamics displayed by *Ec*DnaA-YFP.

SM microscopy revealed a slightly increased estimated residence time compared to *Bs*YFP-DnaA (135 vs 101 ms for *Bs*YFP-DnaA) as well as a slower average diffusion constant of 0.34 $\mu m^2/s$, indicating a somewhat slower movement of *Ec*DnaA-YFP. This is in accordance with the fact that the oscillation of *Ec*DnaA-YFP is visible during a stream acquisition, whereas the pattern of movement of *Bs*YFP-DnaA is not.

The observed oscillation of *Ec*DnaA-YFP might be caused by a regulatory protein chasing DnaA through the cell and inducing the release of DnaA from its binding sites. A similar mechanism was described for the *E. coli* MinCDE sytem, which is a key player for division site selection[121]. MinE oscillates between the cell poles and thereby actively displaces the MinCD complex from the membrane. DnaA oscillation could provide a robust mechanism to control initiation of replication. Removing the chasing regulator could initiate replication or alternatively the action of a positive regulator could stabilize DnaA binding to *oriC*.

Overall I could show a dynamic behavior of DnaA in two bacterial species, indicating that these fast on-off rates might be a general principle to regulate the initiation of replication.

4.12. The Era GTPase localizes in patches close to the cell poles

Era is a conserved RAS-like GTPase, which is important for 16SrRNA maturation and the assembly of the 30S ribosomal subunit[122]. Furthermore it is essential for cell growth in *E. coli* and was proposed to function as a cell cycle checkpoint[106,110]

I was interested in the localization of Era-mVenus in stationary and exponentially growing cells. In stationary cells 4 different localization patterns were observed (figure 33 A). Overall Era-mVenus either localized in patches or dispersed in the cytoplasm. In exponentially growing cells a similar localization pattern was observed, albeit the fluorescence signal was much weaker. In a stream acquisition small mobile or static foci were detectable (figure 34 B, yellow and red arrow). Interestingly, the foci localized close to the cell poles, where also the ribosomes are located. As Era plays a role in ribosome biogenesis, a localization near the ribosomes can be expected. Prior localization of Era using immunoelectron microscopy was reported to be near the internal surface of the cytoplasmic membrane and in patches presumably corresponding to sites of septation[123].

Previous unpublished data from M. Eisemann showed a possible interaction between YabA and Era. Depletion of Era was further shown to lead to an overinitation of replication[107], implying a possible connection between Era and the initiation of replication. SM analysis of Era-mVenus in a *yabA* deletion strain or during blocked replication or translation could help to further investigate its function in *B. subtilis*.

Abbreviations

A	…	AAA+	ATPases associated with diverse cellular activities
		ADP (ATP)	adenosine diphosphate (adenosine triphosphate)
		Amp^R	ampicillin resistance
		APS	ammonium peroxodisulfate
B	…	bp	base pair(s)
C	…	CDF	cumulative distribution function
		CFP	cyan fluorescent protein
		CIP	calf intestinal phosphatase
		Cm^R	chloramphenicol-resistance
D	…	DAPI	4',6-diamidino-2-phenylindole
		Δx	deletion mutation in gen x
		DiaA	DnaA initiator-associated
		DNA	deoxyribonucleic acid
		dNTPs	deoxynucleotide triphosphate(s)
		DSM	Difco sporulation medium
E	…	EDTA	N,N,N',N'-Ethylendiamintetraacetat-Dinatriumsalz
		Erm	Erythromycin
		et al.	et alii
		EtOH	Ethanol
F	…	FRAP	fluorescence recovery after photobleaching
G	…	g	Gram
		GFP	green fluorescent protein
H	…	h	hour(s)
I	…	IHF	integration host factor
		IPTG	isopropyl β- D -1-thiogalactopyranoside
K	…	kb	kilobase
		kDa	kilo dalton
L	…	l	liter
		LB	Luria Bertani
		Lin	Lincomycin
M	…	M	molar
		ml (μl)	milliliter (microliter)
		min	minute(s)
		MW	molecular weight
N	…	Neo	kanamycin
		nt	nucleotide(s)

O	...	OD_{xxx}	optical density at xxx nm
		oriC	origin of replication
		ORC	origin recognition complex
P	...	p	probability
		p.a.	pro analysi
		PCR	polymerase chain reaction
		%	percent
		PhD	Doctor of Philosophy
		pre-RC	prereplication complex
		P_{xyl}	xylose promotor
R	...	RIDA	regulatory inactivation of DnaA
		rpm	revolutions per minute
		RT	room temperature
		RU	response/resonance units
S	...	SDS(-PAGE)	sodium dodecyl sulfate (-polyacrylamide gel electrophoresis)
		SM	single molecule
		$Spec^R$	spectinomycin resistance
		s (ms)	second(s) (milliseconds)
T	...	TEMED	tetramethylehtylenediamine
		Tet^R	tetracyclin resistance
U	...	U	unit(s)
		UV	ultraviolet
V	...	V	volt
		v/v	volume per volume
W	...	wt	wild type
		w/v	weight per volume
Y	...	YFP	yellow fluorescent protein
X	...	X-YPF,	protein X, labeled with fluorescent protein (YFP, CFP or GFP)
		X-CFP,	
		X-GFP	

Bibliography

1. F. Kunst, N. Ogasawara, I. Moszer, A. M. Albertini, G. Alloni, V. Azevedo, M. G. Bertero, P. Bessières, A. Bolotin, S. Borchert, R. Borriss, L. Boursier, A. Brans, M. Braun, S. C. Brignell, S. Bron, S. Brouillet, C. V. Bruschi, B. Caldwell, V. Capuano, N. M. Carter, S. K. Choi, J. J. Cordani, I. F. Connerton, N. J. Cummings, R. A. Daniel, F. Denziot, K. M. Devine, A. Düsterhöft, S. D. Ehrlich, P. T. Emmerson, K. D. Entian, J. Errington, C. Fabret, E. Ferrari, D. Foulger, C. Fritz, M. Fujita, Y. Fujita, S. Fuma, A. Galizzi, N. Galleron, S. Y. Ghim, P. Glaser, A. Goffeau, E. J. Golightly, G. Grandi, G. Guiseppi, B. J. Guy, K. Haga, J. Haiech, C. R. Harwood, A. Hènaut, H. Hilbert, S. Holsappel, S. Hosono, M. F. Hullo, M. Itaya, L. Jones, B. Joris, D. Karamata, Y. Kasahara, M. Klaerr-Blanchard, C. Klein, Y. Kobayashi, P. Koetter, G. Koningstein, S. Krogh, M. Kumano, K. Kurita, A. Lapidus, S. Lardinois, J. Lauber, V. Lazarevic, S. M. Lee, A. Levine, H. Liu, S. Masuda, C. Mauël, C. Médigue, N. Medina, R. P. Mellado, M. Mizuno, D. Moestl, S. Nakai, M. Noback, D. Noone, M. O'Reilly, K. Ogawa, A. Ogiwara, B. Oudega, S. H. Park, V. Parro, T. M. Pohl, D. Portelle, S. Porwollik, A. M. Prescott, E. Presecan, P. Pujic, B. Purnelle, G. Rapoport, M. Rey, S. Reynolds, M. Rieger, C. Rivolta, E. Rocha, B. Roche, M. Rose, Y. Sadaie, T. Sato, E. Scanlan, S. Schleich, R. Schroeter, F. Scoffone, J. Sekiguchi, A. Sekowska, S. J. Seror, P. Serror, B. S. Shin, B. Soldo, A. Sorokin, E. Tacconi, T. Takagi, H. Takahashi, K. Takemaru, M. Takeuchi, A. Tamakoshi, T. Tanaka, P. Terpstra, A. Togoni, V. Tosato, S. Uchiyama, M. Vandebol, F. Vannier, A. Vassarotti, A. Viari, R. Wambutt, H. Wedler, T. Weitzenegger, P. Winters, A. Wipat, H. Yamamoto, K. Yamane, K. Yasumoto, K. Yata, K. Yoshida, H. F. Yoshikawa, E. Zumstein, H. Yoshikawa, and A. Danchin, *"The complete genome sequence of the gram-positive bacterium Bacillus subtilis"*, Nature, **390**, pp. 249–256, Nov. 1997.

2. C. D. Soufo, H. J. D. Soufo, M.-F. Noirot-Gros, A. Steindorf, P. Noirot, and P. L. Graumann, *"Cell-cycle-dependent spatial sequestration of the DnaA replication initiator protein in Bacillus subtilis"*, Dev. Cell, **15**, pp. 935–941, Dec. 2008.

3. K. Skarstad, E. Boye, and H. B. Steen, *"Timing of initiation of chromosome replication in individual Escherichia coli cells"*, EMBO J., **5**, pp. 1711–1717, July 1986.

4. R. S. Fuller, B. E. Funnell, and A. Kornberg, *"The dnaA protein complex with the E. coli chromosomal replication origin (oriC) and other DNA sites"*, Cell, **38**, pp. 889–900, Oct. 1984.

5. M. Matsui, A. Oka, M. Takanami, S. Yasuda, and Y. Hirota, *"Sites of dnaA protein-binding in the replication origin of the Escherichia coli K-12 chromosome"*, J. Mol. Biol., **184**, pp. 529–533, Aug. 1985.

6. D. Bramhill and A. Kornberg, *"Duplex opening by dnaA protein at novel sequences in initiation of replication at the origin of the E. coli chromosome"*, Cell, **52**, pp. 743–755, Mar. 1988.

7. K. Sekimizu, D. Bramhill, and A. Kornberg, *"ATP activates dnaA protein in initiating replication of plasmids bearing the origin of the E. coli chromosome"*, Cell, **50**, pp. 259–265, July 1987.

8. A. Roth, B. Urmoneit, and W. Messer, *"Functions of histone-like proteins in the initiation of DNA replication at oriC of Escherichia coli"*, Biochimie, **76**, pp. 917–923, Jan. 1994.

9. T. Ishida, N. Akimitsu, T. Kashioka, M. Hatano, T. Kubota, Y. Ogata, K. Sekimizu, and T. Katayama, *"DiaA, a novel DnaA-binding protein, ensures the timely initiation of Escherichia coli chromosome replication"*, J. Biol. Chem., **279**, pp. 45546–45555, Oct. 2004.

10. J. P. Erzberger, M. L. Mott, and J. M. Berger, *"Structural basis for ATP-dependent DnaA assembly and replication-origin remodeling"*, Nat. Struct. Mol. Biol., **13**, pp. 676–683, Aug. 2006.

11. S. Ozaki, H. Kawakami, K. Nakamura, N. Fujikawa, W. Kagawa, S.-Y. Park, S. Yokoyama, H. Kurumizaka, and T. Katayama, *"A common mechanism for the ATP-DnaA-dependent formation of open complexes at the replication origin"*, J. Biol. Chem., **283**, pp. 8351–8362, Mar. 2008.

12. R. Donczew, J. Zakrzewska-Czerwińska, and A. Zawilak-Pawlik, *"Beyond DnaA: The Role of DNA Topology and DNA Methylation in Bacterial Replication Initiation"*, J. Mol. Biol., **426**, pp. 2269–2282, June 2014.

13. M. Krause and W. Messer, *"DnaA proteins of Escherichia coli and Bacillus subtilis: coordinate actions with single-stranded DNA-binding protein and interspecies inhibition during open complex formation at the replication origins"*, Gene, **228**, pp. 123–132, Mar. 1999.

14. A. V. Ludlam, M. W. McNatt, K. M. Carr, and J. M. Kaguni, *"Essential amino acids of Escherichia coli DnaC protein in an N-terminal domain interact with DnaB helicase"*, J. Biol. Chem., **276**, pp. 27345–27353, July 2001.

15. L. Fang, M. J. Davey, and M. O'Donnell, *"Replisome assembly at oriC, the replication origin of E. coli, reveals an explanation for initiation sites outside an origin"*, Mol. Cell, **4**, pp. 541–553, Oct. 1999.

16. Y. Abe, T. Jo, Y. Matsuda, C. Matsunaga, T. Katayama, and T. Ueda, *"Structure and function of DnaA N-terminal domains: specific sites and mechanisms in inter-DnaA interaction and in DnaB helicase loading on oriC"*, J. Biol. Chem., **282**, pp. 17816–17827, June 2007.

17. M. J. Davey, L. Fang, P. McInerney, R. E. Georgescu, and M. O'Donnell, *"The DnaC helicase loader is a dual ATP/ADP switch protein"*, EMBO J., **21**, pp. 3148–3159, June 2002.

18. M. Makowska-Grzyska and J. M. Kaguni, *"Primase directs the release of DnaC from DnaB"*, Mol. Cell, **37**, pp. 90–101, Jan. 2010.

19. J. M. Kaguni, *"Replication initiation at the Escherichia coli chromosomal origin"*, Curr. Opin. Chem. Biol., **15**, pp. 606–613, Oct. 2011.

20. A. C. Leonard and J. E. Grimwade, *"Regulating DnaA complex assembly: it is time to fill the gaps"*, Curr. Opin. Microbiol., **13**, pp. 766–772, Dec. 2010.

21. J. P. Erzberger, M. M. Pirruccello, and J. M. Berger, *"The structure of bacterial DnaA: implications for general mechanisms underlying DNA replication initiation"*, EMBO J., **21**, pp. 4763–4773, Sept. 2002.

22. M. D. Sutton, K. M. Carr, M. Vicente, and J. M. Kaguni, *"Escherichia coli DnaA protein. The N-terminal domain and loading of DnaB helicase at the E. coli chromosomal origin"*, J. Biol. Chem., **273**, pp. 34255–34262, Dec. 1998.

23. A. C. Leonard and J. E. Grimwade, *"Regulation of DnaA assembly and activity: taking directions from the genome"*, Annu. Rev. Microbiol., **65**, pp. 19–35, Jan. 2011.

24. S. Nozaki, H. Niki, and T. Ogawa, *"Replication initiator DnaA of Escherichia coli changes its assembly form on the replication origin during the cell cycle"*, J. Bacteriol., **191**, pp. 4807–4814, Aug. 2009.

25. K. Boeneman, S. Fossum, Y. Yang, N. Fingland, K. Skarstad, and E. Crooke, *"Escherichia coli DnaA forms helical structures along the longitudinal cell axis distinct from MreB filaments"*, Mol. Microbiol., **72**, pp. 645–657, May 2009.

26. K. E. Duderstadt, K. Chuang, and J. M. Berger, *"DNA stretching by bacterial initiators promotes replication origin opening"*, Nature, Oct. 2011.

27. N. Fujikawa, H. Kurumizaka, O. Nureki, T. Terada, M. Shirouzu, T. Katayama, and S. Yokoyama, *"Structural basis of replication origin recognition by the DnaA protein"*, Nucleic Acids Res., **31**, pp. 2077–2086, Apr. 2003.

28. J. Garner, P. Durrer, J. Kitchen, J. Brunner, and E. Crooke, *"Membrane-mediated release of nucleotide from an initiator of chromosomal replication, Escherichia coli DnaA, occurs with insertion of a distinct region of the protein into the lipid bilayer"*, J. Biol. Chem., **273**, pp. 5167–5173, Feb. 1998.

29. J. M. Kaguni, *"DnaA: controlling the initiation of bacterial DNA replication and more"*, Annu. Rev. Microbiol., **60**, pp. 351–375, Jan. 2006.

30. W. Messer and C. Weigel, *"DnaA initiator–also a transcription factor"*, Mol. Microbiol., **24**, pp. 1–6, Apr. 1997.

31. A. I. Goranov, L. Katz, A. M. Breier, C. B. Burge, and A. D. Grossman, *"A transcriptional response to replication status mediated by the conserved bacterial replication protein DnaA"*, Proc. Natl. Acad. Sci. U. S. A., **102**, pp. 12932–12937, Sept. 2005.

32. Y. Ogura, Y. Imai, N. Ogasawara, and S. Moriya, *"Autoregulation of the dnaA-dnaN operon and effects of DnaA protein levels on replication initiation in Bacillus subtilis"*, J. Bacteriol., **183**, pp. 3833–3841, July 2001.

33. M. Eisemann, *"Characterization of DnaA mutant proteins from Bacillus subtilis – novel insights into the initiation of replication"*, PhD thesis, University of Freiburg, 2012.

34. M. Wolański, R. Donczew, A. Zawilak-Pawlik, and J. Zakrzewska-Czerwińska, *"oriC-encoded instructions for the initiation of bacterial chromosome replication"*, Front. Microbiol., **5**, p. 735, Jan. 2014.

35. S. Tabata, A. Oka, K. Sugimoto, M. Takanami, S. Yasuda, and Y. Hirota, *"The 245 base-pair oriC sequence of the E. coli chromosome directs bidirectional replication at an adjacent region"*, Nucleic Acids Res., **11**, pp. 2617–2626, May 1983.

36. C. Margulies and J. M. Kaguni, *"Ordered and sequential binding of DnaA protein to oriC, the chromosomal origin of Escherichia coli"*, J. Biol. Chem., **271**, pp. 17035–17040, July 1996.

37. S. Schaper and W. Messer, *"Interaction of the initiator protein DnaA of Escherichia coli with its DNA target"*, J. Biol. Chem., **270**, pp. 17622–17626, July 1995.

38. F. G. Hansen, B. B. Christensen, and T. Atlung, *"Sequence characteristics required for cooperative binding and efficient in vivo titration of the replication initiator protein DnaA in E. coli"*, J. Mol. Biol., **367**, pp. 942–952, Apr. 2007.

39. H. Gille, J. B. Egan, A. Roth, and W. Messer, *"The FIS protein binds and bends the origin of chromosomal DNA replication, oriC, of Escherichia coli"*, Nucleic Acids Res., **19**, pp. 4167–4172, Aug. 1991.

40. C. Nievera, J. J.-C. Torgue, J. E. Grimwade, and A. C. Leonard, *"SeqA blocking of DnaA-oriC interactions ensures staged assembly of the E. coli pre-RC"*, Mol. Cell, **24**, pp. 581–592, Nov. 2006.

41. K. C. McGarry, V. T. Ryan, J. E. Grimwade, and A. C. Leonard, *"Two discriminatory binding sites in the Escherichia coli replication origin are required for DNA strand opening by initiator DnaA-ATP"*, Proc. Natl. Acad. Sci. U. S. A., **101**, pp. 2811–2816, Mar. 2004.

42. V. T. Ryan, J. E. Grimwade, J. E. Camara, E. Crooke, and A. C. Leonard, *"Escherichia coli prereplication complex assembly is regulated by dynamic interplay among Fis, IHF and DnaA"*, Mol. Microbiol., **51**, pp. 1347–1359, Mar. 2004.

43. S. Moriya, T. Fukuoka, N. Ogasawara, and H. Yoshikawa, *"Regulation of initiation of the chromosomal replication by DnaA-boxes in the origin region of the Bacillus subtilis chromosome"*, EMBO J., **7**, pp. 2911–2917, Sept. 1988.

44. T. Fukuoka, S. Moriya, H. Yoshikawa, and N. Ogasawara, *"Purification and characterization of an initiation protein for chromosomal replication, DnaA, in Bacillus subtilis"*, J. Biochem., **107**, pp. 732–739, May 1990.

45. M. Krause, B. Rückert, R. Lurz, and W. Messer, *"Complexes at the replication origin of Bacillus subtilis with homologous and heterologous DnaA protein"*, J. Mol. Biol., **274**, pp. 365–380, Dec. 1997.

46. S. Moriya, T. Atlung, F. G. Hansen, H. Yoshikawa, and N. Ogasawara, *"Cloning of an autonomously replicating sequence (ars) from the Bacillus subtilis chromosome"*, Mol. Microbiol., **6**, pp. 309–315, Feb. 1992.

47. M. Wolański, D. Jakimowicz, and J. Zakrzewska-Czerwińska, *"Fifty years after the replicon hypothesis: cell-specific master regulators as new players in chromosome replication control"*, J. Bacteriol., **196**, pp. 2901–2911, Aug. 2014.

48. J. W. Zyskind and D. W. Smith, *"The bacterial origin of replication, oriC"*, Cell, **46**, pp. 489–490, Aug. 1986.

49. K. Skarstad and T. Katayama, *"Regulating DNA replication in bacteria"*, Cold Spring Harb. Perspect. Biol., **5**, p. a012922, Apr. 2013.

50. M. LU, *"SeqA: A negative modulator of replication initiation in E. coli"*, Cell, **77**, pp. 413–426, May 1994.

51. T. Katayama, S. Ozaki, K. Keyamura, and K. Fujimitsu, *"Regulation of the replication cycle: conserved and diverse regulatory systems for DnaA and oriC"*, Nat. Rev. Microbiol., **8**, pp. 163–170, Mar. 2010.

52. G. B. Ogden, M. J. Pratt, and M. Schaechter, *"The replicative origin of the E. coli chromosome binds to cell membranes only when hemimethylated"*, Cell, **54**, pp. 127–135, July 1988.

53. J. L. Campbell and N. Kleckner, *"E. coli oriC and the dnaA gene promoter are sequestered from dam methyltransferase following the passage of the chromosomal replication fork"*, Cell, **62**, pp. 967–979, Sept. 1990.

54. K. Kurokawa, S. Nishida, A. Emoto, K. Sekimizu, and T. Katayama, *"Replication cycle-coordinated change of the adenine nucleotide-bound forms of DnaA protein in Escherichia coli"*, EMBO J., **18**, pp. 6642–6652, Dec. 1999.

55. T. Katayama and K. Sekimizu, *"Inactivation of Escherichia coli DnaA protein by DNA polymerase III and negative regulations for initiation of chromosomal replication"*, Biochimie, **81**, pp. 835–840, Aug. 1999.

56. M. Su'etsugu, T.-R. Shimuta, T. Ishida, H. Kawakami, and T. Katayama, *"Protein associations in DnaA-ATP hydrolysis mediated by the Hda-replicase clamp complex"*, J. Biol. Chem., **280**, pp. 6528–6536, Feb. 2005.

57. J. Kato and T. Katayama, *"Hda, a novel DnaA-related protein, regulates the replication cycle in Escherichia coli"*, EMBO J., **20**, pp. 4253–4262, Aug. 2001.

58. M. Su'etsugu, K. Nakamura, K. Keyamura, Y. Kudo, and T. Katayama, *"Hda monomerization by ADP binding promotes replicase clamp-mediated DnaA-ATP hydrolysis"*, J. Biol. Chem., **283**, pp. 36118–36131, Dec. 2008.

59. A. Roth and W. Messer, *"High-affinity binding sites for the initiator protein DnaA on the chromosome of Escherichia coli"*, Mol. Microbiol., **28**, pp. 395–401, Apr. 1998.

60. R. Kitagawa, H. Mitsuki, T. Okazaki, and T. Ogawa, *"A novel DnaA protein-binding site at 94.7 min on the Escherichia coli chromosome"*, Mol. Microbiol., **19**, pp. 1137–1147, Mar. 1996.

61. R. Kitagawa, T. Ozaki, S. Moriya, and T. Ogawa, *"Negative control of replication initiation by a novel chromosomal locus exhibiting exceptional affinity for Escherichia coli DnaA protein"*, Genes Dev., **12**, pp. 3032–3043, Oct. 1998.

62. H. Okumura, M. Yoshimura, M. Ueki, T. Oshima, N. Ogasawara, and S. Ishikawa, *"Regulation of chromosomal replication initiation by oriC-proximal DnaA-box clusters in Bacillus subtilis"*, Nucleic Acids Res., **40**, pp. 220–234, Jan. 2012.

63. K. Kasho and T. Katayama, *"DnaA binding locus datA promotes DnaA-ATP hydrolysis to enable cell cycle-coordinated replication initiation"*, Proc. Natl. Acad. Sci. U. S. A., **110**, pp. 936–941, Jan. 2013.

64. K. Fujimitsu, T. Senriuchi, and T. Katayama, *"Specific genomic sequences of E. coli promote replicational initiation by directly reactivating ADP-DnaA"*, Genes Dev., **23**, pp. 1221–1233, May 2009.

65. K. Kasho, K. Fujimitsu, T. Matoba, T. Oshima, and T. Katayama, *"Timely binding of IHF and Fis to DARS2 regulates ATP-DnaA production and replication initiation"*, Nucleic Acids Res., **42**, pp. 13134–13149, Dec. 2014.

66. V. Castilla-Llorente, D. Muñoz Espín, L. Villar, M. Salas, and W. J. J. Meijer, *"Spo0A, the key transcriptional regulator for entrance into sporulation, is an inhibitor of DNA replication"*, EMBO J., **25**, pp. 3890–3899, Aug. 2006.

67. M. Boonstra, I. G. de Jong, G. Scholefield, H. Murray, O. P. Kuipers, and J.-W. Veening, *"Spo0A regulates chromosome copy number during sporulation by directly binding to the origin of replication in Bacillus subtilis"*, Mol. Microbiol., **87**, pp. 925–938, Feb. 2013.

68. L. Rahn-Lee, B. Gorbatyuk, O. Skovgaard, and R. Losick, *"The conserved sporulation protein YneE inhibits DNA replication in Bacillus subtilis"*, J. Bacteriol., **191**, pp. 3736–3739, June 2009.

69. L. Rahn-Lee, H. Merrikh, A. D. Grossman, and R. Losick, *"The sporulation protein SirA inhibits the binding of DnaA to the origin of replication by contacting a patch of clustered amino acids"*, J. Bacteriol., **193**, pp. 1302–1307, Mar. 2011.

70. K. H. Jameson, N. Rostami, M. J. Fogg, J. P. Turkenburg, A. Grahl, H. Murray, and A. J. Wilkinson, *"Structure and Interactions of the Bacillus subtilis Sporulation Inhibitor of DNA Replication, SirA, with Domain I of DnaA"*, Mol. Microbiol., July 2014.

71. W. F. Burkholder, I. Kurtser, and A. D. Grossman, *"Replication initiation proteins regulate a developmental checkpoint in Bacillus subtilis"*, Cell, **104**, pp. 269–279, Jan. 2001.

72. J.-W. Veening, H. Murray, and J. Errington, *"A mechanism for cell cycle regulation of sporulation initiation in Bacillus subtilis"*, Genes Dev., **23**, pp. 1959–1970, Aug. 2009.

73. M.-F. Noirot-Gros, E. Dervyn, L. J. Wu, P. Mervelet, J. Errington, S. D. Ehrlich, and P. Noirot, *"An expanded view of bacterial DNA replication"*, Proc. Natl. Acad. Sci. U. S. A., **99**, pp. 8342–8347, June 2002.

74. A. I. Goranov, A. M. Breier, H. Merrikh, and A. D. Grossman, *"YabA of Bacillus subtilis controls DnaA-mediated replication initiation but not the transcriptional response to replication stress"*, Mol. Microbiol., **74**, pp. 454–466, Oct. 2009.

75. H. Merrikh and A. D. Grossman, *"Control of the replication initiator DnaA by an anti-cooperativity factor"*, Mol. Microbiol., pp. 1–13, Sept. 2011.

76. G. Scholefield and H. Murray, *"YabA and DnaD inhibit helix assembly of the DNA replication initiation protein DnaA"*, Mol. Microbiol., **90**, pp. 147–159, Oct. 2013.

77. H. Murray and J. Errington, *"Dynamic control of the DNA replication initiation protein DnaA by Soj/ParA"*, Cell, **135**, pp. 74–84, Oct. 2008.

78. T. A. Leonard, P. J. Butler, and J. Löwe, *"Bacterial chromosome segregation: structure and DNA binding of the Soj dimer–a conserved biological switch"*, EMBO J., **24**, pp. 270–282, Jan. 2005.

79. G. Scholefield, R. Whiting, J. Errington, and H. Murray, *"Spo0J regulates the oligomeric state of Soj to trigger its switch from an activator to an inhibitor of DNA replication initiation"*, Mol. Microbiol., **79**, pp. 1089–1100, Feb. 2011.

80. G. Scholefield, J. Errington, and H. Murray, *"Soj/ParA stalls DNA replication by inhibiting helix formation of the initiator protein DnaA"*, EMBO J., pp. 1–14, Jan. 2012.

81. E. Maloney, S. C. Madiraju, M. Rajagopalan, and M. Madiraju, *"Localization of acidic phospholipid cardiolipin and DnaA in mycobacteria"*, Tuberculosis (Edinb)., **91 Suppl 1**, pp. S150–5, Dec. 2011.

82. M. Hayashi, Y. Ogura, E. J. Harry, N. Ogasawara, and S. Moriya, *"Bacillus subtilis YabA is involved in determining the timing and synchrony of replication initiation"*, FEMS Microbiol. Lett., **247**, pp. 73–79, July 2005.

83. M.-F. Noirot-Gros, M. Velten, M. Yoshimura, S. McGovern, T. Morimoto, S. D. Ehrlich, N. Ogasawara, P. Polard, and P. Noirot, *"Functional dissection of YabA, a negative regulator of DNA replication initiation in Bacillus subtilis"*, Proc. Natl. Acad. Sci. U. S. A., **103**, pp. 2368–2373, Feb. 2006.

84. P. Youngman, J. B. Perkins, and R. Losick, *"Construction of a cloning site near one end of Tn917 into which foreign DNA may be inserted without affecting transposition in Bacillus subtilis or expression of the transposon-borne erm gene"*, Plasmid, **12**, pp. 1–9, July 1984.

85. D. M. Woodcock, P. J. Crowther, J. Doherty, S. Jefferson, E. DeCruz, M. Noyer-Weidner, S. S. Smith, M. Z. Michael, and M. W. Graham, *"Quantitative evaluation of Escherichia coli host strains for tolerance to cytosine methylation in plasmid and phage recombinants"*, Nucleic Acids Res., **17**, pp. 3469–3478, May 1989.

86. P. S. Lee and A. D. Grossman, *"The chromosome partitioning proteins Soj (ParA) and Spo0J (ParB) contribute to accurate chromosome partitioning, separation of replicated sister origins, and regulation of replication initiation in Bacillus subtilis"*, Mol. Microbiol., **60**, pp. 853–869, May 2006.

87. K. Ireton and A. D. Grossman, *"A developmental checkpoint couples the initiation of sporulation to DNA replication in Bacillus subtilis"*, EMBO J., **13**, pp. 1566–1573, Apr. 1994.

88. P. S. Lee, D. C.-H. Lin, S. Moriya, and A. D. Grossman, *"Effects of the chromosome partitioning protein Spo0J (ParB) on oriC positioning and replication initiation in Bacillus subtilis"*, J. Bacteriol., **185**, pp. 1326–1337, Feb. 2003.

89. P. J. Lewis and A. L. Marston, *"GFP vectors for controlled expression and dual labelling of protein fusions in Bacillus subtilis"*, Gene, **227**, pp. 101–109, Feb. 1999.

90. H. J. Defeu Soufo and P. L. Graumann, *"Dynamic movement of actin-like proteins within bacterial cells"*, EMBO Rep., **5**, pp. 789–794, Aug. 2004.

91. D. B. Kearns and R. Losick, *"Cell population heterogeneity during growth of Bacillus subtilis"*, Genes Dev., **19**, pp. 3083–3094, Dec. 2005.

92. M. Steinmetz and R. Richter, *"Plasmids designed to alter the antibiotic resistance expressed by insertion mutations in Bacillus subtilis, through in vivo recombination"*, Gene, **142**, pp. 79–83, May 1994.

93. K. Mullis, F. Faloona, S. Scharf, R. Saiki, G. Horn, and H. Erlich, *"Specific enzymatic amplification of DNA in vitro: the polymerase chain reaction"*, Cold Spring Harb. Symp. Quant. Biol., **51 Pt 1**, pp. 263–273, Jan. 1986.

94. F. Sanger, S. Nicklen, and A. R. Coulson, *"DNA sequencing with chain-terminating inhibitors"*, Proc. Natl. Acad. Sci. U. S. A., **74**, pp. 5463–5467, Dec. 1977.

95. U. K. Laemmli, *"Cleavage of structural proteins during the assembly of the head of bacteriophage T4"*, Nature, **227**, pp. 680–685, Aug. 1970.

96. D. H. Williamson and D. J. Fennell, *"Apparent dispersive replication of yeast mitochondrial DNA as revealed by density labelling experiments"*, Mol. Gen. Genet., **131**, pp. 193–207, Jan. 1974.

97. T. A. Vida and S. D. Emr, *"A new vital stain for visualizing vacuolar membrane dynamics and endocytosis in yeast"*, J. Cell Biol., **128**, pp. 779–792, Mar. 1995.

98. G. S. Gordon, D. Sitnikov, C. D. Webb, A. Teleman, A. Straight, R. Losick, A. W. Murray, and A. Wright, *"Chromosome and low copy plasmid segregation in E. coli: visual evidence for distinct mechanisms"*, Cell, **90**, pp. 1113–1121, Sept. 1997.

99. J. Schindelin, I. Arganda-Carreras, E. Frise, V. Kaynig, M. Longair, T. Pietzsch, S. Preibisch, C. Rueden, S. Saalfeld, B. Schmid, J.-Y. Tinevez, D. J. White, V. Hartenstein, K. Eliceiri, P. Tomancak, and A. Cardona, *"Fiji: an open-source platform for biological-image analysis"*, Nat. Methods, **9**, pp. 676–682, July 2012.

100. L. A. K. Kleine Borgmann, H. Hummel, M. H. Ulbrich, and P. L. Graumann, *"SMC condensation centers in Bacillus subtilis are dynamic structures"*, J. Bacteriol., **195**, pp. 2136–2145, May 2013.

101. P. Thévenaz, U. E. Ruttimann, and M. Unser, *"A pyramid approach to subpixel registration based on intensity"*, IEEE Trans. Image Process., **7**, pp. 27–41, Jan. 1998.

102. E. Meijering, O. Dzyubachyk, and I. Smal, *"Methods for cell and particle tracking"*, Methods Enzymol., **504**, pp. 183–200, Jan. 2012.

103. H. Murray and A. Koh, *"Multiple regulatory systems coordinate DNA replication with cell growth in Bacillus subtilis"*, PLoS Genet., **10**, p. e1004731, Oct. 2014.

104. S. Geers, *"Control of initiation of replication and Identification of enzymes mediating DNA break repair in Bacillus subtilis"*, PhD thesis, University of Freiburg, 2011.

105. C. E. Caldon, P. Yoong, and P. E. March, *"Evolution of a molecular switch: universal bacterial GTPases regulate ribosome function"*, Mol. Microbiol., **41**, pp. 289–297, July 2001.

106. P. E. March, C. G. Lerner, J. Ahnn, X. Cui, and M. Inouye, *"The Escherichia coli Ras-like protein (Era) has GTPase activity and is essential for cell growth"*, Oncogene, **2**, pp. 539–544, June 1988.

107. T. Morimoto, P. C. Loh, T. Hirai, K. Asai, K. Kobayashi, S. Moriya, and N. Ogasawara, *"Six GTP-binding proteins of the Era/Obg family are essential for cell growth in Bacillus subtilis"*, Microbiology, **148**, pp. 3539–3552, Nov. 2002.

108. A. Sayed, S. i. Matsuyama, and M. Inouye, *"Era, an essential Escherichia coli small G-protein, binds to the 30S ribosomal subunit"*, Biochem. Biophys. Res. Commun., **264**, pp. 51–54, Oct. 1999.

109. T. I. Meier, R. B. Peery, S. R. Jaskunas, and G. Zhao, *"16S rRNA is bound to era of Streptococcus pneumoniae"*, J. Bacteriol., **181**, pp. 5242–5249, Sept. 1999.

110. R. A. Britton, B. S. Powell, S. Dasgupta, Q. Sun, W. Margolin, J. R. Lupski, and D. L. Court, *"Cell cycle arrest in Era GTPase mutants: a potential growth rate-regulated checkpoint in Escherichia coli"*, Mol. Microbiol., **27**, pp. 739–750, Feb. 1998.

111. E. Cho, N. Ogasawara, and S. Ishikawa, *"The functional analysis of YabA, which interacts with DnaA and regulates initiation of chromosome replication in Bacillus subtils"*, Genes Genet. Syst., **83**, pp. 111–125, Apr. 2008.

112. A. M. Breier and A. D. Grossman, *"Whole-genome analysis of the chromosome partitioning and sporulation protein Spo0J (ParB) reveals spreading and origin-distal sites on the Bacillus subtilis chromosome"*, Mol. Microbiol., **64**, pp. 703–718, May 2007.

113. W. K. Smits, A. I. Goranov, and A. D. Grossman, *"Ordered association of helicase loader proteins with the Bacillus subtilis origin of replication in vivo"*, Mol. Microbiol., **75**, pp. 452–461, Jan. 2010.

114. C. Bruand, M. Velten, S. McGovern, S. Marsin, C. Sérèna, S. D. Ehrlich, and P. Polard, *"Functional interplay between the Bacillus subtilis DnaD and DnaB proteins essential for initiation and re-initiation of DNA replication"*, Mol. Microbiol., **55**, pp. 1138–1150, Feb. 2005.

115. F. Y. Marston, W. H. Grainger, W. K. Smits, N. H. Hopcroft, M. Green, A. M. Hounslow, A. D. Grossman, C. J. Craven, and P. Soultanas, *"When simple sequence comparison fails: the cryptic case of the shared domains of the bacterial replication initiation proteins DnaB and DnaD"*, Nucleic Acids Res., **38**, pp. 6930–6942, Nov. 2010.

116. W. Zhang, S. Allen, C. J. Roberts, and P. Soultanas, *"The Bacillus subtilis primosomal protein DnaD untwists supercoiled DNA"*, J. Bacteriol., **188**, pp. 5487–5493, Aug. 2006.

117. C. Y. Bonilla and A. D. Grossman, *"The primosomal protein DnaD inhibits cooperative DNA binding by the replication initiator DnaA in Bacillus subtilis"*, J. Bacteriol., **194**, pp. 5110–5117, Sept. 2012.

118. P. Hammar, M. Walldén, D. Fange, F. Persson, O. Baltekin, G. Ullman, P. Leroy, and J. Elf, *"Direct measurement of transcription factor dissociation excludes a simple operator occupancy model for gene regulation"*, Nat. Genet., **46**, pp. 405–408, Apr. 2014.

119. M. C. Konopka, I. A. Shkel, S. Cayley, M. T. Record, and J. C. Weisshaar, *"Crowding and confinement effects on protein diffusion in vivo"*, J. Bacteriol., **188**, pp. 6115–6123, Sept. 2006.

120. M. Kumar, M. S. Mommer, and V. Sourjik, *"Mobility of cytoplasmic, membrane, and DNA-binding proteins in Escherichia coli"*, Biophys. J., **98**, pp. 552–559, Feb. 2010.

121. D. M. Raskin and P. A. de Boer, *"Rapid pole-to-pole oscillation of a protein required for directing division to the middle of Escherichia coli"*, Proc. Natl. Acad. Sci. U.S.A., **96**, pp. 4971–4976, Apr 1999.

122. C. Tu, X. Zhou, J. E. Tropea, B. P. Austin, D. S. Waugh, D. L. Court, and X. Ji, *"Structure of ERA in complex with the 3' end of 16S rRNA: implications for ribosome biogenesis"*, Proc. Natl. Acad. Sci. U. S. A., **106**, pp. 14843–14848, Sept. 2009.

123. N. Gollop and P. March, *"Localization of the membrane binding sites of Era in Escherichia coli"*, Res. Microbiol., **142**, pp. 301–307, Jan. 1991.

List of Figures

List of Tables

Acknowledgments

First of all, I would like to thank Prof. Peter Graumann for his excellent supervision. I very much appreciated our discussion, his encouragement and his cordiality during this work.

I am very grateful for collaborations with Prof. Dr. Bernhard Schmitt, Prof. Dr. Stephan Dahlke from the (Department of mathematics, Phillips-University Marburg) and Dr. Sean Murray (MPI for terrestrial microbiology, Marburg, AG Sourjik).

Thanks to Prof. Dr. Hironori Niki, National Institut of Genetics, Japan for the gift of the *E. coli* DnaA-eYFP sandwich fusion.

I thank Dr. Christine Kaimer who introduced me to working with *Bacillus subtilis*.
Our two "microscopy guys", Dr. Felix Dempwolff and Stephan Altenburger I would like to thank for keeping the microscopes running.

Our amazing technicians, both in Freiburg and in Marburg, I thank for "keeping the lab running". I would like to extend my thanks to Sabrina Steidel for helping not only in the cleaning kitchen.

Dr. Ana Hervas Veguillas and Dr. Marc Eisemann who shared the joy and curses DnaA had to offer.

Special thanks go to all the former and current members of the Graumann lab – I enjoyed our great time together! Many thanks go the the former and current members of the "Front-lab".

Many thanks to Dr. Felix Dempwolff and Dr. Lukas Lewark for proofreading.

Ich möchte mich auch bei meinen Freunden Anne, Anja, Julia, Kerstin S., Kerstin D., Katharina, Charles und Manuel bedanken.

Abschließend möchte ich mich bei meiner ganzen Familie bedanken. Mein besonderer Danke geht dabei an meine Eltern Christine und Andreas Schenk für Ihre Liebe und grenzenlose Unterstützung. Lukas danke ich für die gemeinsame Zeit, die liebevolle Unterstützung und seine bedingungslose Liebe.

Appendix

Supplemental movies

Supplemental movies of single molecule microscopy

Exposure time 41 ms, 24 frames/s. Scale bar: 2 μm. Pixel size: 100 nm.

Suppl. movie 1: *B. subtilis* cells expressing YFP-DnaA from an ectopic site.

Suppl. movie 2: *B. subtilis* cells expressing YFP-YabA from an ectopic site in a *yabA* deletion strain.

Suppl. movie 3: *E. coli* cells expressing DnaA-YFP from its original site.

Supplemental movies of DnaA-YFP oscillation in *E. coli*

Exposure time 200 ms, 5 frames/s. Scale bar: 2 μm. Pixel size: 80 nm.

Suppl. movie 4: *E. coli* cells expressing DnaA-YFP from its original site.

Suppl. movie 5: *E. coli* cells expressing DnaA-YFP from its original site. Addition of 200 μml rifampicin.